ABSTRACT

THE (p,t) REACTION ON RARE EARTH NUCLEI

By

Ronald William Goles

The (p,t) reaction on ^{141}Pr, ^{159}Tb, ^{165}Ho and ^{169}Tm has been carried out for the purpose of studying the general systematics of the (p,t) reaction on rare earth nuclei. All experiments were conducted at the bombarding energy of 30 MeV with the exception of the ^{141}Pr(p,t) experiment which was carried out at 40 MeV.

The (p,t) reaction on ^{141}Pr was found to strongly populate collective vibrational states in the more or less spherical ^{139}Pr nucleus. Angular distributions of states populated through this reaction were collected between 15° and 65° at 5° intervals and have been compared with distorted wave calculations.

In each of the remaining deformed nuclei studied, a strong population of the ground state rotational band was observed with at least six band members being excited in each case. Moreover, a β vibrational band in ^{157}Tb and γ vibrational bands in ^{157}Tb and ^{163}Ho were also found to be strongly excited through this reaction. Angular distributions of states below 1.25 MeV of excitation populated through the ^{159}Tb(p,t) reaction were taken between 10° and 75° at 5° intervals and have been compared with distorted wave predictions.

In addition, γ ray experiments involving the ξ/β^+ decay of ^{167}Yb were conducted in order to complement the ^{169}Tm(p,t) experiment. This decay scheme study has established the existence of twelve new excited states and the probable placement of a thirteenth in the daughter nucleus ^{167}Tm. Moreover, these thirteen states together with the well established low energy level structure of the ^{167}Tm nucleus form a consistant framework for the placement of 52 new γ rays associated with the decay of ^{167}Yb.

THE (p,t) REACTION ON RARE EARTH NUCLEI

By

Ronald William Goles

A THESIS

Submitted to
Michigan State University
in partial fulfillment of the requirements
for the degree of

DOCTOR OF PHILOSOPHY

Department of Chemistry

1971

For my mother

ACKNOWLEDGEMENTS

I wish to thank Dr. Wm. C. McHarris for suggesting this very interesting area of study. His patience and help during the experimental work and the preparation of this thesis are sincerely appreciated. I would also like to thank Dr. W. H. Kelly, Dr. B. H. Wildenthal and Dr. J. A. Nolen for their valuable advice concerning many aspects of experimental work.

A very special thank you is extended to Dr. R. A. Warner for his invaluable suggestions and experimental assistance.

Dr. B. Preedom, Mr. I. D. Proctor, Mr. J. A. Rice and Dr. G. F. Trentelman are gratefully acknowledged for their help in data acquisition and/or analysis.

I acknowledge the financial assistance of the National Science Foundation, U. S. Atomic Energy Commission and Michigan State University.

Finally, I wish to thank my scientific assistant, Mary, who always cheerfully found time to help her husband in his scientific endeavors.

TABLE OF CONTENTS

Chapter Page

APPENDICES

LIST OF TABLES

LIST OF FIGURES

Figure Page

Chapter I

Introduction

The purpose of this thesis is to investigate the general systematics of the (p,t) reaction on rare earth nuclei. Until quite recently this area of study has been left literally unresearched, although the (p,t) reaction work that has been done on intermediate to heavy mass nuclei (Ba64, Ba68, Bj66, Re67, Ma66) has served to establish the direct nature of this reaction at moderate bombarding energies.

Direct reactions are particularly useful in the study of nuclear properties since their associated mechanisms are simple and are easily understood. Models of direct reaction mechanisms have been developed and from these have come computer codes (Ba62, Ku65) which are capable of predicting quite accurately observed experimental phenomena such as angular scattering probabilities.

Pick-up reactions are a general type of direct nuclear reaction which are characterized by the transfer of a nucleon or group of nucleons from the target nucleus to an impinging, interacting projectile. To be more specific, the (p,t) reaction is pictured as proceeding through a one step transfer process in which the incident proton plucks out an ordered pair of neutrons from the target nucleus and scatters away in the form of a triton.

The particular target nuclei used in this study are: ^{141}Pr, ^{159}Tb, ^{165}Ho and ^{169}Tm. The ^{141}Pr(p,t) reaction was chosen to initiate this study, because the spherical shape of the ^{141}Pr nucleus together with the well known level structure of the residual nucleus, ^{139}Pr, allowed a straight forward analysis of the experimental data. The results of this analysis then served to establish the basic characteristics of the (p,t) reaction on rare earth nuclei.

Having completed the ^{141}Pr(p,t) study and knowing a little more of what to expect, the (p,t) reactions on the remaining strongly deformed nuclei were conducted. In addition, γ-ray experiments involving the ε/β^+ decay of ^{167}Yb were carried out to complement the ^{169}Tm(p,t) reaction experiment.

The results of these studies have shown the (p,t) reaction to be a very powerful tool for probing the collective properties of nuclei, two neutrons removed from stability.

Chapter II. Nuclear Models

The interpretation of experimental results obtained for the (*p*,*t*) reaction on rare-earth nuclei leans quite heavily upon the use of several models of the nucleus. In this chapter, those nuclear models which are to be used in the following chapters will be reviewed.

2.1. Shell Model

One of the most successful models of the nucleus is the shell model with spin-orbit interaction (Ma55). In this model individual nucleons are considered to move in stationary orbits determined by an effective spherically symmetric potential which is meant to approximate the nucleon-nucleon interactions occurring within the nucleus. Moreover, within the nucleus these orbiting nucleons are pictured as being paired off in such a way that values of many nuclear parameters are determined solely by a single unpaired nucleon.

The great success of this model lies in its ability to predict nuclear properties such as "magic numbers", nuclear isomerism, and ground state spin systematics for even and odd mass nuclei.

However, because of the simplifications used, the simple shell model cannot describe correlated or collective motion of nucleons within the nucleus and is therefore incapable of describing the collective properties exhibited by nuclei such as large quadrupole moments and low lying collective excited states.

2.2. Liquid-Drop Model

The collective model of the nucleus (Pr63) separates the nucleus into a core and extracore nucleons. The core is treated macroscopically as a deformable drop of nuclear liquid in interaction with the few extra-core nucleons that occupy unfilled shell model orbitals. Such a system can undergo two types of collective motion - surface vibrations in which the shape is distorted in an oscillatory fashion with preservation of volume and volume vibrations with preservation of shape. Since the nuclear fluid is nearly incompressible, the lowest excitations are associated with surface vibrations.

Clearly, this model of the nucleus is extremely useful in describing vibrationally excited states of spherical nuclei. For instance, in odd mass spherical nuclei, low lying vibrational states are pictured as being constructed from the various possible couplings of the vibrational angular momenta of the core λ, called the multipole order, with the spin, I, of the ground state. Thus, in the case of a quadrupole vibration, $\lambda=2$, one would expect to observe a multiplet of vibrationally excited states with spins ranging from $|I-2|$ to $I+2$. To first order, this multiplet of core excited states are degenerate; however, residual interactions between the odd nucleon and the core in practice lifts their degeneracy.

In spite of the success of the liquid drop model in explaining the low lying excited states associated with spherical nuclei, it is inadequate to explain the level structure exhibited by permanently deformed nuclei. Clearly the nuclear system is capable of motions not envisaged by the simple liquid drop model.

2.3. Unified Model

Bohr (Bo52) and Bohr and Mottelson (Bo53) tried to fuse the individual-particle and liquid-drop aspects of the nuclear system into a single "unified" model. Briefly, the model consists of a deformed rotating-vibrating nuclear core which provides a non-spherical field in which individual nucleons move. The quantum state of the model is defined by the quantum numbers $\vec{I}$, K, Ω, and M, where $\vec{I}$ is the total core plus odd nucleon(s) angular momentum of the state, K is the projection of $\vec{I}$ on the symmetry axis of the body-fixed frame, M is the projection of $\vec{I}$ in a fixed arbitrary direction (the laboratory Z axis)and Ω is the component of the total angular momentum of the odd nucleon(s) $\vec{j}$ along the symmetry axis of the body-fixed frame. For nuclei with cylindrical symmetry, which is true for low-lying rotational states, the angular momentum of the core $\vec{R}$ will be perpendicular to the symmetry axis and K will equal Ω. A vector diagram relating the quantities just described is illustrated in Fig. 2.1.

2.3.1. Rotational Spectra

The unified model of deformed odd mass nuclei predicts that for each vibrational state of the even-even core and for each assignment of the odd nucleon to a deformed single particle state, rotational energy states characterized by quantum number $K=\Omega$ will be produced by the rotational motion of the core. The energies of these rotational states are related to the total spin of the system through the following relationship,

$$E_I = \hbar^2/2\mathcal{I}\,[I(I+1) + (-1)^{I+1/2}a(I+1/2)\delta_{I,1/2}] + E_\circ \qquad \text{(II-1)}$$

with I taking on values K, $K+1$, $K+2$, . . .

2.3.2. Vibrational States

As in the previous model of the nucleus, the liquid drop picture of the deformed vibrating nuclear core is assumed. However, the phonon

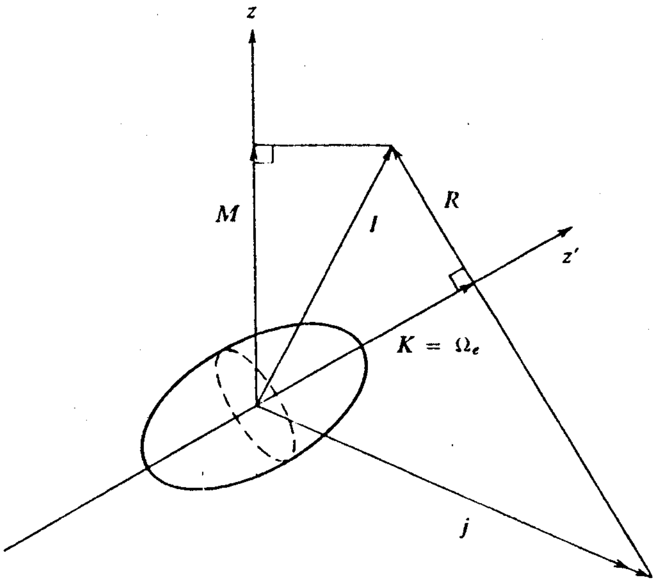

Fig. 2.1. Coupling scheme for deformed nuclei.

angular momentum λ is no longer a good quantum number, since in general it is coupled to the rotational motion of the core. Nevertheless, ν, its projection along the body fixed symmetry axis may still be used. A vibrationally excited state built upon the ground state is characterized by a K quantum number which is related to the ground state projection number $K_\circ$ and projection number ν by the following relationship,

$$K = |K_\circ + \nu| \qquad \text{(II-2)}$$

There are two exceptionally simple low energy vibrational modes of excitation which are common to most deformed nuclei: β vibrations whose angular momentum is perpendicular to the body fixed symmetry axis of the nucleus and γ vibrations whose components along the symmetry axis are ±2. From above arguments, the unified model of the nucleus would predict that a β vibration would give rise to a single excited band characterized by the K quantum number $K{=}K_\circ$ while the γ vibrations can give rise to two bands characterized by K quantum numbers $|K_\circ \pm 2|$.

Chapter III. DWBA Scattering Theory

The general formalism of DWBA scattering theory has been presented in detail in several excellent references (Ba62, Sa64, SaA65). It is the purpose of this chapter to outline this theory briefly in order to present the basic assumptions and approximations used in the analysis of the present experimental results.

3.1. Basic Theory

Consider the general reaction, $A(a,b)B$, which is symbolic for the following nuclear reaction expression:

$$A + a \rightarrow B + b \qquad \text{(III-1)}$$

where A, a, B and b represent the target, impinging particle, residual nucleus and scattered particle, respectively. Following Satchler (SaA65), the total Hamiltonian for this system, H, can be expressed in terms of either colliding pairs of particles, as is shown below.

$$H = H_{Aa} = H_{Bb} \qquad \text{(III-2)}$$

Furthermore, the prior and post forms of the total Hamiltonian H_{Aa} and H_{Bb}, respectively, can be expressed as

$$H_{Aa} = H_A + H_a + T_{Aa} + V_{Aa} \qquad \text{(III-3)}$$

and

$$H_{Bb} = H_B + H_b + T_{Bb} + V_{Bb}$$

where, if G and g are allowed to represent either A and a or B and b,

H_G and H_g are the internal Hamiltonians of these particles, T_{Gg} is their relative kinetic energy operator, and V_{Gg} is the interaction potential acting between the two particles.

The total wave function of the system Ψ_{Gg} is thus defined by the equation

$$(H_{Gg} - E)\ \Psi^{(\pm)}_{Gg}\ (\xi_G \xi_g, \vec{r}_{Gg}) = 0 \qquad \text{(III-4)}$$

where E represents the total energy of the system, ξ_G and ξ_g are the internal coordinates of G and g respectively, and the (+) and (-) designate the usual outgoing or incoming wave boundary conditions. If it is assumed that the internal coordinates of "g" are independent of those for "G", the total wavefunction of the system may be factored and written as follows,

$$\Psi_{Gg} = \phi\ (\xi_G, \xi_g)\ \phi(\vec{r}_{Gg}) = \phi_G(\xi_G)\phi_g(\xi_g)\phi(\vec{r}_{Gg}) \qquad \text{(III-5)}$$

where ϕ_G and ϕ_g are eigenfunctions of the internal coordinates of G and g, respectively, and satisfy the following eigenvalue equations

$$H_G\ \phi_G = E_G\ \phi_G$$

and (III-6)

$$H_g\ \phi_g = E_g\ \phi_g$$

The total energy of the system may now be written as

$$E = E_{Gg} + \hbar^2\kappa_{Gg}/2\mu_{Gg}$$

or (III-7)

$$E = E_G + E_g + \hbar^2\kappa^2{}_{Gg}/2\mu_{Gg}$$

where κ_{Gg} is the wave number of the relative motion of the pair G and g and μ_{Gg} is their reduced mass.

Having the expression for the total eigenfunction of the system, the transition amplitude for the reaction $A(a,b)B$ can be represented exactly by (To61, Go64):

$$t = \left\langle \phi_\beta e^{i\vec{\kappa}_\beta \cdot \vec{r}_\beta} \middle| v_\beta \middle| \Psi_\alpha^{(+)} \right\rangle \qquad \text{(III-8a)}$$

or

$$t = \left\langle \Psi_\beta^{(-)} \middle| v_\alpha \middle| \Psi_\alpha e^{i\vec{\kappa}_\alpha \cdot \vec{r}_\alpha} \right\rangle \qquad \text{(III-8b)}$$

where the abbreviations $\alpha \equiv Aa$ and $\beta \equiv Bb$ has been used. The subscript a on $\Psi_a^{(+)}$ signifies the solution with incoming waves in the a channel only but outgoing waves in all open channels. Thus, asymptotically, the wave function $\Psi_a^{(+)}$ will have the form

$$\Psi_\alpha^{(+)} \rightarrow \phi_\alpha e^{i\kappa_\alpha \cdot r_\alpha} + \sum_\gamma f_{\alpha\gamma} \left(\frac{e^{i\vec{\kappa}_\gamma \cdot \vec{r}_\gamma}}{r} \right) \Psi_\gamma \qquad \text{(III-9)}$$

where the sum is over all open channels γ and

$$f_{\alpha\gamma} \propto \left\langle \Psi_\gamma e^{i\vec{\kappa}_\beta \cdot \vec{r}_\beta} \middle| v_\beta \middle| \Psi_\alpha^{(+)} \right\rangle \qquad \text{(III-10)}$$

If the entire wave function $\Psi_{Gg}^{(\pm)}$ were known, then the problem of calculating the transition amplitude and thus the scattering reaction cross section would be solved. However, since the interaction potentials v_{Aa} and v_{Bb} of Eq. III-5 are not known, approximations must now be made in order to solve the transition amplitude equation.

At this point in the analysis a second potential U_β in the β channel together with its eigenfunction χ_β are usually introduced, where

χ_β satifies the time independent Schrödinger equation,

$$\left[(E-E_\beta) - T_\beta - U_\beta\right] \chi_\beta^\pm (\vec{r}_\beta,\vec{\kappa}_\beta) = 0 \qquad \text{(III-11)}$$

The potential U_β which has been introduced is quite general in form and is subject to only two basic restrictions: it is required that $U_\beta \to 0$ as $r_\beta \to \infty$ and that U_β be diagonal in the β system. Using the Gell-Mann-Goldberger relation (To61, Go64, SaA65) for scattering by two potentials, Eq. III-8a can be transformed as follows:

$$t = \left\langle \phi_\beta \chi_\beta^- \middle| \nu_\beta - U_\beta \middle| \Psi_\alpha^+ \right\rangle + \left\langle \phi_\beta \chi_\beta^- \middle| U_\beta \middle| \phi_\alpha e^{i\vec{\kappa}_\alpha \cdot \vec{r}_\alpha} \right\rangle \qquad \text{(III-12a)}$$

Similarly, the transformation of III-8b has the analogous form,

$$t = \left\langle \Psi_\beta^{(-)} \middle| \nu_\alpha - U_\alpha \middle| \phi_\alpha \chi_\alpha^+ \right\rangle + \left\langle \phi_\beta e^{i\vec{\kappa}_\beta \cdot \vec{r}_\beta} \middle| U_\alpha \middle| \phi_\alpha \chi_\alpha^+ \right\rangle \qquad \text{(III-12b)}$$

Now, since the arbitrary potential U_β or U_α is assumed to be diagonal in the β or α system, the second term in these expressions for the transition amplitude will be zero except for the case of elastic scattering. Excluding this possibility, the exact expression for the post and prior interaction forms of the transition amplitudes become

$$t_{\text{post}} = \left\langle \phi_\beta \chi_\beta^{(-)} \middle| \nu_\beta - U_\beta \middle| \Psi_\alpha^{(+)} \right\rangle \qquad \text{(III-13a)}$$

and

$$t_{\text{prior}} = \left\langle \Psi_\beta^{(-)} \middle| \nu_\alpha - U_\alpha \middle| \phi_\alpha \chi_\alpha^{(+)} \right\rangle \qquad \text{(III-13b)}$$

In order to evaluate the transition amplitudes in III-13, one has to choose a U_β or U_α which will make possible the replacement of $\Psi^{(\pm)}$ by some computable quantity. The distorted-wave Born approximation

(DWBA) follows from the observation that elastic scattering is usually the dominant process occurring in any scattering situation. In other words, this observation implies that the optical potential that describes elastic scattering will be the dominant part of the interactions ν_{Aa} and ν_{Bb}. Clearly then, if U_α and U_β are chosen as the optical potentials for describing the scattering of a on A and b on B respectively, the expressions $\nu_\alpha - U_\alpha$ and $\nu_\beta - U_\beta$ will become small perturbing residual interactions responsible for the reaction, and the problem can clearly be treated by perturbation techniques. Radial eigenfunctions of optical model potentials satisfying Eq. III-11 can easily be calculated. The perturbation expression for Ψ_α^+ thus becomes

$$\Psi_\alpha^{(+)} \simeq \phi_\alpha \chi_\alpha^{(+)} (\vec{r}_\alpha) \qquad \text{(III-14)}$$

while the distorted-wave approximation to the post interaction form of the transition amplitude III-13a is

$$t_{\text{post}}\,(\text{DW}) = \left\langle \phi_\beta \chi_\beta^{(-)} \middle| \nu_\beta - U_\beta \middle| \phi_\alpha \chi_\alpha^{(+)} \right\rangle \qquad \text{(III-15)}$$

The analogous prior interaction form of this amplitude can be written as

$$t_{\text{prior}}(\text{DW}) = \left\langle \phi_\beta \chi_\beta^{(-)} \middle| \nu_\beta - U_\beta \middle| \phi_\alpha \chi_\alpha^{(+)} \right\rangle \qquad \text{(III-16)}$$

It is useful at this point to separate the integrand of the transition amplitude into factors which are dependent upon internal and relative coordinates. Letting $\mathcal{V}$ represent either the post or prior interaction potentials, one can express the transition amplitude corresponding to the reaction $A(a,b)B$ as follows:

$$t = J \int d\vec{r}_\beta \int d\vec{r}_\beta \, \chi_\beta^{(-)}(\vec{\kappa}_\beta, \vec{r}_\beta) \left\langle B,b|v|A,a \right\rangle \chi_\alpha^{(+)}(\vec{\kappa}_\alpha, \vec{r}_\alpha) \qquad \text{(III-17)}$$

Here $\vec{r}_\alpha$ and $\vec{r}_\beta$ are vectors connecting the centers of mass of A and a and B and b, respectively, while J is the Jacobian of the transformation to these relative coordinates. The distorted waves χ_α and χ_β are elastic scattering wave functions calculated from Eq. III-11 which describe the relative motion of the pair a, A(asymptotically with relative momentum $\vec{\kappa}_\alpha$)before collision and the pair b, B (with $\vec{\kappa}_\beta$) after collision, respectively.

The remaining factor in the amplitude III-17 is the matrix element of the interaction causing the inelastic event taken between internal states of the colliding pairs

$$\left\langle B,b|v|A,a \right\rangle = \int \phi_B^* \phi_b^* v \phi_A \phi_a d\xi \qquad \text{(III-18)}$$

where ξ represents all pertinent <u>internal</u> coordinates. This matrix element or form factor contains all the information regarding nuclear structure, angular momentum selection rules and even the type of reaction being considered.

3.2. Differential Cross Section

Having obtained an expression for the transition amplitude, t, connecting two non-identical nuclear states A and B via the $A(a,b)B$ reaction, one has the tools for calculating the differential cross section for the scattering between these two states. For unpolarized projectiles and target nuclei, the expression relating the differential scattering cross section to the transition amplitude can be shown (Sa64) to have the following form:

$$\frac{d\sigma}{d\Omega} = \frac{\mu_\alpha \mu_\beta}{(2\pi\hbar)^2} \frac{\kappa_\beta}{\kappa_\alpha} \frac{\Sigma |t|^2}{(2J_A+1)(2S_a+1)} \qquad \text{(III-19)}$$

where J_A and S_A are the spin quantum numbers of the target and projectile respectively and where the sum is taken over all spin projection numbers of the impinging particle, target, residual nucleus and scattered particle.

Thus, in order to obtain theoretical differential cross sections for a scattering event, one has now only to evaluate the appropriate form factor $\langle B,b|v|A,a\rangle$.

3.3. Form Factors for Pick-up Reactions

Pick-up reactions are a general type of nuclear reaction which are characterized by the transfer of a nucleon or a group of nucleons from the target nucleus to an impinging particle with which the target interacts. In order to adapt the previously developed DWBA formalism to the particular case of pick-up reactions, one has to make the following assignments to the components of the general reaction $A(a,b)B$:

$$b = a + x$$

and (III-20)

$$A = B + x$$

Here x denotes the nucleon or cluster of nucleons plucked out of nucleus A by the incident interacting particle a.

As was shown in Section 1 of this chapter, the prior interaction form of the form factor is given by

$$f = \langle Bb|\nu_{Aa} - U_{Aa}|Aa\rangle \qquad \text{(III-21)}$$

In order to evaluate this matrix element, some explicit form for the interaction potential responsible for the reaction must be derived. Since the target nucleus A is pictured as being composed of a core "B" and a bound particle or cluster "x", the interaction potential ν_{Aa} may conveniently be written as a sum of two terms

$$\nu_{Aa} = \nu_{xa} + \nu_{Ba} \tag{III-22}$$

The perturbing interaction responsible for the reaction may be written as

$$\nu_{Aa} - U_{Aa} = \nu_{xa} + (\nu_{Bb} - U_{Aa}) \tag{III-23}$$

It is customary at this point to take ν_{xa} as the important interaction responsible for pick-up, since from previous arguments one would expect cancellation of ν_{Ba} with U_{Aa}. Furthermore, it is generally assumed that ν_{xa} is central, that is, scalar in $\vec{r}_{xa}$ so that "a" and "x" are in an S-state of relative motion within b. The nuclear matrix element III-21 may now be written explicitly as:

$$f = \iiint \phi_{\beta}^{*}(\xi_{\beta})\phi_{b}^{*}(\xi_{a}\xi_{x},\vec{r}_{ax})\nu_{xa}(\xi_{x}\xi_{a},\vec{r}_{ax})\phi_{a}(\xi_{a})\phi_{A}(\xi_{B}\xi_{x},\vec{r}_{Bx})d\xi_{a}d\xi_{x}d\xi_{b} \tag{III-24}$$

where ξ_i represents the internal coordinates of particle i while $\vec{r}_{ij}$ is the vector joining the centers of mass of particles i and j.

Since the interaction potential ν_{xa} is independent of ξ_B, the matrix element III-24 may be simplified by integrating over this variable. The overlap of the target with the residual nucleus, $\langle B|A\rangle$, projects out the bound state wave function of the particle or cluster.

This overlap is usually evaluated by expanding ϕ_A in terms of ϕ_B and ϕ_x.

$$\phi_A = \sum_{J_B j M_B} (J_B, j, M_B, M_A - M_B | J_A M_A) \phi_{J_B M_B}(\xi_B) \Omega^{B,A}_{j\mu}(\xi_x, \vec{r}_{Bx}) \tag{III-25}$$

where J_B and M_B are the spin and projection numbers of B, j and μ are the angular momentum and projection numbers of x, $\phi_B(\xi_B)$ is the wave-function of nucleus B with internal coordinates ξ_B and $\Omega^{B,A}_{j\mu}$ is the wave function of the bound particle or cluster x. Substituting this expression of ϕ_A into the overlap integral, one has

$$\langle \phi_B | \phi_A \rangle = \sum_{j} (J_B, j, M_B, M_A - M_B | J_A M_A) \Omega^{B,A}_{j\mu}(\xi_x, \vec{r}_{Bx}) \tag{III-26}$$

The indexes B,A are carried as a reminder that Ω depends upon the initial and final nuclear state.

The angular dependence of $\Omega^{B,A}_{j\mu}$ may now be removed by expanding in spherical harmonics

$$\Omega^{B,A}_{j\mu} = \sum_{S\ell M} (i)^{\ell} Y^{M}_{\ell}(\theta_{Bx}\phi_{Bx}) \phi^{BA,\ell j}_{S,\mu-M}(r_{Bx}\xi_x)(\ell SM, \mu-M | j\mu) \tag{III-27}$$

where S is the intrinsic spin of particle x. S need not be single valued if x is a cluster.

Upon substitution of III-27 into III-24, one obtains the following general expression for pick-up form factors:

$$f = \sum_{j^{\ell}SM} (J_B, j, M_B, M_A - M_B | J_A M_A)(i)^{\ell} Y_{\ell}^{M}(r_{Bx})(\ell SM, \mu - M | j\mu)$$

$$\iint \phi_b(\xi_a \xi_x, \vec{r}_{ax}) \nu_{xa}(\xi_a \xi_x, \vec{r}_{ax}) \; \phi_{S,\mu-M}^{BA,\ell j}(\xi_x, \vec{r}_{Bx}) \phi_a(\xi_a) d\xi_a d\xi_x$$

(III-28)

The above equation marks the point of departure for two different approaches which are commonly used in the evaluation of the form factor III-28. A brief description of each method along with the additional assumptions and approximations which characterize each will now be discussed.

3.3.1. Cluster transfer and Zero Range Approximation.

The cluster model of two neutron pick-up reactions treats the two neutrons as a structureless elementary particle of spin 0 and mass 2. In particular, the (p,t) reaction is pictured as proceeding through the transfer of a "dineutron" from the target nucleus to the interacting incident proton. Because the two neutrons are treated as being elementary, calculation of the (p,t) form factor proceeds exactly as in single nucleon transfer reactions such as (p,d) reactions.

Upon adopting this approach, one may immediately simplify the matrix element III-28 by expanding ϕ_b in terms of ϕ_a and ϕ_x as follows

$$\phi_b = \sum_{S a j_x M_a} (S_a j_x M_a, M_x | S_b M_b) \phi_{S_a M_a}(\xi_a) \phi_{j_x M_x}(\vec{r}_{xa}, \xi_x)$$

(III-29)

Substitution of III-29 into the matrix element contained in Eq. III-28 one arrives at the following expression

$$< b|\nu_{xa}|x,a> = \sum_{S_a j_x M_a} (S_a j_x M_a, M_x | S_b M_b)$$

$$\times \iint \phi_{S_a M_a} \phi_{j_x M_x} \nu_{xa} \phi^{AB\ell j}_{S,\mu-M} \; \phi_{J_a M_a} d\xi_a d\xi_x \qquad \text{(III-30)}$$

Noting that the cluster assumption has eliminated the dependence of ν_{xa} on the internal coordinates and using the orthogonal properties of the ϕ_a's, the integration over ξ_a yields the result

$$< b|\nu_{xa}|x,a> = (S_a S_x M_a, M_x | S_b M_b) \;\times \int \phi_{S_x M_x} \nu_{xa} \; \phi^{BA,\,\ell j}_{S,\,\mu-M}(\vec{r}_{xa}, \xi_a) d\xi_x$$

(III-31)

where the sum over j_x has been reduced to a single term with $J_x=S_x$, since "a" and "x" are assumed to be in a relative S-state. Furthermore, for the dineutron transfer $S_x=0$; however, S_x will be carried along for generality.

The remaining integral of Eq. III-31 can easily be carried out by noting that since "x" is considered an elementary particle, $\phi^{AB,\,\ell j}_{S,\,\mu-M}\,(\xi_x, \vec{r}_{Bx})$ will be factorable into functions dependent upon internal and relative coordinates as is shown in Eq. III-32.

$$\phi^{BA,\,\ell j}_{S,\,\mu-M} = R_{\ell j}(r_{Bx}) \Psi_{S,\,\mu-M}(\xi_x)$$

(III-32)

Similarly,

$$\phi_{j_x M_x}(\xi_x, r_{ax}) = \Theta(r_{ax})\Psi_{S_x M_x}(\xi_x) \qquad \text{(III-33)}$$

Substituting the above quantities into equation III-31, one obtains the following result:

$$\langle b|\nu_{xa}|xa\rangle = (S_a S_x M_a, M_x|S_b M_b) R_{\ell j}(r_{Bx})\nu_{ax}(r_{ax})\Theta(r_{ax})$$

$$\times\ \delta_{S_x, S}\ \delta_{M_x, \mu-M} \qquad \text{(III-34)}$$

Finally, using this result in Eq. III-28, one has the following expression for the cluster transfer form factor:

$$f = \sum_{j\ell} (J_B j M_B, M_A - M_B|J_A M_A)(S_a S_x M_a, M_b - M_a|S_b M_b)$$

$$\times\ (i)^{\ell} Y_{\ell}^{M}(r_{Bx})\nu_{ax}(r_{ax})\Theta(r_{ax})(\ell S_x m, M_x|j M_A - M_B)$$

$$\times\ R_{\ell j}(r_{Bx}) \qquad \text{(III-35)}$$

where $m = M_A + m_a - M_B - M_b$

In the above expression, the radial functions $R_{\ell j}$ are assumed to be proportional to shell model eigenfunctions and are taken to be the bound state wave functions of the dineutron in a Woods-Saxon well. The form of this well in which the cluster is bound is given by

$$U(r) = V_o\left(\frac{1}{1+e^{x}}\right)\ ;\ x = (r - 1.25A^{1/3}f)/0.65\,f \qquad \text{(III-36)}$$

where A is the mass number of the residual nucleus and V_0 is chosen to reproduce the experimental two neutron separation energy.

The zero range approximation, which has been used with this cluster transfer approach, consists of setting

$$V(r_{ax})\theta(r_{ax}) = D_0\delta(r_{ax}) \qquad \text{(III-37)}$$

where D_0 is a constant characteristic of the reaction being considered.

This rather extreme approximation is imposed in order to reduce the six-dimensional unseparable integral of Eq. III-17 to a three-dimensional one which can be handled easily by present DWBA computer codes. The effect of this approximation (SaA65) is to introduce correlations between the various functions which are varying rapidly in the nuclear interior. This phenomenon in turn tends to overestimate the contributions to the scattering cross sections from the interior of the nucleus.

Combining the zero range approximation, III-37, with equation III-35, one obtains the general result that the form factor corresponding to a particular ℓsJ cluster transfer will be proportional to the bound state wave function of that cluster.

3.3.2. Two nucleon matrix element.

As an alternative to the gross approximations inherent in the cluster transfer formalism, one can attempt to calculate the form factor corresponding to two neutron pick-up through direct use of Eq. III-28. In this approach, one gives up the idea of further simplifying the two neutron matrix element expressions and instead attempts to approximate the functional quantities present within it realistically.

Rewriting the two nucleon matrix elements contained in Eq. III-28,

$$< b|V_{ax}|x,a> = \iint \phi_b(\xi_b)V_{ax}\phi^{BA,\ell j}_{S,\mu-M}\phi_a \qquad \text{(III-38)}$$

the functional quantities which are used by the distorted-wave code DWUCK (Ku71) in the finite range evaluation of this expression will now be outlined.

For $\phi_b(\xi_b)$, the internal wavefunction of the triton, a Gaussian form is assumed (Ku71, Ch70)

$$\phi_b(\xi_b) = N\exp(-\eta^2[r^2_{12} + r^2_{1a} + r^2_{2a}]) \qquad \text{(III-39)}$$

where η is the size parameter of the triton, N a normalization constant, and $\vec{r}_{ij} = \vec{r}_i - \vec{r}_j$.

Since two neutron pick-up is now being considered, the interaction potential, V_{ax}, becomes the sum of two terms

$$V_{ax} = V_{a1} + V_{a2} \qquad \text{(III-40)}$$

where again a Gaussian form for these nucleon-nucleon interactions, V_{ai}, is assumed and has the form,

$$V_{ij} = U_o\exp(-\beta^2 r_{ij}{}^2) \qquad \text{(III-41)}$$

where β is the reciprocal of the range of the nucleon-nucleon interaction, while U_o determines the strength of this interaction.

The two neutron wave function $\phi^{\mathrm{B,A}\ell\mathrm{j}}_{\mathrm{S},\mu-\mathrm{M}}$ determined from the overlap of the target and residual nucleus is usually expressed in terms of single neutron wave functions as follows

$$\phi^{\ell_1\ell_2}_{L\lambda}(r_1,r_2) = \sum_{\lambda_1\lambda_2} (\ell_1\ell_2\lambda_1\lambda_2|L\Lambda)\phi_{\ell_1\lambda_1}(r_2)\phi_{\ell_2\lambda_2}(r_2) \tag{III-42}$$

The wave functions of the two initially bound neutrons $\phi_{\ell_1\lambda_1}$ and $\phi_{\ell_2\lambda_2}$ are then taken to be those of a particle bound in a Wood-Saxon well of the form,

$$U(r) = -V_o 1/(1+e^x) + (\hbar^2/m_\pi \cdot c)^2 V_s 1/r \frac{d}{dr}\left(\frac{1}{1+e^x}\vec{\ell}\cdot\vec{S}\right) \tag{III-43}$$

where

$$x = (r-r_o A^{1/3})/a \tag{III-44}$$

In the above expression, $\vec{\ell}$ and $\vec{s}$ are the orbital and spin angular momenta of the neutron, A is the mass of the target nucleus less one, r_o is the real nuclear radius parameter, a is the diffusivity parameter, V_s is the spin-orbit well depth and V_O is the real Woods-Saxon well depth which is adjusted so that individual neutrons are bound by one-half the two neutron separation energy.

Having made these substitutions in the two neutron matrix elements, one has only to integrate this expression in order to obtain an expression for the form factor III-28. The methods employed in integrating Eq. III-38 are the subjects of several papers (Ku71, Ch70, Ba67) and will not be dealt with here.

3.3.3. Finite Range Correction. Once an expression for the two neutron matrix elements and the resultant form factor III-28 is obtained, one is faced with calculating a six-dimensional integral III-17 in order to evaluate the expression for the transition amplitude. This procedure, if carried out, involves rather excessive computational difficulties and is unsuitable for present DWBA computer programs. The distorted wave code DWUCK employs an approximate correction factor Λ to the usual zero range approximation in order to correct for the effects due to the finite range of the nucleon-nucleon interactions. This factor has the form

$$\Lambda(r) = \left\{ 1+ \frac{M_b M_x R^2}{M_a{}^2 \hbar^2} \quad [U_b(r)-U_a(r)-U_x(r)-BE_x] \right\}^{-1} \tag{III-45}$$

where U_i is the optical model potential for particle i, M_i is the mass of particle i, BE_x is the magnitude of the binding energy of the particle x and R is the range of the interaction.

It has been shown (Ku71, Ch70) that with the correction factor III-45, the zero range code approximates fairly well the correct finite range calculations for two neutron transfer reactions.

CHAPTER IV

Experimental Apparatus and Methods

4.1. The (*p*,*t*) Reaction

The investigations of the (*p*,*t*) reaction on ^{141}Pr, ^{159}Tb, ^{165}Ho and ^{169}Tm have not all been carried out using the same methods and apparatus. As a result, Sections 4.1.1. through 4.1.3. will deal with matters common to all experiments, while Sections 4.1.4. and 4.1.5. will deal with the details of specific experiments.

4.1.1. Cyclotron and Beam Transport

The experimental proton beams were provided by the Michigan State variable-energy sector-focused cyclotron. Through use of quadrupole focusing magnets located at appropriate positions along the beam line, the transport system illustrated in Figure 4.1. focused the extracted beam on slits *S*1 and *S*3 whose apertures determined the beam energy spread on the target. The proton beams were energy analyzed and dispersed by bending magnets *M*3 and *M*4, each of which turns the beam through 45°. The magnetic fields of these analyzing magnets were measured with NMR probes placed in the central fields of *M*3 and *M*4. Bending magnet *M*5 was then used to deflect the beam into the desired experimental area. Additional quadrupole focusing just prior to the experimental areas allowed one to vary the beam dispersion on target.

4.1.2. Target Fabrication

In conjunction with experiments concerning the (*p*,*t*) reaction on rare-earth isotopes, thin metallic targets of ^{141}Pr, ^{159}Tb, ^{165}Ho and ^{169}Tm have been prepared by vacuum evaporation at the Michigan State

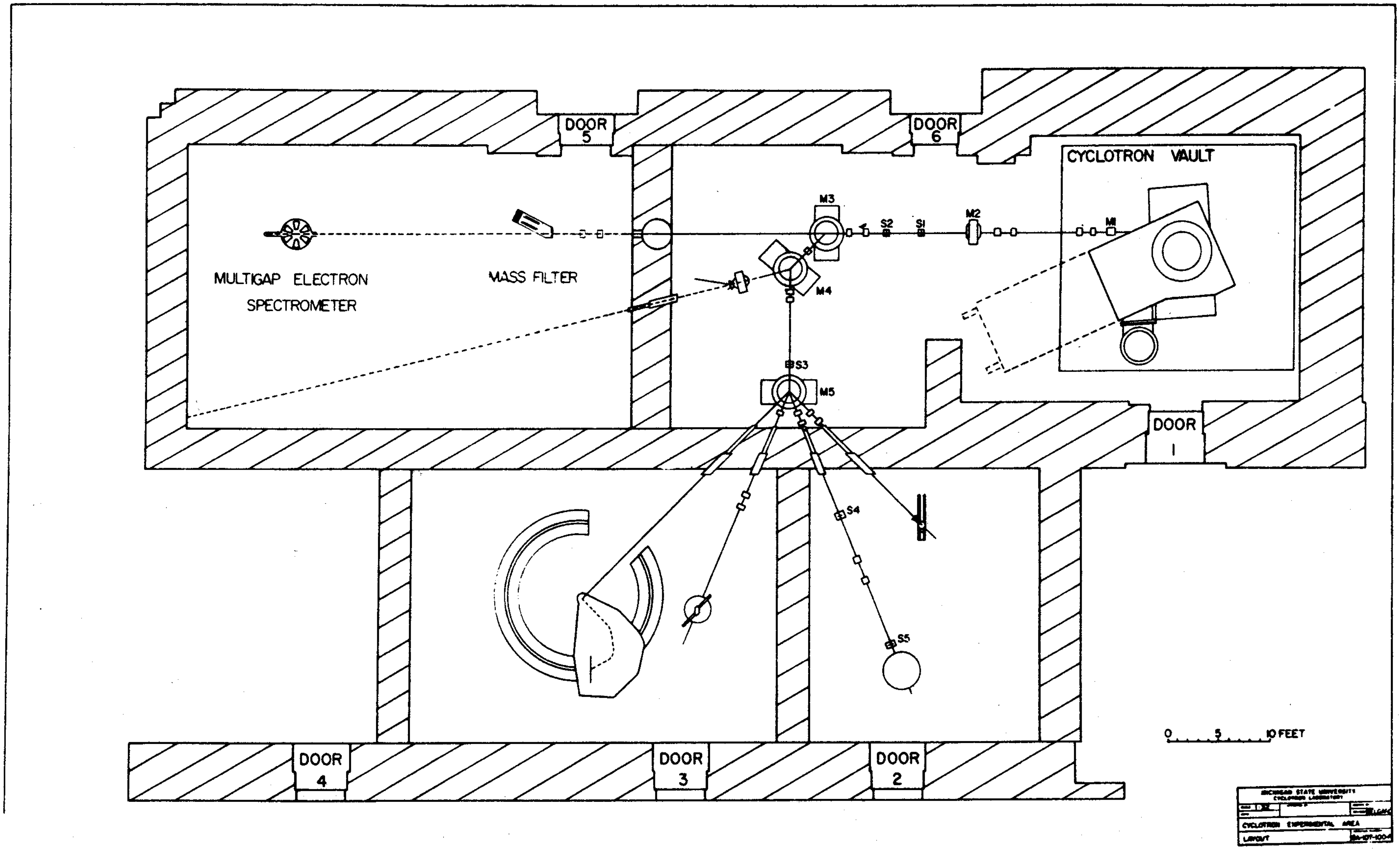

Fig. 4.1. Michigan State University cyclotron, beam transport system and experimental areas.

Cyclotron Laboratory. The details of the vacuum system used are described elsewhere (Go69).

The foils themselves were prepared by evaporating the 99.9% pure metallic rare earth from a 5-mil tantalum boat onto a 20-μg/cm^2 carbon backing. In order to insure a good uniformity of the foils, the carbon backings were always placed 4-6 in. above the evaporation crucible or boat.

The carbon backings used in the fabrication of targets had no observable effects on the data taken since their thinness precluded significant beam degradation, while their high (p,t) Q value disallowed any possibility of interference.

Target thicknesses of fabricated targets were determined through use of an ^{241}Am α gauge. This apparatus measures the energy loss suffered by $\simeq$5.5 MeV α-particles as they traverse a target. This information can then be directly related to the target thickness through use of range-energy tables (Wi66). A precision of ±5% is assumed for this method of measurement.

4.1.2.A. ^{141}Pr Targets

^{141}Pr targets readily oxidize when exposed to air. As a result, these targets were stored under vacuum. The target thickness of the foil used in obtaining the triton angular distribution was 793-μg/cm^2.

4.1.2.B. ^{159}Tb Target

Studies of the (p,t) reaction on ^{159}Tb were all conducted using a 454μg/cm^2 target. Although ^{159}Tb does not oxidize readily, this target was also stored under vacuum to minimize the effects of long term exposure to air.

4.1.2.C. ^{165}Ho and ^{169}Tm Targets

Target thicknesses of ^{165}Ho and ^{169}Tm used in this experiment were ≃300-μg/cm^2. These targets showed no signs of long term deterioration from prolonged exposure to air and were not stored under vacuum.

4.1.3. The Faraday Cup and Charge Collection

The beam used in irradiating rare-earth targets was stopped and collected by either an aluminum or a carbon Faraday cup. The differential and integral charge collected during an experiment was monitored with an Elcor model A310B current digitizer and integrator.

An aluminum beam stop has the advantage of only producing short-lived activities upon being bombarded by the beam. However, significant γ-ray backgrounds are produced during the periods of bombardment which makes this beam stop unsuitable for experiments involving photographic plates. During such runs, a carbon Faraday cup was used which produced lower radiation levels during bombardment.

4.1.4. ^{141}Pr(p,t) Experiment

In the study of the (p,t) reaction on ^{141}Pr, an ≃800-μg/cm^2 target of metallic ^{141}Pr was bombarded with 500-nA beams of 40-MeV protons accelerated by the Michigan State University sector-focused cyclotron. An $E,\Delta E$ detector telescope was used to measure the energies of the tritons produced while a monitor counter kept track of the number of protons elastically scattered at right angles to the beam direction.

4.1.4.A. The Scattering Chamber

The 36" scattering chamber used in this experiment was equipped with a central, remotely rotatable target ladder capable of holding a scintillator and several targets, a remotely movable arm capable of mounting a detector telescope at various radial positions, and an unmotorized arm capable of mounting a stationary detector or monitor, again, at several radial positions

The target and detector angle readout device was reproducible well within a ±0.15° limit.

A plexiglass window in the scattering chamber together with a closed circuit television system allowed the beam spot to be observed on a scintillator and finely adjusted with quadrupole focusing.

4.1.4.B. The Detector Telescope and Monitor Counter

The ΔE-E detector telescope used in this experiment was composed of two cooled Si surface barrier detectors. The ΔE detector is a thin diode incapable of stopping the least energetic particle of interest and is always placed closest to the target. The E detector, which is placed behind the ΔE counter, is a much thicker diode which is chosen so that the total thickness of the two detectors, $E+\Delta E$, is sufficient to stop the most energetic particle of interest. The ΔE and E detector thicknesses chosen for this experiment were 925 μ and 2025 μ, respectively.

The solid angle subtended by the detectors was determined by a collimator slit placed directly in front of the detector package and the radial position of the detector telescope. In this experiment a 110-mil thick tantalum collimator with an oval aperture of 0.120"×0.260" was used at a ≃10" radial distance from the target.

Cooling of the detectors was achieved by circulating ethanol at dry ice temperature through a cooling plate in contact with the copper detector mount in the telescope. This was done in order to reduce electronic noise within the detectors to a minimum.

A NaI(Tl) detector placed at right angles to the beam was used to monitor elastically scattered protons. The number of elastic events recorded for a given irradiation is proportional to the product of the effective target thickness and the total charge collected during the irradiation. As a result, relative cross-sections may be obtained which are independent of the errors associated with target thickness measurements, target nonuniformities, beam drift, and target deterioration. The monitor output is also a very sensitive means of determining analyzer dead times.

4.1.4.C. Electronics and Particle Identification

Having described the hardware associated with the detection system, the electronic methods used to measure energies and identify particles will now be discussed.

For each particle "seen" by the detection system, three signals are received from the detector telescope: A pulse "ΔE" from the ΔE detector proportional to the differential energy loss of the particle, a pulse "E" from the E detector proportional to the energy of the particle emerging from ΔE detector, and a pulse, "Σ", proportional to the total energy of the particle, obtained by summing the "E" and "ΔE" pulses at the detector telescope. The summing circuit which produces the Σ pulse appears in Fig. 4.2. The ΔE, E and Σ pulses taken off the detector telescope are then passed through charge sensitive preamplifiers and sent on to the data acquisition area. Here they go through the electronics setup illustrated in Fig. 4.3 which, in addition to amplifying and shaping the pulses, requires the simultaneous presence of Σ and ΔE signals before these latter two pulses are sent on to a coupled pair of 8192-channel digital to analog convertors (ADC's). The computer code

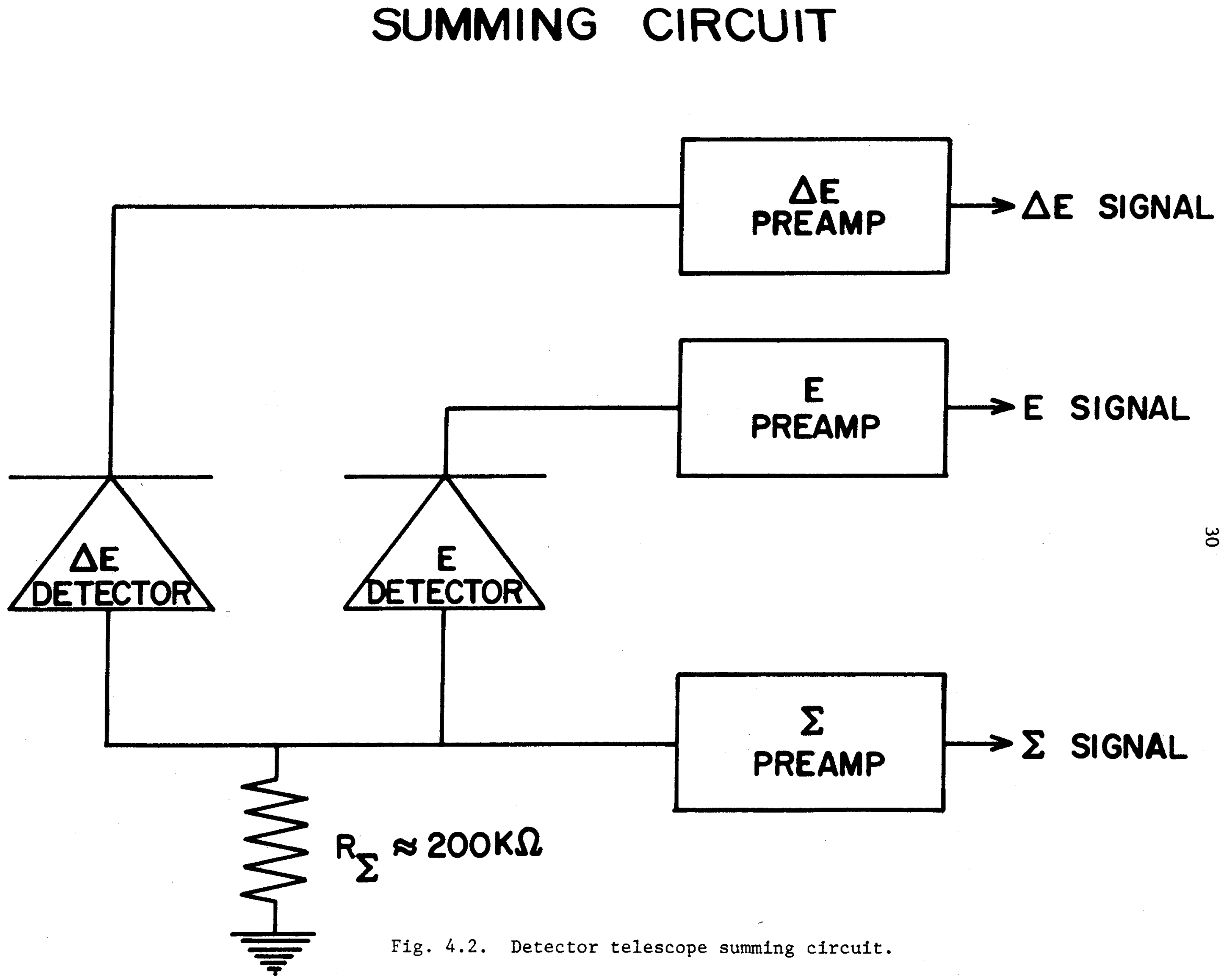

Fig. 4.2. Detector telescope summing circuit.

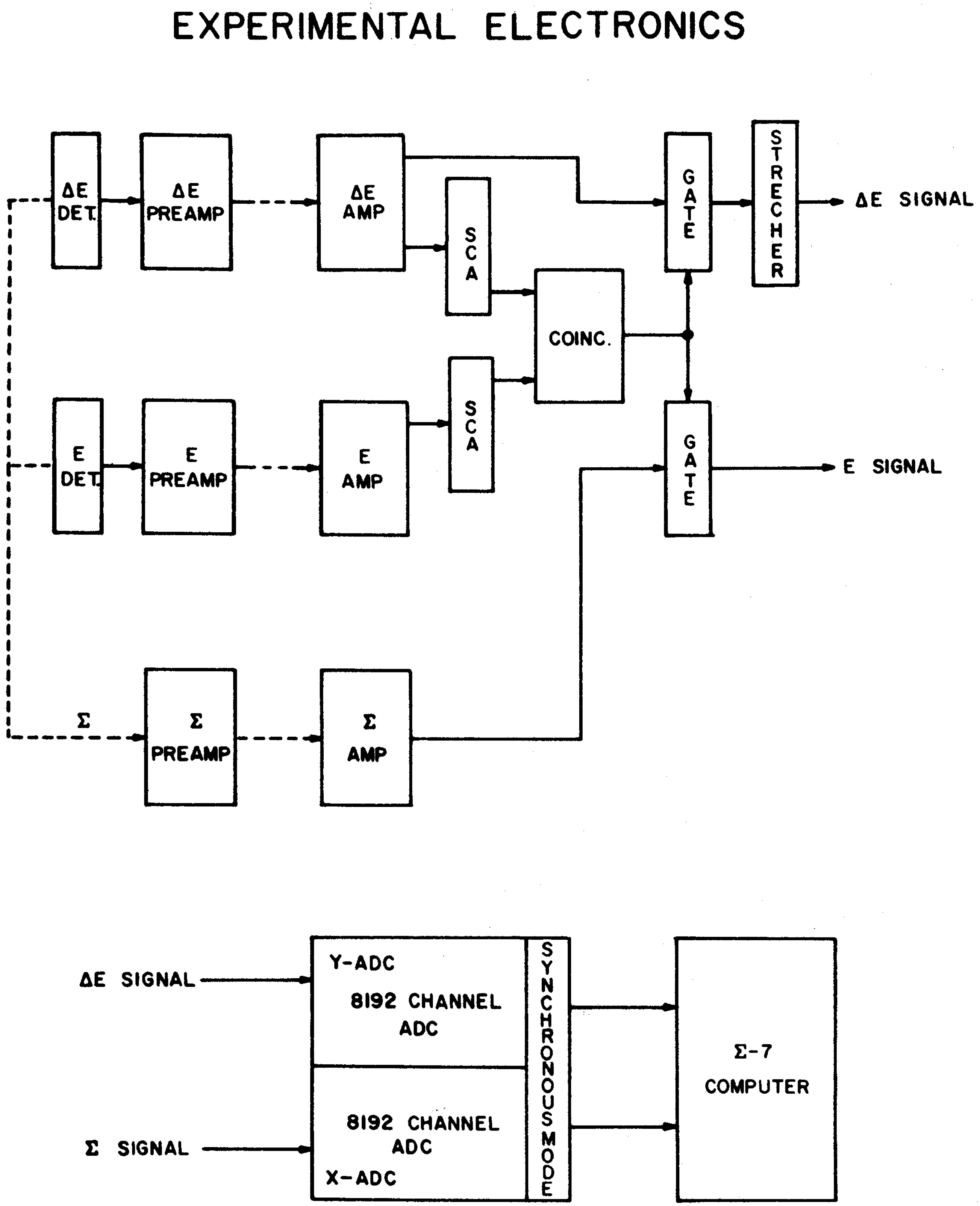

Fig. 4.3. Experimental electronics associated with the *E*–Δ*E* detector telescope.

TOOTSIE (Ba70) stores this digitized two-dimensional information and is capable of displaying it on a storage scope. Just such a two-dimensional display is illustrated in Fig. 4.4. Now, because particles differing in mass and/or charge but having the same total kinetic energy will exhibit different differential energy losses, different particles "seen" by the detector telescope will fall into distinctly different non-overlapping bands in this Σ-ΔE two-dimensional space. The computer code then allows gate lines to be drawn about the desired particle band or bands in the form of polynomial fits to points designated in this Σ-ΔE plane. These gate lines are then used to route all total energy pulses Σ, falling within a given pair to any one of several 8192-channel memory blocks where the total energy spectrum is stored.

4.1.4.D. Dead Time Correction

In order to correct for pulses lost due to ADC dead time, the elastic scattering portion of the monitor counter spectra was simultaneously scaled and sent to the channel zero associated with the pair of ADC's used in the spectral analysis. The pulses sent to channel zero are scaled only during time intervals when the ADC's are idle. Thus, the ratio of these two numbers will be a measure of the fractional number of counts lost during the counting period.

4.1.5. ^{159}Tb(p,t), ^{165}Ho(p,t) and ^{169}Tm(p,t) Experiments

In the investigation of the (p,t) reaction on ^{159}Tb, ^{165}Ho and ^{169}Tm, $\simeq$300-μg/cm^2 targets were bombarded with 30-MeV protons accelerated by the Michigan State University sector-focused cyclotron. The scattered tritons were analyzed by an Enge-split-pole magnetic spectrometer and collected on Kodak NTB nuclear emulsions.

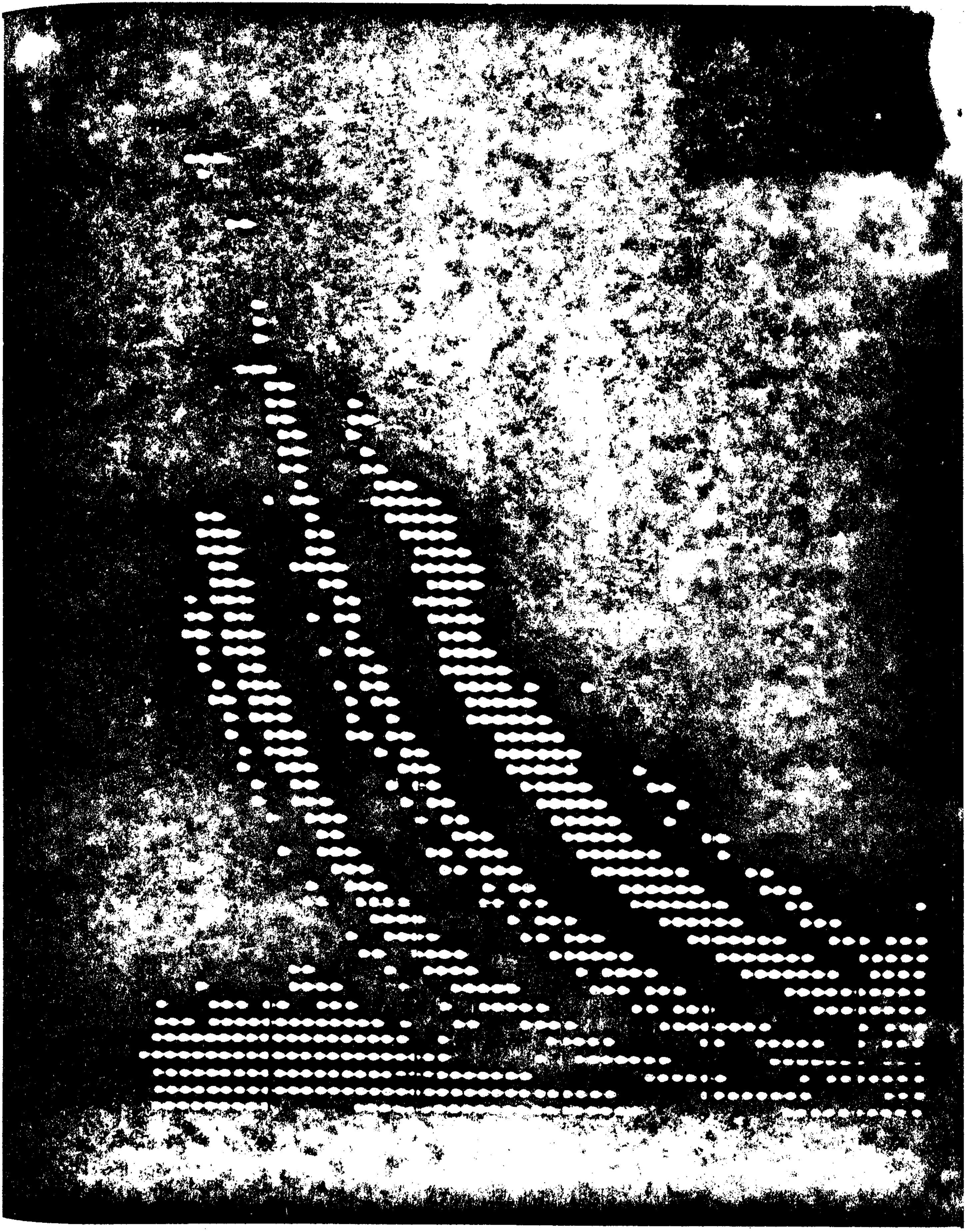

Fig. 4.4. TOOTSIE two dimensional E-ΔE display illustrating three particle bands.

4.1.5.A. The Magnetic Spectrograph

An Enge split-pole, double focusing magnetic spectrograph was used to momentum analyze the scattered tritons produced through the (p,t) reaction on ^{159}Tb, ^{165}Ho, and ^{169}Tm. This spectrograph is mounted on a rail and is capable of being rotated about a stationary centrally located 14" scattering chamber from -5° to 160°. The 14" scattering chamber is equipped with a remotely rotatable central target post, a series of removable ports located about its perimeter and a sliding seal which forms the contact between the chamber and the spectrograph. A 0.372"× 0.387" slit located ≃10" from the central target post at the junction of the chamber and spectrograph defined the solid angle of acceptance for the spectrograph.

The spectrograph was chosen for this series of experiments because of its high transmission and resolution capabilities. Kinematic broadening effects were completely compensated for through a proper positioning of the focal plane. This allowed for the use of large solid angles without a corresponding kinematic loss in energy resolution. Kinematic focal plane positions were computed with the computer code SPECKINE (Tr70).

SPECKINE also allowed for calculations of dispersion matched quadrupole settings which disperse the beam energy on target in such a way that the spectrograph magnet will focus all rays producing a given excitation. Perfect dispersion matching would make experimental resolution independent of the bombarding beam energy width. Clearly, dispersion matching allowed for much higher bombarding currents on target than could normally be tolerated if the beam width was directly related to resolution.

Particle identification was achieved solely through the momentum analysis of the spectrograph magnet. A fortuitous combination of reaction Q values always caused the tritons to be much more rigid than all other observable reaction products.

4.1.5.B. Monitor Counter

A 5-mm ϕ cooled Si(Li) solid state detector placed at right angles to the beam was used to monitor the elastic scattering events produced during the angular distribution experiment of ^{159}Tb.

4.1.5.C. Plate Reading

The photographic plates which recorded scattering events were scanned using a microscope whose plate platform could be continuously moved both in a horizontal and vertical direction. A vernier associated with horizontal motion (motion along the energy axis) allowed relative plate positions to be read to within ±0.005 mm.

Under normal scanning conditions plates were viewed under a 200 power magnification and read in 1/4 mm strips. However, in the cases of high track densities and/or high resolution these conditions were varied in order to suit the particular situation at hand.

4.2. $^{167}\text{Yb} \xrightarrow{\varepsilon/\beta^+} {}^{167}\text{Tm}$ Experiment

The states of ^{167}Tm have also been investigated through the ε,β^+ decay of ^{167}Yb. Gamma-ray singles and coincidence experiments have been conducted in order to construct the ^{167}Yb decay scheme.

4.2.1. Source Preparation

Samples of the 18.5-min ^{167}Yb were produced by bombarding the oxide of 100% abundant naturally occurring ^{169}Tm with 23.5-MeV protons accelerated by the Michigan State University sector-focused cyclotron.

Samples were bombarded for approximately 3 min with average beam currents of 2-μA, and the resulting activities were counted for periods not exceeding 3 half-lives

The ^{167}Yb activity produced by the (*p*,3*n*) reaction is extremely clean since the major competing reactions (*p*,2*n*) and (*p*,*n*), lead to stable and relatively long-lived isotopes respectively. Furthermore, the relatively long-lived ^{167}Tm activity decays almost entirely to a single state in ^{167}Er, giving rise to only 2 significant γ rays.

γ rays not associated with the decay of ^{167}Yb were identified through a crude half-life study and from the γ-ray spectra of residual activities left after all ^{167}Yb had decayed away. The only major contamination identified in the ^{167}Yb γ-ray spectra were the 207.9-keV and 531.8-keV γ rays from the ^{167}Tm decay.

4.2.2. γ-Ray Singles Experiments

The energies and relative intensities of γ rays associated with the decay of ^{167}Yb were determined by a series of γ-ray singles experiments. The low energy portion (E_γ <200 keV) of the γ-ray spectrum was taken with a Si(Li) x-ray detector. This detector easily resolved several closely spaced low energy γ rays allowing accurate relative intensity measurements to be made.

Spectra above 200 keV were taken using Ge(Li) detectors with and without Pb absorbers. Graded lead absorbers placed between the source and the detector were used to discriminate against low energy, high intensity γ rays so that "hotter" sources could be counted in order to bring out the high energy, low intensity γ rays associated with the ^{167}Yb decay. Spectra taken without Pb absorbers were used for relative intensity and energy measurements of the stronger γ rays in the spectra and also served to establish a correspondence between spectra taken with and without Pb absorbers so that corrected relative intensities of weaker γ-ray lines could be obtained.

Electronics components used with all γ-ray singles experiments included an FET preamplifier and high voltage supply, a pulse shaping linear amplifier with pole-zero compensation, an analog to digital converter (ADC) and multichannel analyzer.

4.2.3. γ-Ray Coincidence Experiments

γ-ray cascade relationships were established through anti-coincidence and delayed coincidence experiments. These studies were conducted using a Ge(Li) detector in coincidence with an 8"×8" NaI(Tl) split annulus and a 3"×3" NaI(Tl) scintillation counter. A complete description of this coincidence system and its capabilities are discussed elsewhere (Au67). The electronics used in these coincidence experiments is illustrated in Fig. 4.5.

In the anti-coincidence experiment, ^{167}Yb sources were placed at the center of the annulus tunnel which was then blocked by a 3"x3" NaI(Tl) detector at one end and by the Ge(Li) detector at the other. The source in effect was completely surrounded by detectors and represented a very efficient counting system. The single-channel analyzers associated with the NaI(Tl) detectors were set to accept all γ rays above 70 keV. The coincidence resolving time used in this experiment was 100 nsec.

With the exception of the operating mode of the linear gate and the delay of 250 nsec added to the Ge(Li) side of the coincidence

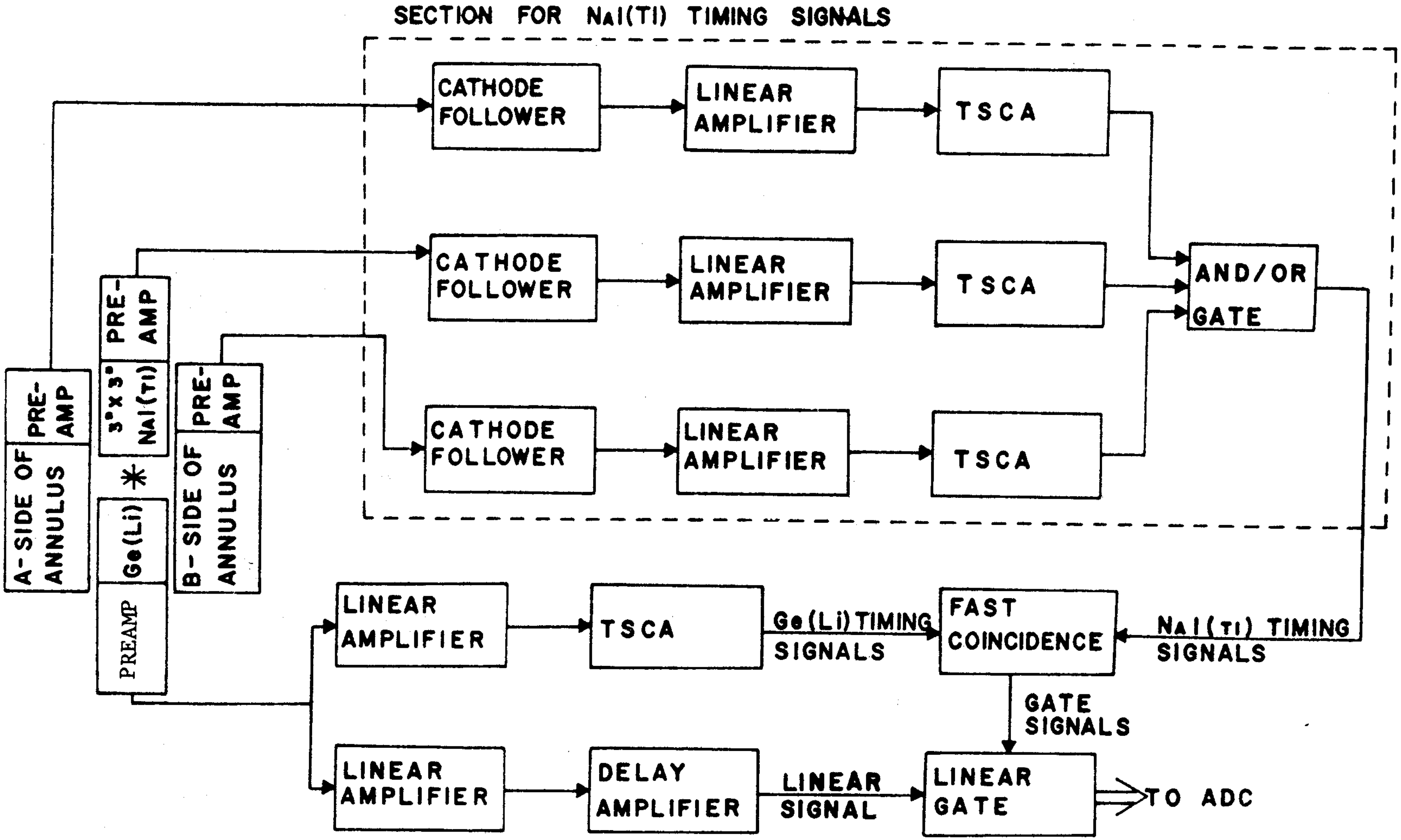

Fig. 4.5. Experimental apparatus associated with γ ray anti- and delayed coincidence experiments.

circuit, the delayed coincidence experiment was conducted exactly as was the previously described anti-coincidence study.

CHAPTER V

DATA REDUCTION

5.1. Peak Areas and Centroids

The areas and centroids of spectral peaks were all determined in the same manner, independent of the type of experiment. These computations were achieved through the use of the computer code MOIRAE (Au68).

MOIRAE allows spectra in the form of computer card inputs to be displayed on an oscilloscope. Having designated representative background points on both sides of a peak, the computer code will determine the background under the peak through use of a polynomial fit to these designated background points. The background fit or difference spectra can then be displayed for visual inspection. Once an acceptable background is obtained and the positions of the high and low sides of the peak are specified, MOIRAE calculates the net area of the peak, the statistical error associated with this area and the peak centroid.

The areas and centroids of composite peaks were determined using the computer code SAMPO (Ro69). SAMPO will strip a composite peak by fitting Gaussian peaks with exponential tails to the data. The characteristics of the fitting peaks were determined from singlet lines appearing in the same spectra. A detailed discussion of this code is given elsewhere (Ro69).

5.2. (p,t) Experiment

5.2.1. Energies

The methods used in obtaining excitation energies corresponding to the various spectral triton peaks differed in the two types of experiments conducted. As a result, these methods will be discussed separately.

5.2.1.A. ^{141}Pr(*p*,*t*) Experiment

The excitation energies of the various triton peaks occurring in the ^{141}Pr spectra were determined internally by making a correspondence between some of the more obvious triton peaks and the well established states of ^{139}Pr (Be69). The centroids of these standard triton peaks together with information concerning the proton bombarding energy, scattering angle and particle masses were used in a FORTRAN kinematic code to establish a calibration curve from which excitation energies of unknown peaks were determined.

In addition, an independent energy measurement of some of the more intense triton groups was conducted using a broad range magnetic spectrometer and a 3-cm ϕ Si position sensitive detector. In this experiment the ground state peak was placed at several different positions along the detector in order to calibrate the detector's length. Excitation measurements were then obtained using methods described in the next section.

5.2.1.B. Spectrograph Experiments

The excitation energies measured with the spectrograph were derived from the relative energy measurements of the various triton lines based on a single peak of known excitation, usually the ground state. Given the excitation energy and the centroid of the reference peak together with the bombarding energy, the scattering angle, the masses of particles involved, and the value of the spectrograph magnetic field, the relativistic computer code SPECTRUM (Ri70) will calculate the excitation energies of all other lines occurring in the spectrum based on their relative focal plane positions. The uncertainties inherent in this type of measurement have been determined to be ±5 keV.

5.2.2. Cross-Sections

In the analysis of angular distribution data both absolute and relative differential cross sections were calculated. Because of the inherent errors involved in measuring absolute cross sections, only relative values were used in the construction of angular distributions. These curves were then renormalized to reflect the magnitudes of the measured absolute curves. Error bars appearing in all angular distributions reflect statistical uncertainties only.

5.3. γ-ray Experiments

The information extracted from γ-ray experiments are γ-ray energies and/or relative intensities. These quantities, in turn, are obtained from measured peak areas and centroids. The methods used in extracting nuclear information from experimentally measured quantities will now be discussed.

5.3.1. γ-Ray Energies

The energies of the stronger γ rays associated with the ^{167}Yb decay were determined internally by counting activities of ^{167}Yb simultaneously with well known γ-ray standards. The centroids of these standard γ-ray peaks served to establish a correspondence between peak position and energy from which energies of other spectral peaks could be determined. The correspondence drawn between centroid and energy took the form of a least-squared linear or quadratic calibration curve. The energies of the lower intensity ^{167}Yb γ rays were then similarly determined by using the stronger ^{167}Yb γ rays as secondary standards. Only those peaks falling within the range of the calibration points were determined in this way.

The standard γ-ray sources used in the primary calibration of the ^{167}Yb spectrum appear in Table 5.1.

5.3.2. γ-Ray Relative Intensities

In order to relate relative peak areas to their relative intensity values, the efficiency of the detection system as a function of energy has to be determined. This can be done in an absolute or relative sense but must be done empirically for each and every detector used. The methods of determining a relative efficiency curve are discussed elsewhere (Do71).

The analytical forms of the relative efficiency curves for the detectors used in this experiment are contained in the computer code MOIRAE *E*(*I*) (Be69). Given the detector used, peak energies and their corresponding areas, this code computes γ-ray relative intensities by correcting each peak area for its corresponding relative detector efficiency and normalizing this result to a single γ-ray intensity defined as 100.

Table 5.1. γ-Ray Calibration Standards

Source	γ-ray energy (keV)	Reference
^{22}Na	1274.53 ±0.10	Le68
^{46}Sc	889.18 ±0.10	Le68
	1120.41 ±0.10	
^{60}Co	1173.226±0.040	Le68
	1132.483±0.046	
^{65}Zn	1115.44 ±0.01	Le68
^{88}Y	897.96 ±0.10	Le68
	1836.08 ±0.07	
^{110m}Ag	657.71 ±0.03	Br69
	706.68 ±0.04	
	763.88 ±0.04	
	884.67 ±0.04	
	1475.73 ±0.04	
	1504.90 ±0.08	
	1562.22 ±0.06	
^{182}Ta	1121.28 ±0.12	Le68
	1221.42 ±0.10	
^{207}Bi	569.63 ±0.08	Le68
	1063.58 ±0.06	
	1769.71 ±0.13	

Chapter VI

^{141}Pr(p,t) Results

6.1. Introduction

The investigation of the general systematics of the (p,t) reaction on rare-earth isotopes was begun with the ^{141}Pr nucleus. The residual nucleus of this reaction, ^{139}Pr, has been extensively studied through the ε/β^+ decays of the ground and meta-stable states of ^{139}Nd. The latest level structure of ^{139}Pr as determined through the decay scheme studies of Beery, Kelly and McHarris (Be69) appears in Figure 6.1. As in other N=79 odd-mass isotones, the energy separation between the $11/2^-$ metastable and the $3/2^+$ ground states is rather small, making the $M4$ transition connecting these two states quite slow. This situation has the effect of allowing the two quite dissimilar isomers to decay almost independently to two completely different sets of states in the daughter nucleus ^{139}Pr. Because of the large number of very dissimilar states established by this decay scheme study, it was decided to begin our investigation of the (p,t) reaction with ^{141}Pr even though the main emphasis of our total study would involve only strongly deformed nuclei.

6.2. DWBA Analysis

The distorted wave predictions for various ℓ-value transfers were calculated using a zero-range, cluster pick-up approach as well as a more rigorous finite-range, two-nucleon transfer formalism.

The distorted wave code JULIE (Sa64) was used in the cluster transfer analysis. The bound-state and optical potential parameters

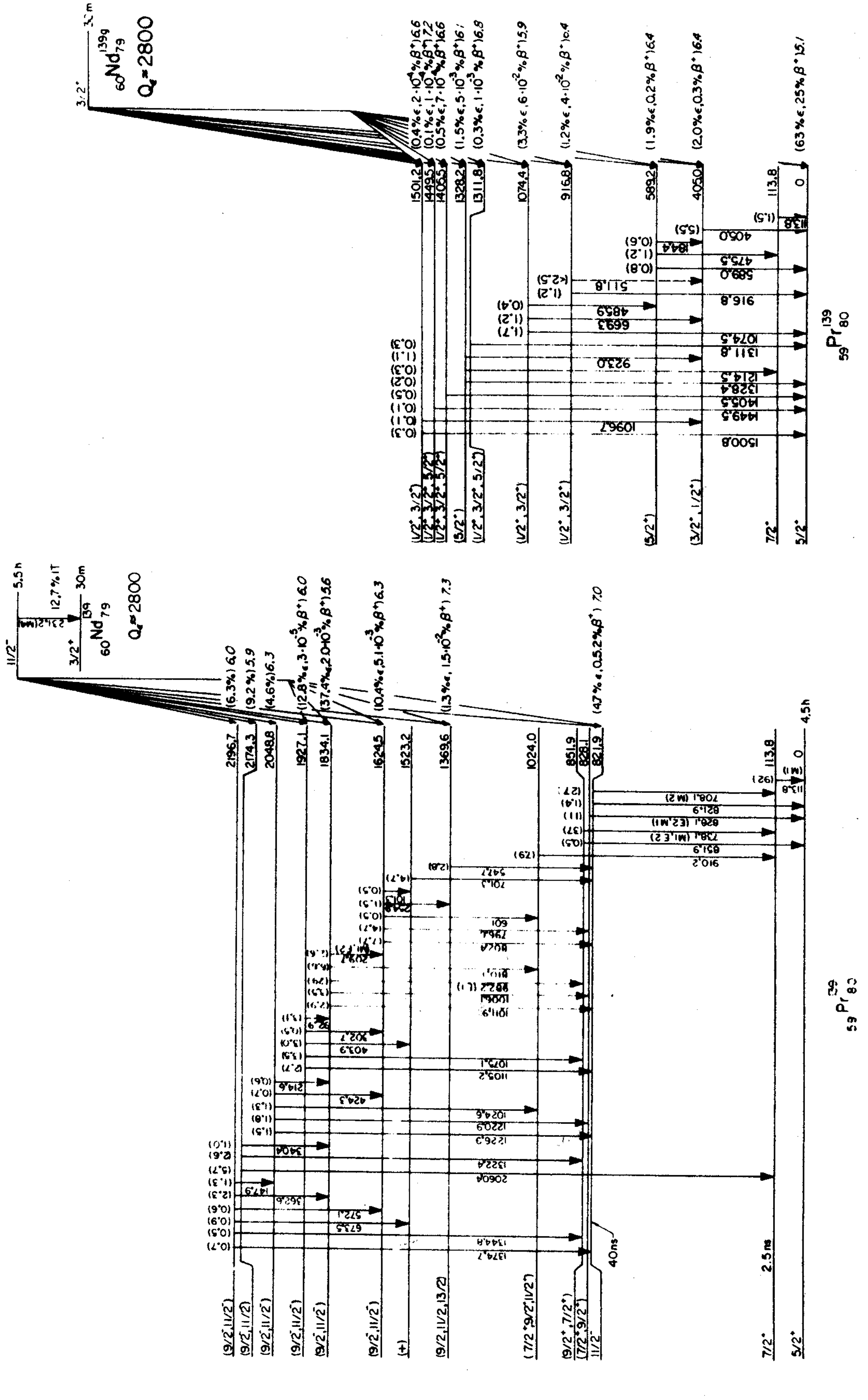

Fig. 6.1. Decay schemes of ^{139m}Nd and ^{139g}Nd.

used in these calculations are listed in Table 6.1. The bound state well depth was always chosen so as to reproduce the binding energy of the two neutrons removed. This binding energy, B_x, was calculated from the formula:

$$B_x(\text{cluster}) = S - E_x \qquad (6.1.)$$

where S is the ground state separation energy of two neutrons and E_x is the excitation energy of the state being considered. Cluster transfer predictions when compared with experimental results will always be denoted by a broken curve.

The finite range, two nucleon transfer calculations were performed using the distorted wave code DWUCK (Ku65). The bound state and optical potentials used in this analysis appear in Table 6.1. The real well depth of each of the two transferred bound neutrons was chosen to reproduce one half their total binding energy. This single neutron binding energy, B_x, was calculated from the following relationship:

$$B_x = (S - E_x) \; / \; 2 \qquad (6.2.)$$

Finite range two nucleon transfer calculations will in this and all succeeding chapters be represented by a continuous curve when being compared with experimental data.

6.3. ^{141}Pr(p,t) Spectra

Triton spectra obtained from the (p,t) reaction on ^{141}Pr were collected with an E-ΔE detector telescope and were with the exception of 70° taken between 15° and 75° at 5° intervals. Typical spectra

Table 6.1.

Optical-Model and Bound-State Well Parameters used in the Distorted-Wave Analysis of the ^{141}Pr(p,t) Reaction

Particle	V_o (MeV)	W_o (MeV)	W_D (MeV)	V_s (MeV)	r_o (f)	a (f)	r'_o (f)	a' (f)	r''_o (f)	a'' (f)	r_{oc} (f)
Proton[1]	49.95	4.97	5.00	6.04	1.16	0.75	1.370	0.63	1.026	0.738	1.25
Triton[2]	169.6	12.00			1.14	0.795	1.48	0.824			1.40
Dineutron					1.25	0.650					1.25
Neutron[3]				λ=25	1.25	0.650					1.25

1) Ref. Fr67
2) Ref. Ig69
3) The value of λ=25 corresponds to $V_s \simeq 8.5$ MeV.

$$U_{OM}(r) = V_c(r) - V_o \frac{1}{1+e^{x}} - (W_o - 4W_D \frac{d}{dx'}) \frac{1}{1+e^{x'}} + (\frac{\hbar}{m_\pi c})^2 V_s \frac{1}{r} \frac{d}{dr} (\frac{1}{1+e^{x''}}) \vec{\ell}\cdot\vec{\sigma}$$

taken at 25° and 35° are illustrated in Figure 6.2. A complete compilation of spectra taken in this experiment together with the pertinent extracted data appears in Appendexes *A* and *B* respectively.

6.4. Angular Distributions

The experimental angular distributions together with their distorted wave predictions are displayed in Figures 6.3-6.4. Figure 6.3. exhibits those states populated through ℓ value transfers from 0 to 3. The angular distribution corresponding to the $5/2^+ \rightarrow 5/2^+$ ground state transition clearly corresponds to an apparently pure $\ell=0$ transfer. The finite range calculation of the transfer of two $d_{3/2}$ neutrons fits the lower angle data much better than does the cluster transfer analysis; however, the latter calculation does a better job of predicting the positions of therelative maxima occurring at 55° than does the finite range approach. The overall agreement between theory and experiment is good, and, since the angular shape of an $\ell=0$ transfer is sufficiently different from all other ℓ-values, the ground state of the residual nucleus ^{139}Pr appears to be populated by a pure $\ell=0$ wave.

The five angular distributions appearing below the $\ell=2$ designation in Figure 6.3 all exhibit a characteristic $\ell=2$ angular shape. Again, at lower angles the finite range $(d_{3/2})^2_{\ell=2}$ calculations fit the data much better than do the cluster predictions, although beyond 25° both theoretical curves are remarkably similar. Moreover, since the states populated through these $\ell=2$ waves have all been previously (Be69) classified as being collective in nature, the purity of these experimental $\ell=2$ curves are assured (Pe63).

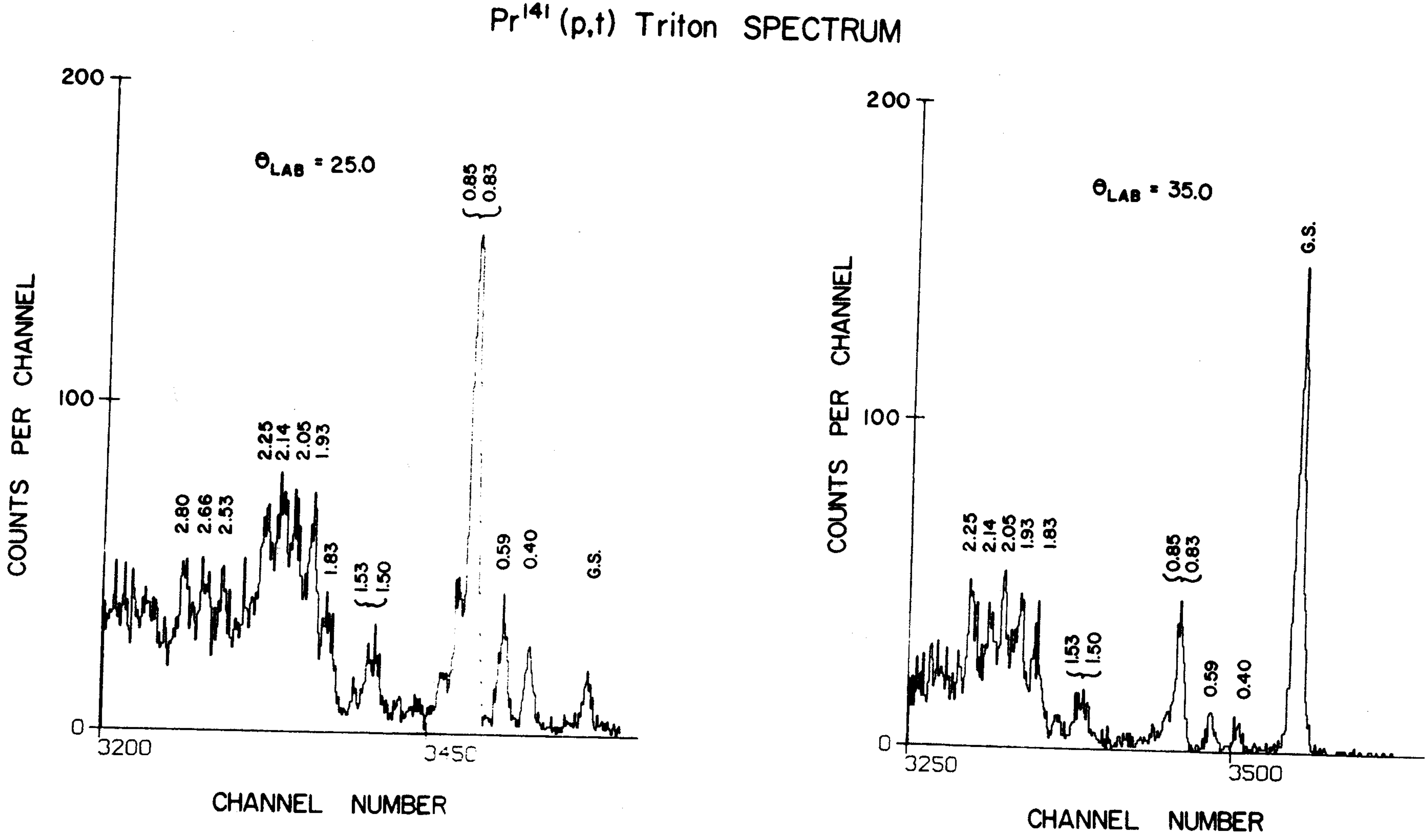

Fig. 6.2. $^{141}\mathrm{Pr}(p,t)$ triton spectra taken with an E-ΔE detector telescope.

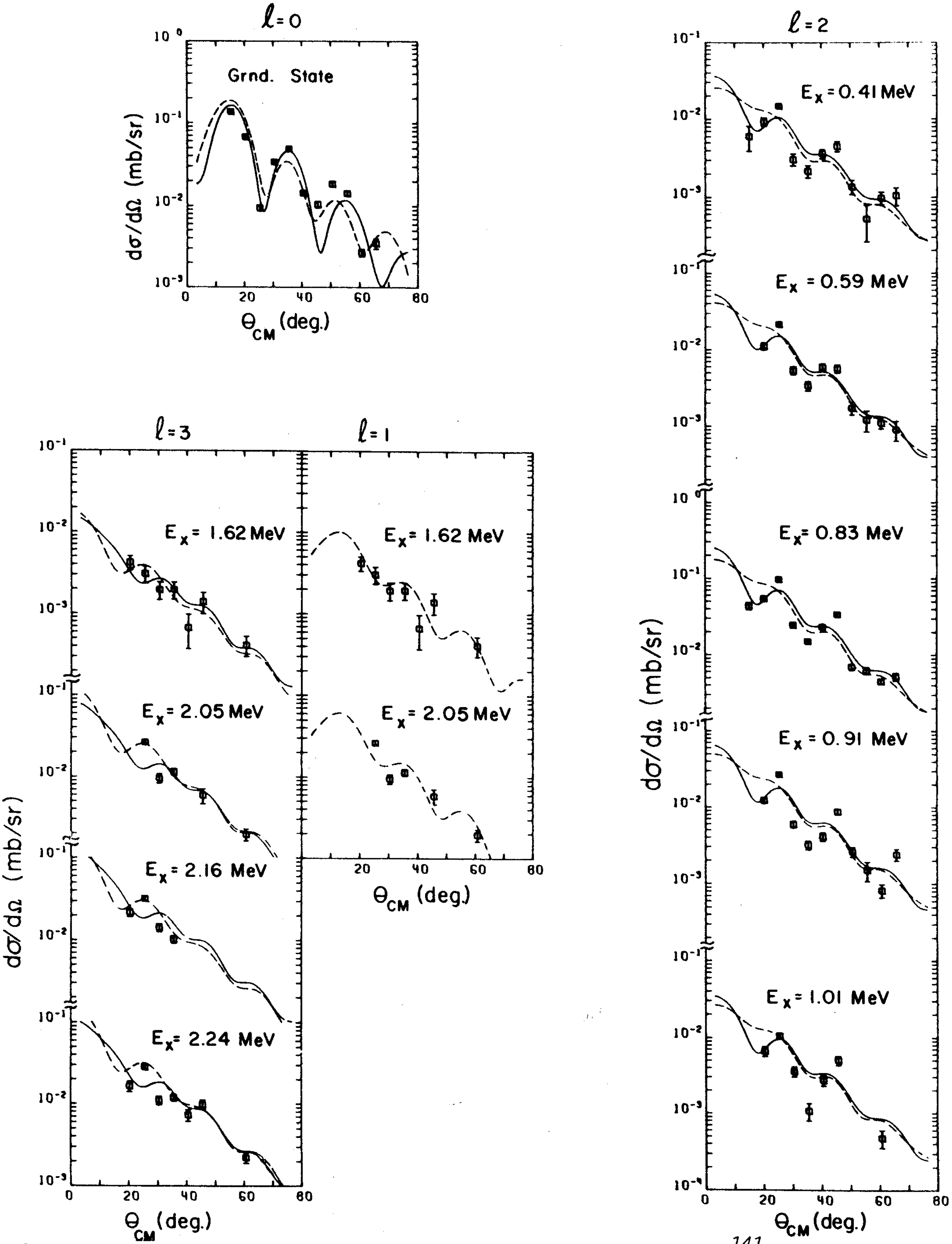

Fig. 6.3. Angular distributions of states populated through the ^{141}Pr(p,t) reaction. Theoretical two neutron pick-up and cluster transfer calculations are represented by continuous and broken curves respectively. Relative cross sections have been normalized to reflect measured absolute values.

The remaining angular distributions appearing in Figure 6.3 correspond to four states populated through ℓ=1 and/or ℓ=3 transfers. The 1620-keV and 2050-keV states clearly exhibit an odd-ℓ character; however, unique ℓ assignments cannot be made on the basis of shape alone, since both ℓ=1 and ℓ=3 angular predictions fit the experimental points equally well.

However, because these relatively low energy states are populated by odd ℓ waves, their origins can only be explained in terms of an octupole core excitation or in terms of a transferred $h_{11/2}$ neutron. The former explanation of course immediately eliminates the possibility of any ℓ=1 strength in the angular distributions of these states.

If, on the other hand, an $h_{11/2}$ neutron participates in the pick-up process leading to these excited odd parity states, then of the possible even parity orbitals available, energetics alone makes a $d_{3/2}$ neutron the most probable candidate for the second neutron transferred. Assuming this transfer configuration, one finds that of the two possible ℓ values associated with these two states only the ℓ=3 value is allowed by the conservation of angular momentum. This pick-up mode, moreover, is consistent with the shell model configurations assigned to states of similar energy characterized by radioactive studies (Be69, Mc69).

The remaining two states in Figure 6.3 appear to exhibit a unique ℓ=3 shape, although the limited number of experimental points in these distributions make these assignments tentative at best.

Figure 6.4 exhibits two angular distributions which probably represent more than one excited state each. An ℓ=6 angular shape has

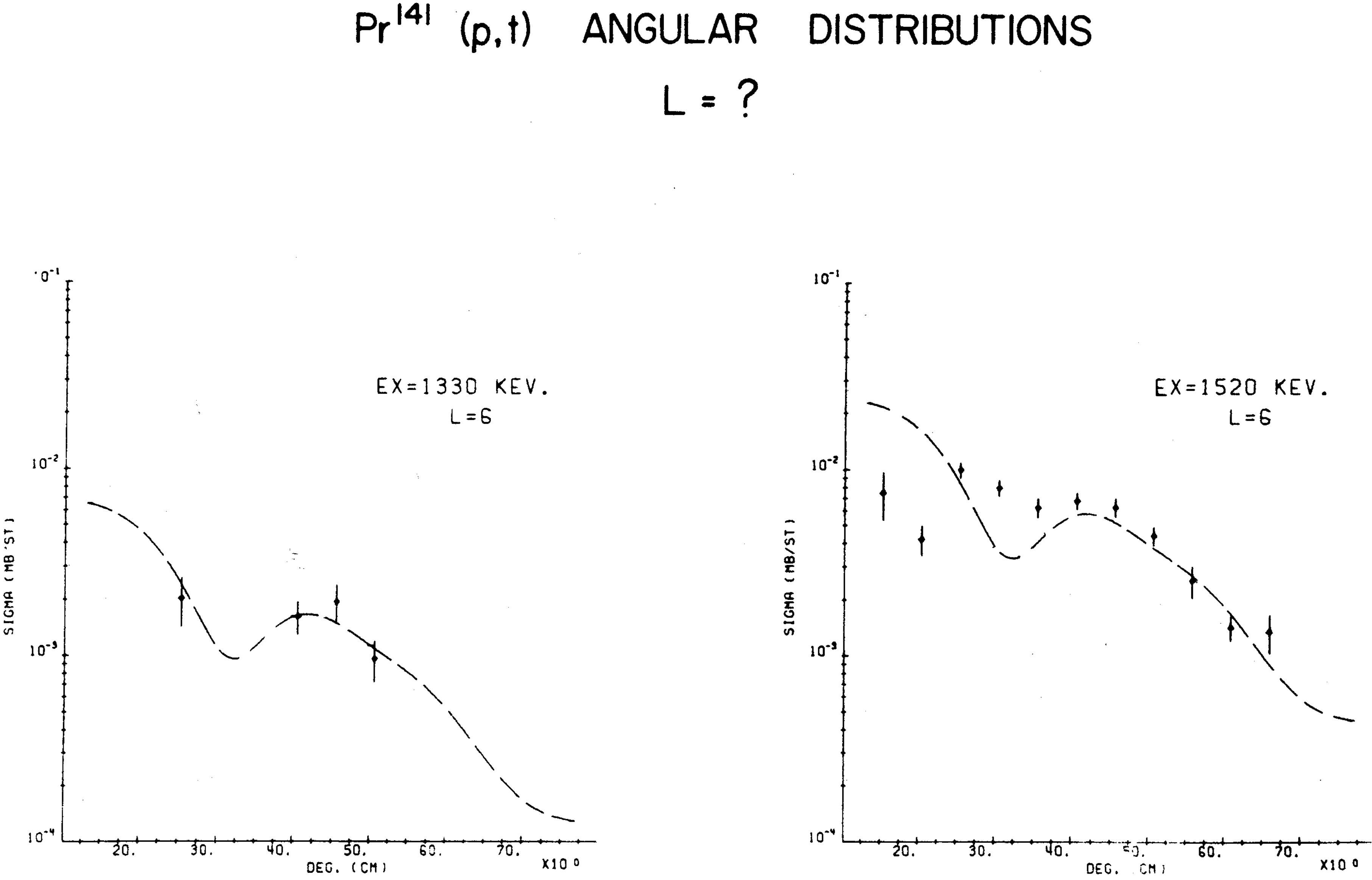

Fig. 6.4. Angular distributions of peaks which might have a composite nature. An ℓ=6 angular shape has been included for comparison sake only.

been included for comparison sake only since both angular shapes are believed to be a composite of several ℓ values.

6.5. Summary

A comparison of the results of our (*p*,*t*) data with the previously described decay scheme studies appears in Table 6.2. The first thing to be noted is that the ℓ values assigned to the transitions to the various states in ^{139}Pr are in every way consistent with the spin and parity assignments of the corresponding states established through radioactivity studies.

Furthermore, the ℓ=2 assignments for the five states listed further corroborate the collective vibrational character previously ascribed to them. Since unique spin assignments have not been made for most of these collective states, an attempt was made to clarify this situation through use of the weak coupling model of collective nuclear motion. Since these states are presumed to be members of a multiplet constructed from the coupling of the $d_{5/2}$ ground state with the first excited 2+ state of the core, the weak coupling model would predict the presence of five pure collective excited states with spins ranging from 1/2 to 9/2 whose relative cross sections are in a ratio of 1:2:3:4:5, respectively, and whose energy center of gravity corresponds to the first 2^+ excitation in the ^{138}Ce nucleus. Although several combinations of these six states would satisfy the latter energy constraint, the former cross sectional relationship expected for pure vibrationally excited states cannot be satisfied by any combination of these states indicating that much mixing within and possibly outside the multiplet must occur.

Table 6.2. States Populated Through the $^{141}\mathrm{Pr}(p,t)$ Reaction

(This work)		(Beery)		
Energy (KeV)	ℓ value	Energy (KeV)	J^π	Classification
0	0	0.	5/2+	$(\pi d_{5/2})^1$
–	–	113.8	7/2+	$(\pi d_{5/2})^2(\pi g_{7/2})^{-1}$
405±10	2	405.0	3/2+,1/2+	$(\pi d_{5/2})^1(2+)$
590±10	2	589.2	5/2+	$(\pi d_{5/2})^1(2+)$
–	–	821.8	11/2–	$(\pi h_{11/2})^1$
830±10	2	828.1	7/2+,9/2+	$(\pi d_{5/2})^1(2+)$
		851.9	9/2+,7/2+	$(\pi d_{5/2})^1(2+)$
910±15	2	916.8	1/2+,3/2+	$(\pi d_{5/2})^1(2+)$
1010±20	2	1024.0	7/2+,9/2+,11/2+	Collective
1330±20	?	1311.8	1/2+,3/2+,5/2+	
		1328.2	5/2+	
		1369.6	9/2+,11/2+,13/2+	
1520±20	?	1501.2	1/2+,3/2+	
		1523.2	(+)	
1623±20	1,3	1624.5	9/2–,11/2–	$(\pi d_{5/2})^1(\nu d_{3/2})^{-1}(\nu h_{11/2})^{-1}$
2050±30	1,3	2048.8	9/2–,11/2–	$(\pi d_{5/2})^1(\nu d_{3/2})^{-1}(\nu h_{11/2})^{-1}$
2160±50	3	2174.3	9/2–,11/2–	$(\pi d_{5/2})^1(\nu d_{3/2})^{-1}(\nu h_{11/2})^{-1}$
2240	3	–	–	–
2660	–	–	–	–
2740	–	–	–	–
2800	–	–	–	–

Finally, in agreement with the model of direct nuclear reactions, only those excited states corresponding to excited neutron components or core excitations were populated by this reaction. Conspicuously absent are the 113-keV $7/2^+$ and the 821.8-keV $11/2^-$ proton states even though neutron and core excited states of similar spin and parity were observed to be strongly populated by this reaction. Additional ^{141}Pr(p,t) experiments conducted at bombarding energies of 35 MeV and 30 MeV further established the direct nature of this reaction at these relatively high proton energies.

Chapter VII.

^{159}Tb(*p*,*t*) Results

7.1. Introduction

Of the three deformed residual nuclei studied, ^{157}Tb is the best characterized. From radioactivity studies involving both conversion electron and γ-ray work (Pe62, B167), the partial level scheme illustrated in Fig. 7.1. was developed. The main features of this level structure are the identification of a rotational band built upon a β vibrational excitation of the K=3/2[411] ground state and the characterization of a K=1/2 band based at 598 keV.

Several investigators (Pe62, B167) have differed as to their interpretation of the rotational band based at 598 keV. There are two possibilities for the origin of such a K=1/2 band. It can be explained as a rotational band superimposed either on the $1/2^+$[411] single particle proton state expected from the Nilsson diagram in this region, or on a γ vibrational state based on the K=3/2 ground state. The vibrational origin of these states is strongly suggested from both systematics and the very small decoupling parameter associated with this band. The empirical value of this decoupling parameter is ∿1/20 of the theoretical value (B167) based on a nuclear deformation of η=5 and is of opposite sign. However, experimentally determined K conversion coefficients imply significant $M1$ admixtures in transitions deexciting this band to the ground band (see table 7.1 and 7.2); these should be formally completely forbidden for states having a vibrational origin, although band mixing could easily account for this phenomenon. In light of the established directness of the (*p*,*t*) reaction at the

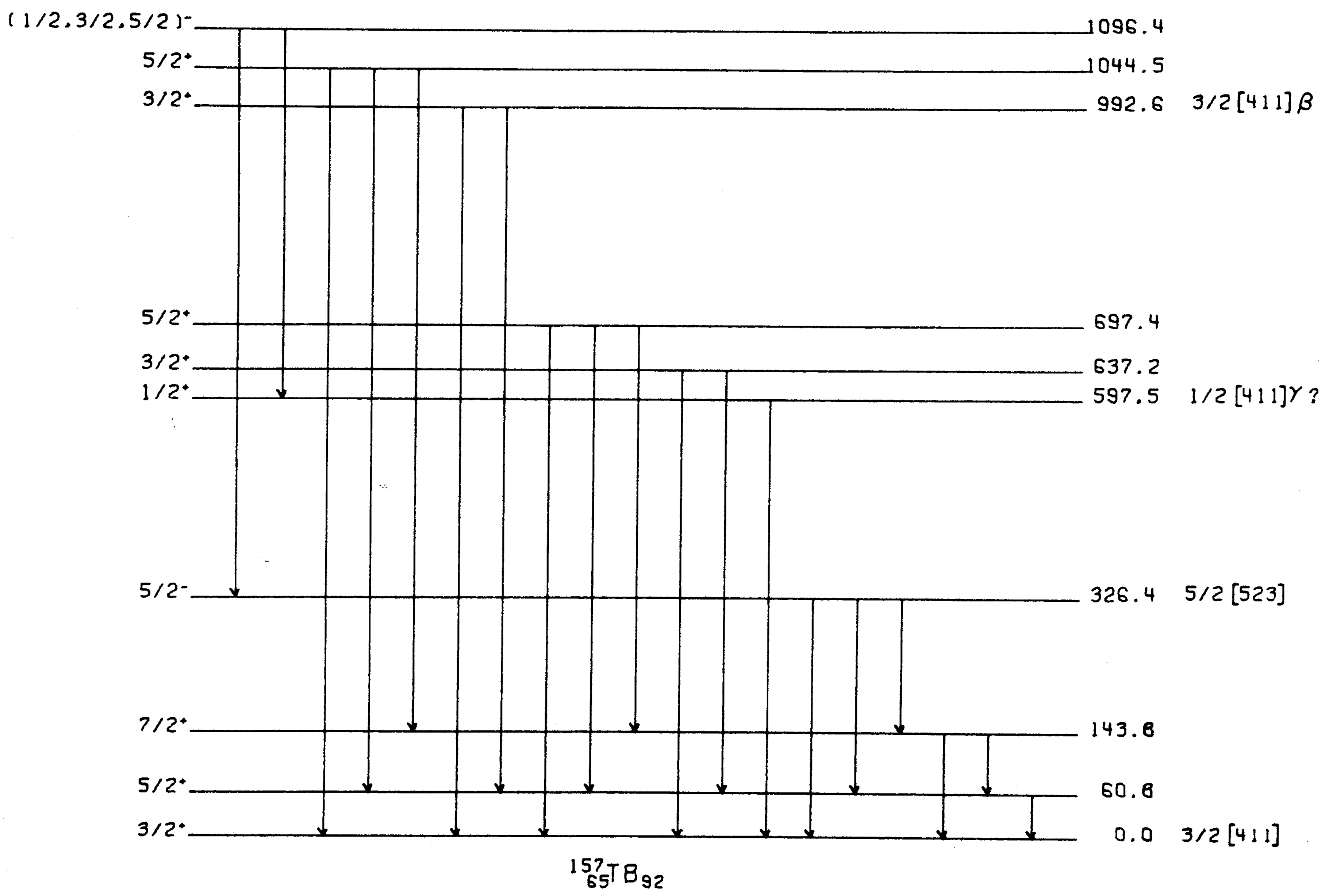

Fig. 7.1. Partial level structure of ^{157}Tb. Arrows represent deexciting γ rays observed when various states are fed by the ε decay of ^{157}Dy.

Table 7.1

Multipolarities Of γ rays Deexciting the γ Vibrational Band in ^{157}Tb

Transition[a] Energy	Band[b] Type	State Depopulated	Fed Grnd. Member	Suggested Multipolarities
554±2	γ	697	143.8	M1,E2
577±2	γ	637	60.8	M1,E2
597±1	γ	597	Grnd.	M1,E2
636±1	γ	{ 637 698	{ Grnd. 60.8	M1,E2

a) Ref. Pe 62
b) Our assignment.

Table 7.2

Multipolarities Of γ rays Deexciting The Vibrational Bands In ^{157}Tb

Transition[a] Energy	Band[b] Type	State Depopulated	Fed Grnd. Member	Suggested Multipolarities
553.1±0.8	γ	697.4	143.8	M1
576.6±0.8	γ	637.2	60.8	M1
597.5±0.6	γ	597.5	Grnd.	M1
931.7±0.8	β	992.6	60.8	E2
984.0±2	β	1044.5	60.8	E2+E0
992.8±2	β	992.6	Grnd.	E2+E0

a) Ref. B167
b) Our assignment.

bombarding energies used in this study, the presence of these *K*=1/2 states in our triton spectra would be a sufficient condition for establishing their collectivity.

7.2. Spectral Results

The ^{159}Tb(*p*,*t*) triton spectrum taken at the laboratory scattering angle of 20° appears in Fig. 7.2. The most striking feature of this spectrum is the strong population of the ground state rotational band, with members certainly up to $13/2^+$ and possibly as high as $17/2^+$ being excited. At 598 keV of excitation one finds three states which, within experimental uncertainty, correspond to the first three members of the previously discussed $K=1/2^+$ rotational band. In addition, if one generates the $7/2^+$ and $9/2^+$ members of this band by parameterizing the simple rotational energy relationship, one finds two additional states populated by this reaction which appear to be the next two higher members of this (γ vibration) band.

The set of three states based at 994 keV of excitation possesses relative intensity characteristics which are remarkably similar to those exhibited by the first three members of the ground state rotational band. If the simple $I(I+1)$ energy spacing is assumed for these levels and one solves for I, one obtains a value remarkably close to 3/2 . Thus in addition to the two previously known members of the β vibrational band, a third has been observed to be populated through this reaction.

The results obtained from this spectrum are summarized in Table 7.3. The theoretical values for the members of the various rotational bands have been calculated using the rotational energy

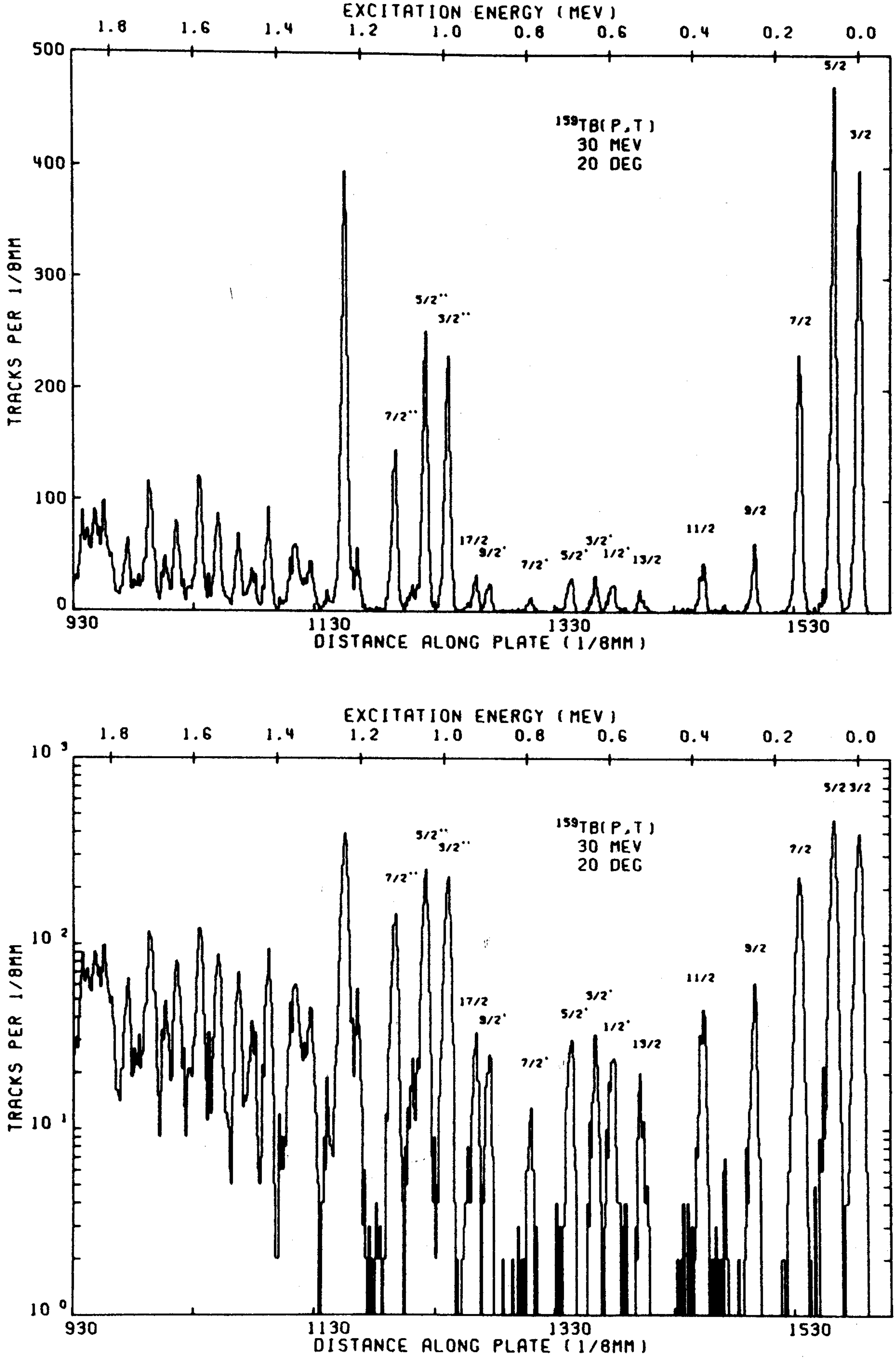

Fig. 7.2. Log and linear displays of the ^{159}Tb(p,t) spectrum taken at the laboratory scattering angle of 20°.

Table 7.3. States Populated Through the ^{159}Tb(p,t) Reaction.

Energy (keV)	Energy[a] (keV)	Theory (keV)	Assignment[b] J^π	Energy (keV)	Energy[a] (keV)	Theory (keV)	Assignment[b] J^π
G S	G S	---	$3/2^+$	1120	---	1124	$7/2''^+$
61	60.8	---	$5/2^+$	1207	---		---
144	143.8	---	$7/2^+$	1238	---	1241	$(9/2''^+)$
254	---	252	$9/2^+$	1276	---		---
325	---		---	1318	---		---
379	---	384	$11/2^+$	1352	---		---
527	---	539	$13/2^+$	1417	---		---
598	597.5	---	$1/2'^+$	1454	---		---
640	637.5	---	$3/2'^+$	1487	---		---
699	697.4	---	$5/2'^+$	1535	---		---
795	---	797	$7/2'^+$	1578	---		---
896	---	898	$9/2'^+$	1602	---		---
927	---	923	$17/2^+$	1631	---		---
947	---		---	1659	---		---
994	992.6	---	$3/2''^+$	1695	---		---
1048	1044.5	---	$5/2''^+$	1749	---		---
1080	---		---				

---

[a] P. H. Blichert-Toft, E. G. Funk, and J. W. Mihelich, Nucl. Phys. A100, (1967) 369-391.

[b] I = member of ground state rotational band; I' = member of $K=K_\circ-2$ γ-vibrational band. I'' = member of $K=K_\circ$ β-vibrational band.

formulas given by equation 2.1. The rotational parameters used in these calculations are tabulated in Table 7.4. A level scheme of states populated through ^{159}Tb(p,t) reaction appears in Figure 7.3.

7.3. Angular Distributions

Because the selection rules governing the (p,t) reaction on odd-mass nuclei will usually allow states to be populated by several ℓ-value transfers, angular distributions of all the known states excited by the ^{159}Tb(p,t) reaction were obtained in order to determine whether this type of experiment could be profitably used in the analysis of odd-mass nuclear states. The spectra collected in this experiment were taken between 10° and 75° at 5° intervals and appear in Appendix *C*. The differential cross sections extracted from these spectra are tabulated in Appendix *D*.

7.3.1. DWBA Analysis

The distorted wave predictions for the various ℓ-value transfers were calculated as described in section 6.2. The optical potential and bound state parameters used in this analysis appear in Table 7.5. The $h_{9/2}$ spherical shell model orbit was used in calculating the bound-state wave functions of the transferred neutrons, since the least bound pair of neutrons in the ^{159}Tb nucleus occupies a Nilsson orbit derived from this spherical state. Again, the finite range and cluster transfer calculations are represented by continuous and broken curves respectively when compared with experimental data.

7.3.2. Ground-State Rotational Band

The angular distributions of the ground state rotational band members appear in Fig. 7.4.

Table 7.4

Rotational Parameters Associated With Bands Populated Through The ^{159}Tb(p,t) Reaction.

Band	$\hbar^2/2\mathcal{J}$ (keV)	a	E_0 (keV)
Grnd.	11.98	-	-44.57
γ	12.90	0.086	589.43
β	10.80	-	953.50

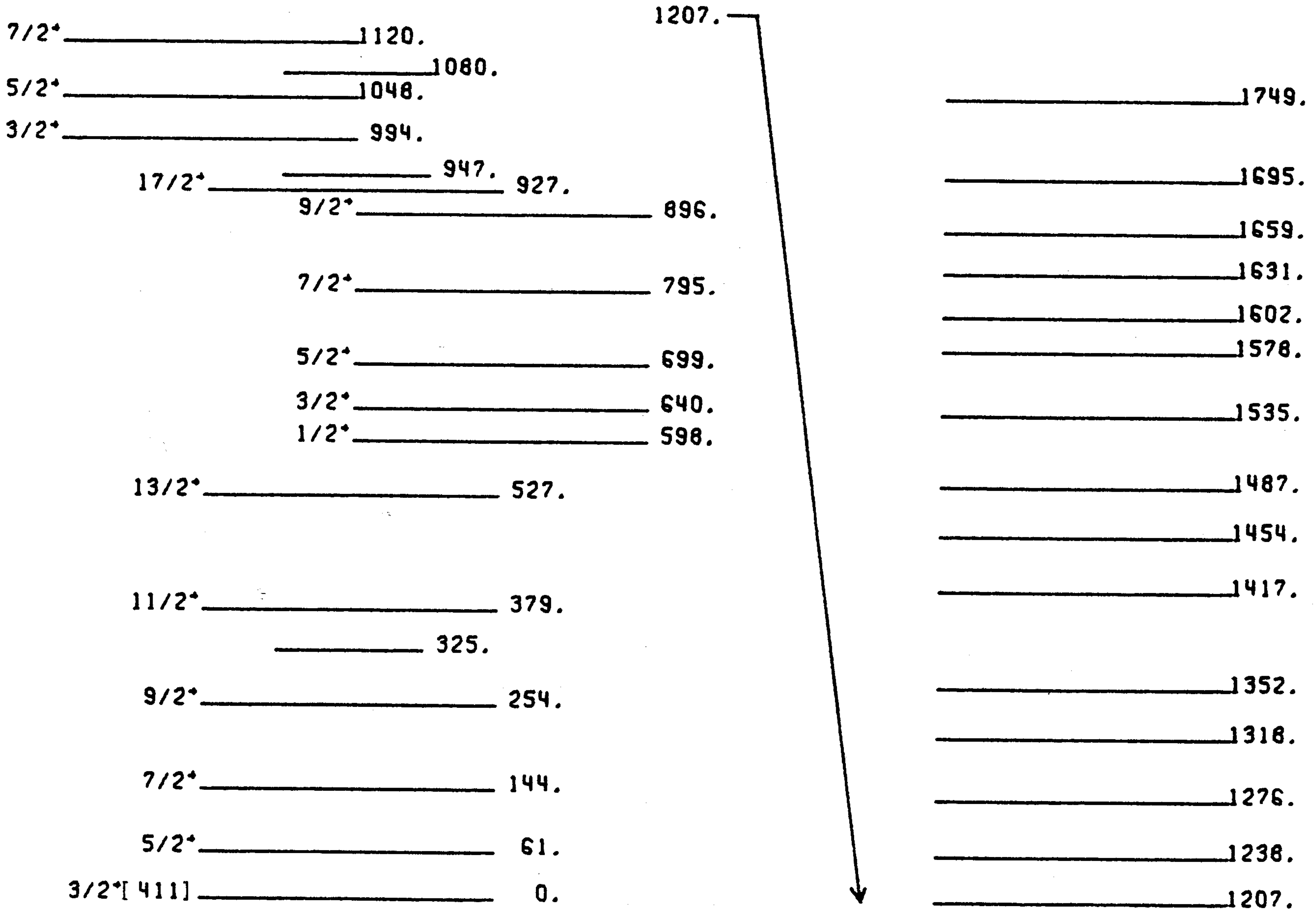

Fig. 7.3. States populated through the ^{159}Tb(p,t) reaction.

Table 7.5.

Optical-Model and Bound-State Well Parameters used in the Distorted-Wave Analysis of the ^{159}Tb(*p*,*t*) Reaction.

Particle	V_o (MeV)	W_o (MeV)	W_D (MeV)	V_s (MeV)	r_o (f)	a (f)	r_o' (f)	a' (f)	r_o'' (f)	a'' (f)	r_{oc} (f)
Proton[1]	52.91	4.97	5.00	6.04	1.16	0.75	1.370	0.63	0.026	0.738	1.25
Triton[2]	169.6	12.00			1.14	0.795	1.48	0.824			1.40
Dineutron					1.14	0.795					1.40
Neutron[3]				λ=25	1.25	0.65					1.25

1) Ref. Fr67
2) Ref. Ig69
3) The value of λ=25 corresponds to $V_s \approx 8.5$ MeV.

$$U_{OM}(r) = V_c(r) - V_o \frac{1}{1+e^{x}} - (W_o - 4W_D \frac{d}{dx'}) \frac{1}{1+e^{x'}} + (\frac{\hbar}{m_\pi c})^2 V_s \frac{1}{r} \frac{d}{dr} (\frac{1}{1+e^{x''}}) \vec{\ell}\cdot\vec{\sigma}$$

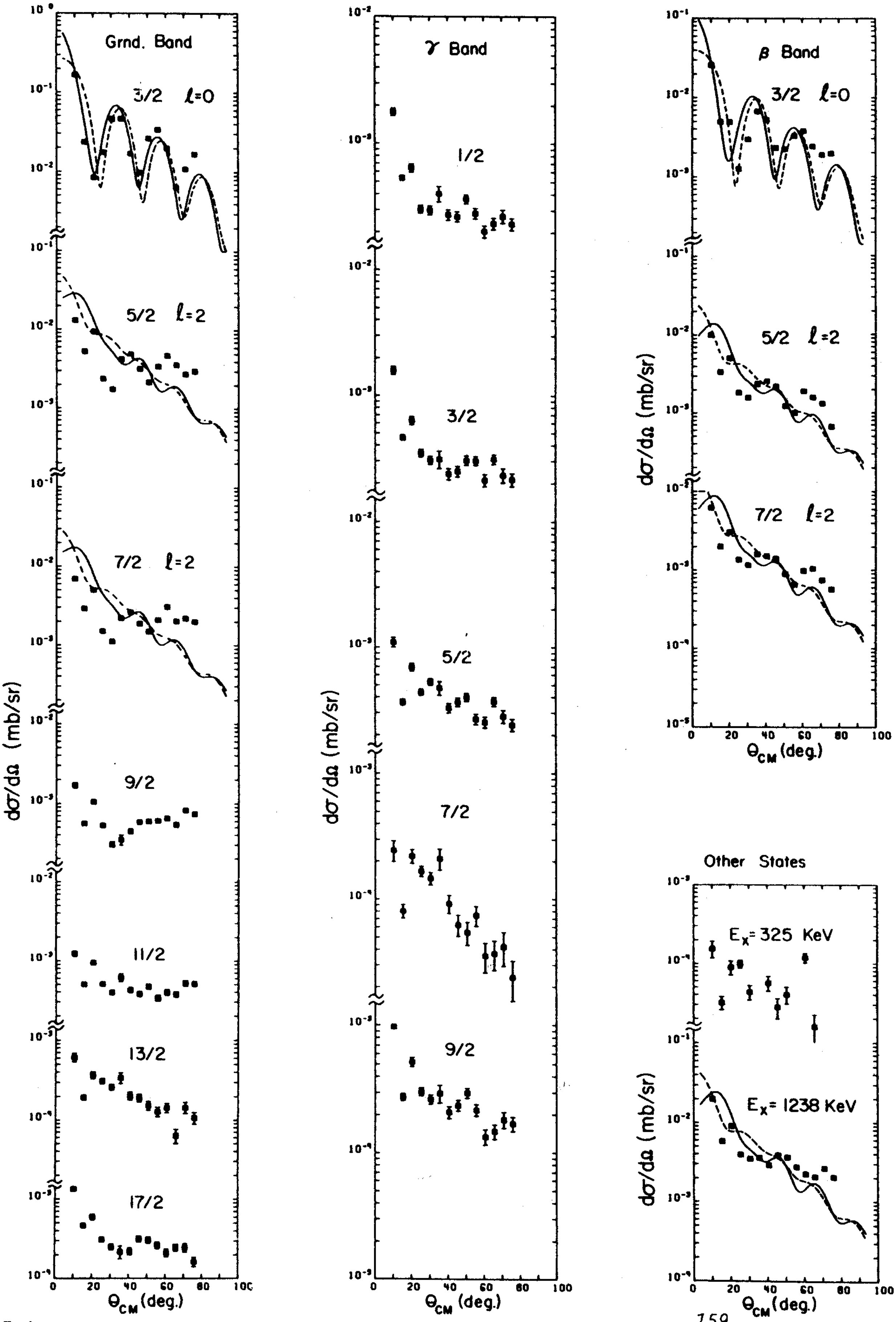

Fig. 7.4. Angular distributions of states populated through the ^{159}Tb(p,t) reaction. Theoretical two neutron pick-up and cluster transfer calculations are represented by continuous and broken curves respectively. Relative cross sections have been normalized to reflect measured absolute values.

As in the previous case of the (*p*,*t*) reaction on the spherical ^{141}Pr nucleus, the $3/2^+ \rightarrow 3/2^+$ ground-state transition proceeds through a strong dominant ℓ=0 transfer. The theoretical ℓ=0 curves predict the positions of the relative maxima and minima quite well but clearly underestimate the strength of the experimentally observed diffraction pattern. This phenomenon was also observed in the ^{141}Pr(*p*,*t*) experiment and is in marked contrast to the ℓ=0 ground state transition accompanying the ^{176}Yb(*p*,*t*) reaction (As71, Hi70), where the angular dependence on cross section is not so pronounced. Again, the finite range, two-neutron pickup calculation does a much better job of fitting the lower angle data than does the cluster transfer prediction, although both approaches do a respectable job of reproducing the experimental ℓ=0 angular shape.

The 5/2 and 7/2 members of the ground state rotational band have very similar angular shapes. The positions of the relative maxima occurring in these curves are reminiscent of ℓ=2 angular shapes; however, the deep minimum occurring at 30° along with the unusual strength of the observed diffraction pattern makes the ℓ=2 assignments for these states extremely uncertain.

The remaining members of the ground state rotational band populated through the (*p*,*t*) reaction on ^{159}Tb exhibit angular distributions which cannot be explained in terms of any single dominant angular momentum transfer.

7.3.3. γ-Vibrational Band

The angular distributions of the various members of the *K*=1/2 γ vibrational band are also illustrated in Fig. 7.4. The angular shapes exhibited by the first three members of this vibrational band are, within statistical uncertainty, identical, indicating a complete absence of $\ell=0$ strength in the transition to the 3/2 member of this band. Moreover, the angular shapes exhibited by these three states, as well as the remaining two members of this band indicate that these states are populated by a complex mixture of several allowed ℓ-values rather than through a single dominant angular momentum transfer. Possibly this phenomenon can be understood and explained in terms of band mixing which from previous arguments certainly must be occurring in this γ vibrational band. Qualitatively one wouldn't expect complex mixed states to be populated through simple, pure angular momentum transfers, and perhaps this is just the underlying reason behind the complex angular shapes exhibited by these states.

7.3.4. β-Vibrational Band

The angular distributions of the members of the β-vibrational band are illustrated in Fig. 7.4. Unlike the γ-vibrational states, the members of this collective band appear to be populated through a single dominant angular momentum transfer. As in the ground state rotational band, the $3/2^+$ band head appears to be populated by an $\ell=0$ wave; however, unlike the ground state transition, the agreement between the experimental angular distribution and theoretical $\ell=0$ curves are something less than spectacular. The positions of the experimental maxima and minima appear to be systematically shifted from their theoretically predicted positions, indicating the possibility of small contributions from higher allowed ℓ values. Nevertheless, the overall shape and underlying strength of this experimental curve undoubtedly express its dominant $\ell=0$ character.

The angular distributions of the remaining two members of this band exhibit a characteristic $\ell=2$ angular shape. The positions of the relative maxima of these curves are predicted quite well by the theory although their relative strengths are once again underestimated.

Recently there has been considerable speculation as to the reality of β vibrational shape oscillations. The very unsystematic disappearance of these bands in some deformed even-even rare-earth nuclei has cast some serious doubts upon the simplistic origin associated with β vibrational bands in general. However, previous γ-ray and conversion electron work (B167) have shown that the first two members of this band behave in a classic manner characteristic of pure β vibrationally excited states. Perhaps the simple manner in which the (p,t) reaction populates these states is a measure or signature of their collective purity. This statement although speculative is consistent with previous arguments surrounding the complex nature of ℓ transfers leading to the previously discussed γ vibrational states and indirectly implies mixing in excited members of the ground state rotational band.

7.3.5. Other States

Angular distributions of two additional states of unknown origin were also determined in this study and appear in Fig. 7.4 under the heading: "Other States".

The 325 keV state appearing in ^{159}Tb(p,t) spectra is a relatively low intensity peak which exhibits no apparent relationship to any other peaks in this energy region. Its angular distribution is flat, unstructured and is in no way related to any single angular momentum curve. Its angular shape, however, is much like those exhibited by the members of the *K*=1/2 γ vibrational band. Perhaps this peak is the *K*=5/2 γ vibrational state; however, this is only mere speculation.

The 1238 keV peak on the other hand is a highly intense, strongly populated peak which might have a composite nature. The angular distribution of this peak appears to have a dominating ℓ=2 angular shape. However, since this peak occurs at or above the pairing gap in this nucleus nothing really can be said about its origin based on these data alone.

7.4. Summary

As was expected from the previous ^{141}Pr(p,t) results, the (p,t) reaction on ^{159}Tb was found to populate collective excited states within the residual nucleus ^{157}Tb strongly. With the exception of a few extremely low intensity states, the entire triton spectrum below the pairing gap was totally accounted for in terms of β- and γ- vibrational and ground-state rotational band members.

Angular distributions of the collective states populated by this reaction showed absolutely no general simplifying tendencies. With the exception of the ground state and the members of the β vibrational band, states were observed to be populated by complex mixtures of angular momentum transfers. Why a very few states should be populated by the lowest possible ℓ value while all others are not is not immediately clear.

Before concluding this chapter, something should be said about the strange 20° differential cross section behavior exhibited by many of the states studied. This strange behavior is manifested in angular distributions by an apparent discontinuity at 20°. Both the 15° and 25° degree points are commonly much smaller than the 20° value, which cannot be understood in terms of any single theoretical curve. This effect, however, appears to be very real since three independent sets of specta taken at 15°, 20° and 25° all reproduce this behavior.

Chapter VIII

^{165}Ho(p,t) Results

8.1. Introduction

In the interpretation of the ^{165}Ho(p,t) spectra, liberal use has been made of the well established level structure of ^{165}Ho (Le68) since experimental facts concerning the residual nucleus of this reaction, ^{163}Ho, are all but nonexistent. A partial level structure of ^{165}Ho appears in Fig. 8.1 where only pertinent states of interest have been included.

8.2. Spectral Results

The characteristics of the triton spectra obtained from ^{165}Ho are very much like those exhibited by the previous ^{159}Tb(p,t) spectra as is graphically shown in Fig. 8.2. In this spectrum, one finds a strong population of the K=7/2$^-$[523] ground state rotational band with level spacings similar to those occurring in the same band in the ^{165}Ho nucleus.

From Coulomb excitation experiments conducted on ^{165}Ho by Seaman et al (Se67) one would expect from systematics to observe the K=3/2$^-$ and 11/2$^-$ γ vibrational bands at ≃500 keV and ≃900 keV, respectively. And indeed one does observe a set of states originating at 562 keV of excitation which appear to have some intensity interrelationships. If one assumes that the 562-keV and the 618-keV states are the first two members of the K=3/2 γ vibrational band and one generates higher members by parameterizing the simple $I(I+1)$ energy relationship, one finds convincing evidence for the presence of additional members

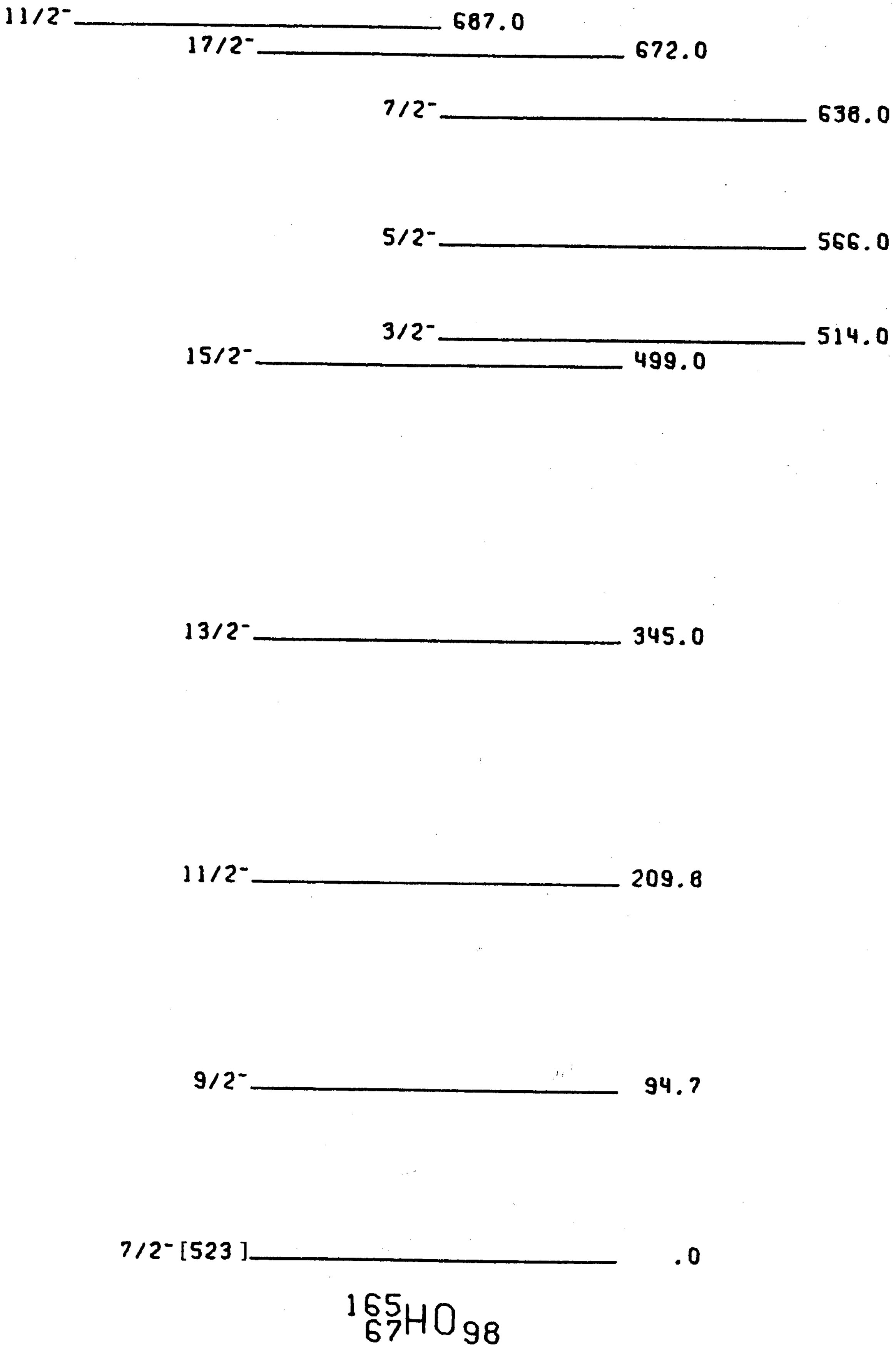

Fig. 8.1. Partial collective level structure of ^{165}Ho.

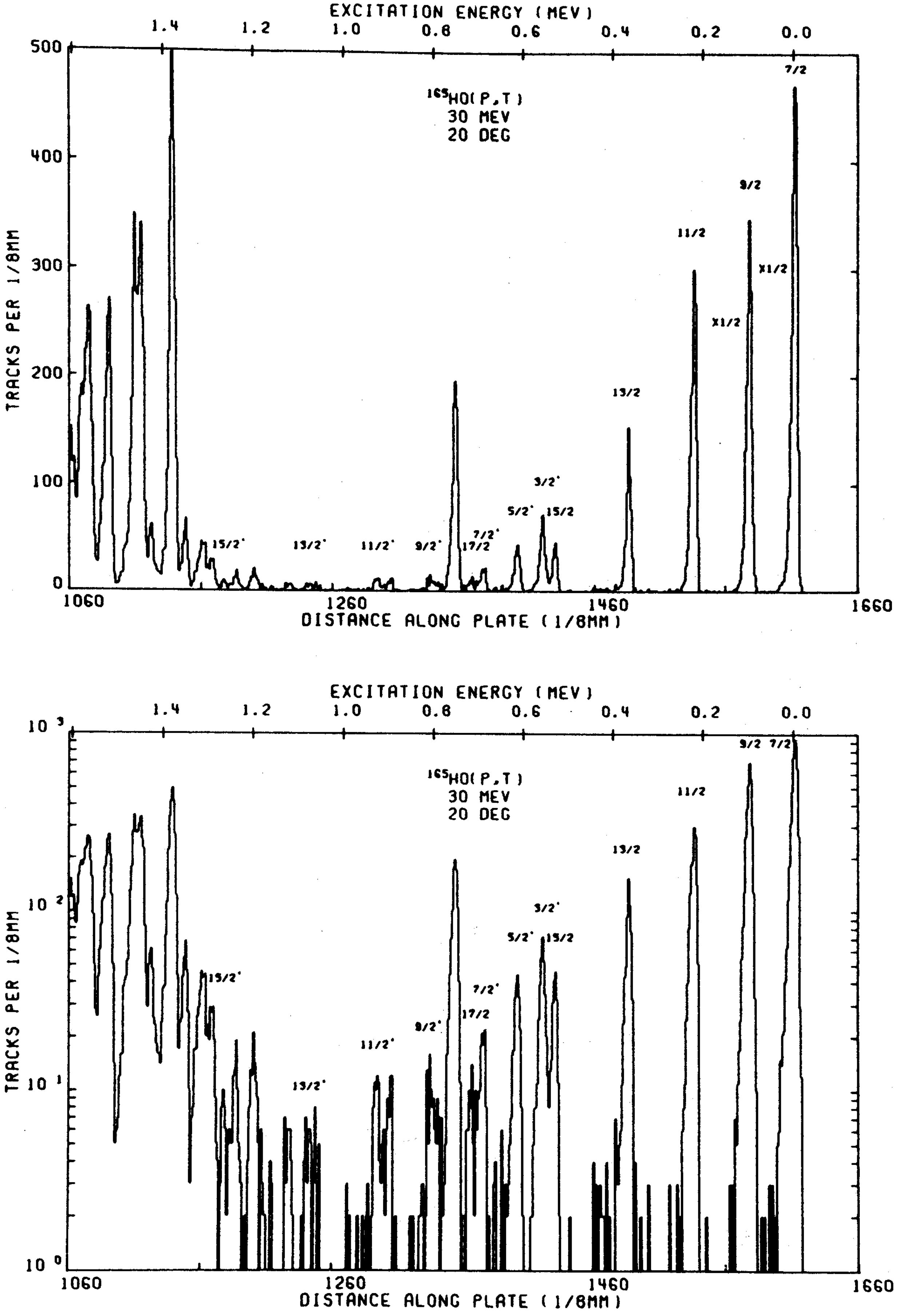

Fig. 8.2. Log and linear displays of the ^{165}Ho(p,t) spectrum taken at the laboratory scattering angle of 20°.

up to a spin of 15/2. However, no evidence for the presence of a K=11/2 γ vibrational band could be found in our spectra. The results of the ^{165}Ho(p,t) spectrum are summarized in table 8.1. Rotational parameters used in the theoretical calculations of rotationally excited states are listed in Table 8.2. A level scheme composed of all states populated through the ^{165}Ho(p,t) reaction appears in Fig. 8.3.

8.3. Summary

As in the case of ^{159}Tb, the (p,t) reaction on ^{165}Ho is found to populate rotational as well as vibrationally excited states in the residual nucleus strongly. The present study has identified six members of the K=7/2 ground state rotational band and seven members of the K=3/2 γ vibrational band. Moreover, with the single exception of the 791-KeV peak, these states completely exhaust the (p,t) reaction strength occurring below the pairing gap in the ^{163}Ho nucleus.

The origin of the strongly excited 791-KeV state cannot be determined from our data since it doesn't appear to have any relationship to any other states in our spectra. Being below the pairing gap, this state certainly must be a collective excitation, but whether it be a β, γ or octupole state is not clear from our data alone.

Table 8.1. States Populated Through the ^{165}Ho(p,t) Reaction.

Energy (keV)	Theory (keV)	Assignment[a] J^π	Energy (keV)	Theory (keV)	Assignment[a] J^π
G S	---	$7/2^-$	1117		---
100	---	$9/2^-$	1156		---
224	222	$11/2^-$	1175		---
369	367	$13/2^-$	1194		---
533	533	$15/2^-$	1232		---
560	---	$3/2'^-$	1245		---
618	---	$5/2'^-$	1259	1256	$15/2'^-$
695	699	$7/2'^-$	1286		---
720	722	$17/2^-$	1308		---
755		---	1345		---
791		---	1373		---
807	804	$9/2'^-$	1419		---
826		---	1441		---
898		---	1457		---
912		---	1513		---
926	931	$11/2'^-$			
1060		---			
1075	1082	$13/2'^-$			

[a] I = member of ground state rotational band; I' = member of $K=K_\circ-2$ γ-vibrational band

Table 8.2.

Rotational Parameters Associated With Bands Populated Through the ^{165}Ho(p,t) Reaction.

Band	$\hbar^2/2\mathcal{I}$ (keV)	a	E_0 (keV)
Grnd.	11.11	-	-175.00
γ	11.60	-	516.50

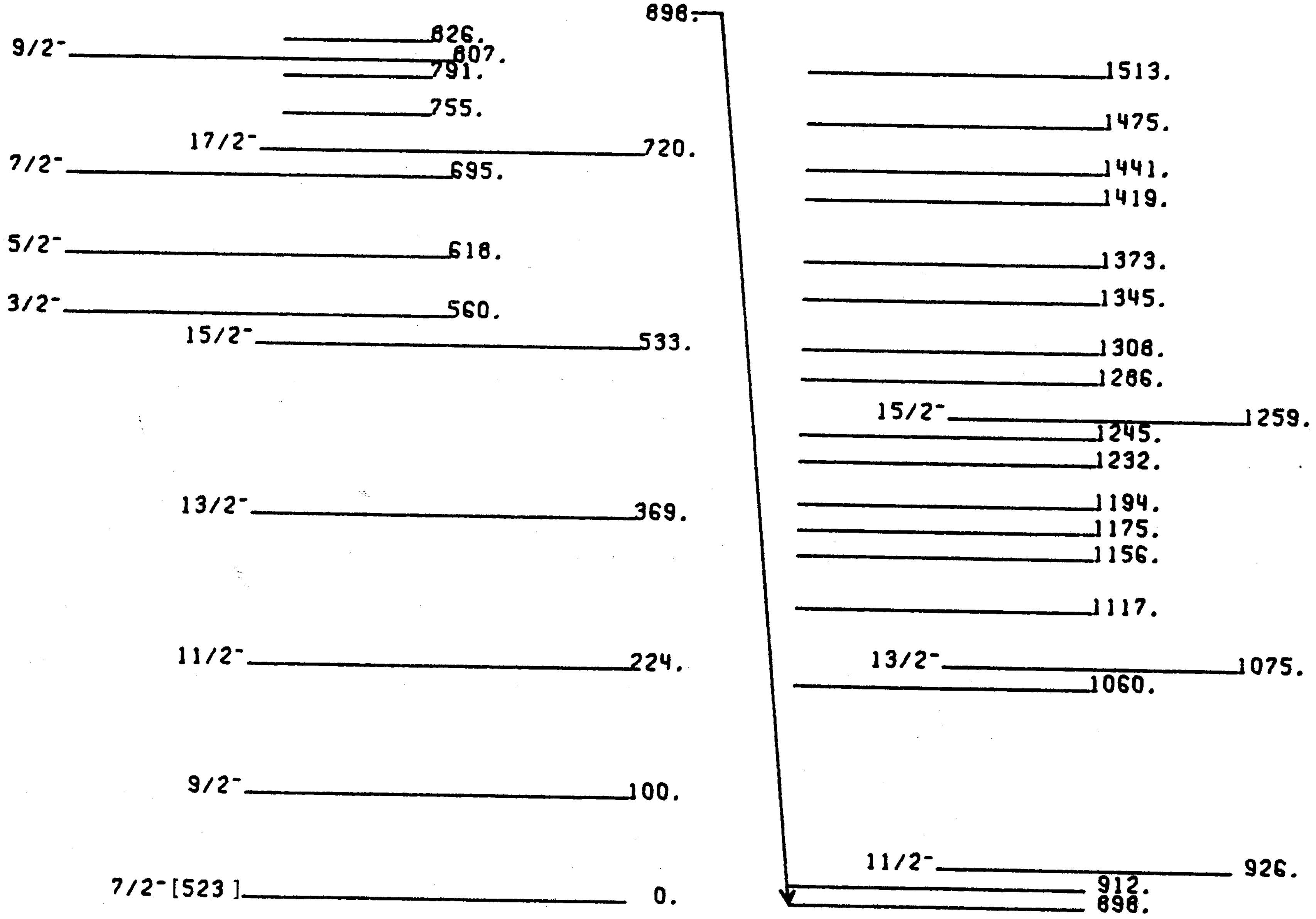

Fig. 8.3. States populated through the ^{165}Ho(p,t) reaction.

Chapter IX

States in ^{167}Tm

The level structure of the ^{167}Tm nucleus has been studied through the (p,t) reaction on ^{169}Tm and through the ε/β^+ decay of ^{167}Yb. It was hoped that the collective characteristics of the (p,t) reaction coupled to the single particle aspects associated with ε/β^+ decay would lead to a more or less complete low energy characterization of the ^{167}Tm nucleus. This chapter will discuss and compare the results obtained from each of these independent but complementary means of investigation.

9.1. ^{169}Tm(p,t) Results

The triton spectrum obtained at 20° from the ^{169}Tm(p,t) reaction appears in Fig. 9.1. As in the previous results, the ground state rotational band of ^{167}Tm is found to be strongly excited by this reaction; however, due to the rather large decoupling parameter associated with this K^+=1/2$^+$[411], the first two members of this band have not been resolved in this experiment. Nevertheless, at least six members of this rotational band are found to be populated through the (p,t) reaction.

Coulomb excitation experiments conducted on ^{169}Tm (Se67) have identified a K^+=3/2$^+$ γ vibrational band at 571 KeV of excitation in this nucleus. Based on this information and the previous results obtained for ^{157}Tb and ^{163}Ho, the series of three-states originating at 600 keV of excitation have all the appearances of being members of a γ vibrational band. However, a consistent energy relationship cannot

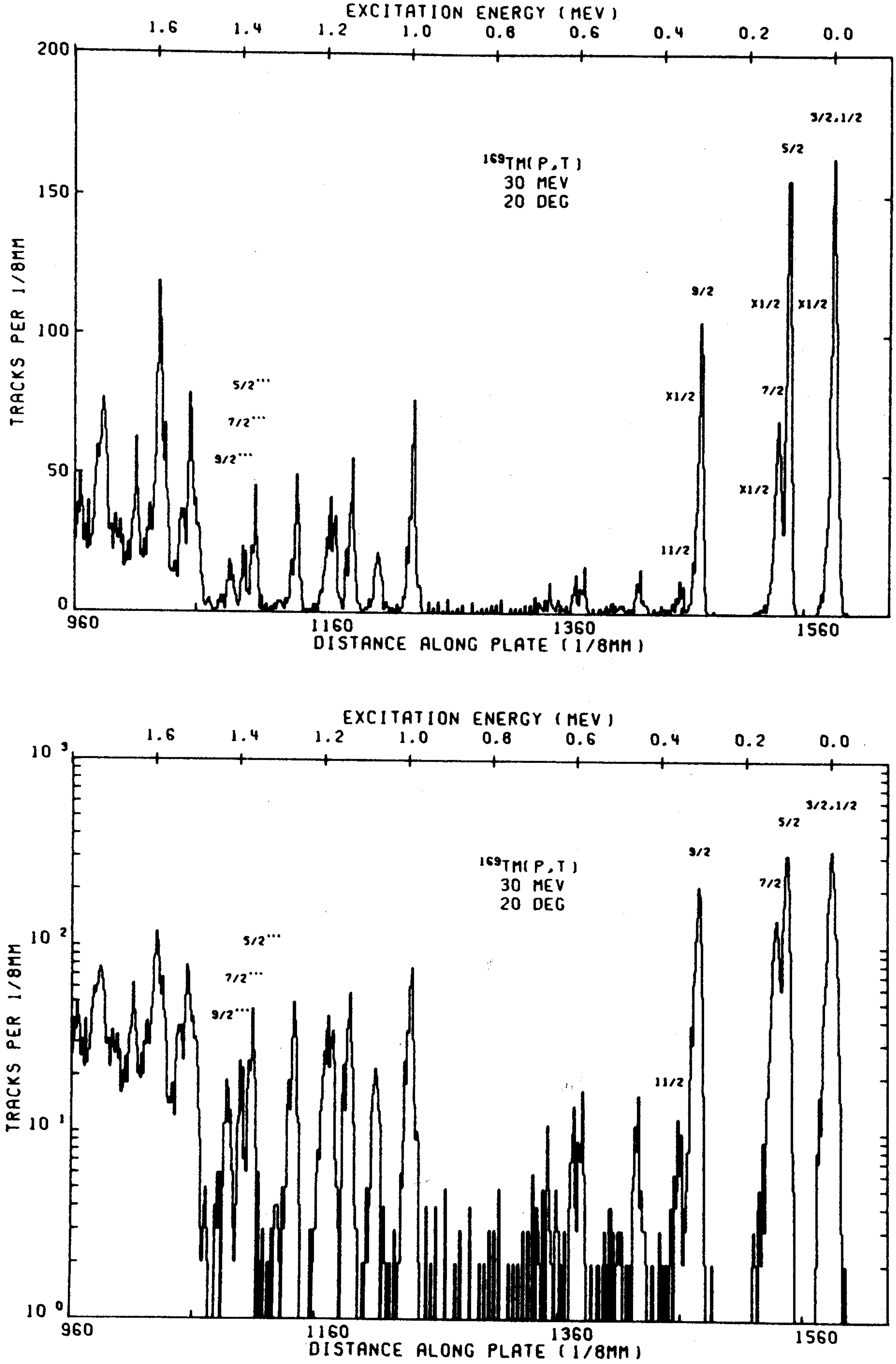

Fig. 9.1. Log and linear displays at the ^{169}Tm(p,t) spectrum taken at the laboratory scattering angle of 20°.

be established between these states for an assumed band head spin of either 3/2 or 5/2. Because of their extremely low intensity, it is entirely possible that only one or two of these states belong to the K=3/2 γ vibrational band expected in this region. If this is indeed the case, the present data are insufficient to make a judgement one way or the other since a minimum of three states is required in order to make the spin assignment.

At 1000 keV of excitation, one finds a series of highly excited, closely spaced peaks whose doublet nature defies all attempts at sorting these states into groups of common origin. Without higher resolution, a meaningful interpretation of states in this region cannot be made.

The series of three states originating at 1380 keV of excitation appears to have some type of common origin. The energy spacings between these peaks suggest, although not too strongly, a K=5/2 rotational band. Since these states appear to be above the pairing gap in this nucleus, one can only speculate as to their K=5/2 γ vibrational origin.

The results of the analysis of the ^{169}Tm(p,t) spectrum are summarized in Table 9.1. A level structure reflecting the states populated through the ^{169}Tm(p,t) reaction appears in Fig. 9.2.

9.2. γ-Ray Studies of the ^{167}Yb Decay

The states of ^{167}Tm have been investigated through the γ-ray studies of the ε/β^+ decay of ^{167}Yb. This study has firmly established the existence of twelve new excited states and the probable placement of a thirteenth in the daughter nucleus ^{167}Tm. Moreover, these thirteen

Table 9.1. States Populated Through the ^{169}Tm(p,t) Reaction.

Energy (keV)	Energy[a] (keV)	Assignment[b] J^π
10	G S	$1/2^+$
	10.4	$3/2^+$
117	116.6	$5/2^+$
142	142.4	$7/2^+$
329	326.5	$9/2^+$
374	371.0	$11/2^+$
470	---	---
604	---	---
624	---	---
663	---	---
682	---	---
706	---	---
1010	---	---
1092	---	---
1154	---	---
1192	---	---
1210	---	---
1283	---	---
1320	---	---
1380	---	$5/2'''^+$
1404	---	$7/2'''^+$
1434	1435[c]	$9/2'''^+$
1457	---	---
1486	---	---
1526	---	---
1574	---	---
1598	---	---
1625	---	---
1655	---	---

a) Ref. Wi69

b) I and I''' are members of the ground and γ vibrational bands respectively.

c) Energy calculated from the first two members of this band.

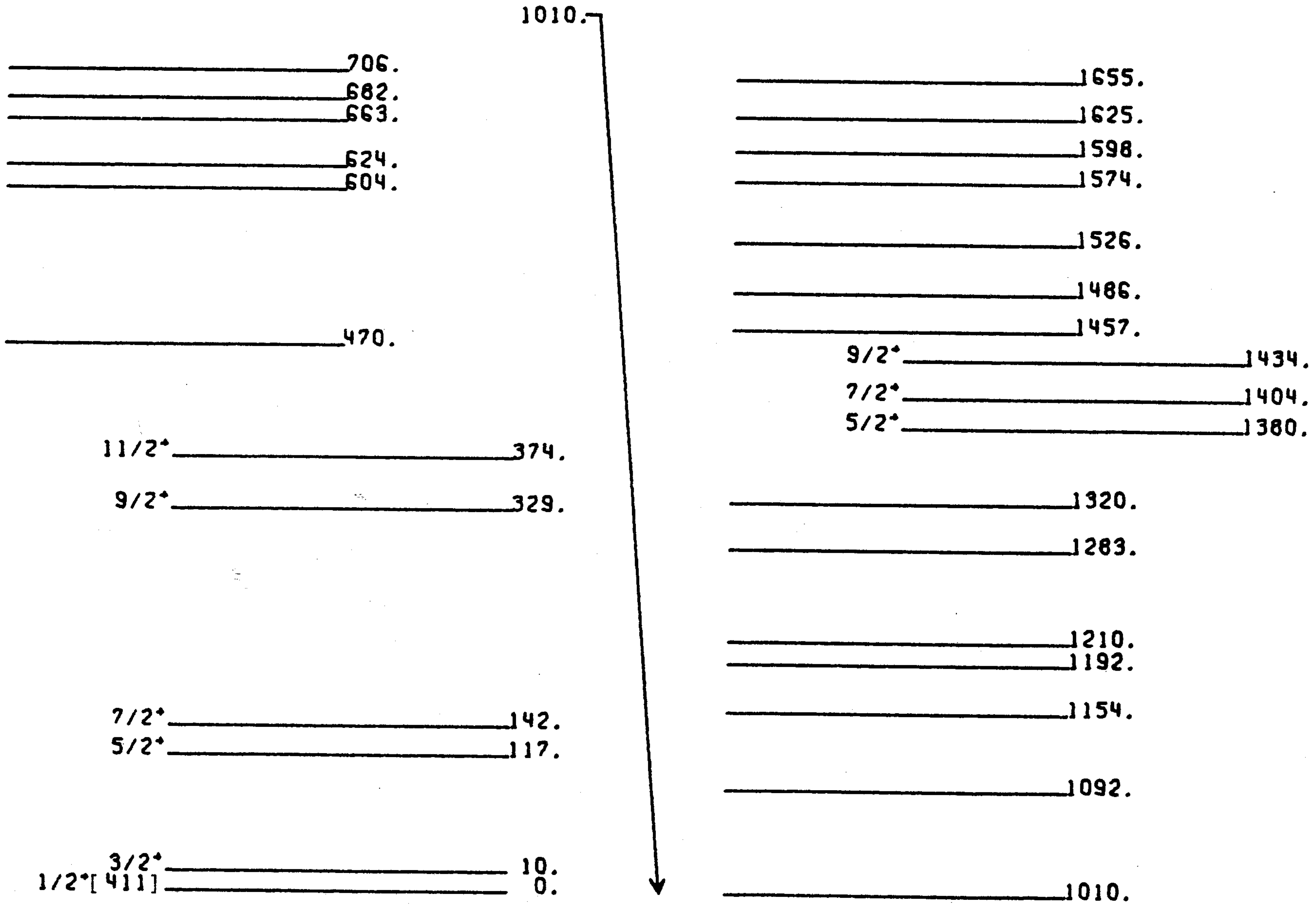

Fig. 9.2. States populated through the ^{169}Tm(p,t) reaction.

states, together with the well established level structure below 300 keV of excitation in the ^{167}Tm nucleus, form a consistent framework for the placement of 52 new γ-rays associated with the decay of ^{167}Yb.

9.2.1. Introduction

In 1954 the 18.5 min. ^{167}Yb activity was first produced (Ha54). Since then a number of studies involving both conversion electron (Ha59, Gr65) and γ ray work (Ha59, Wi60, Gr65, Ta65, Pa67) have contributed to the now well known low energy level scheme of ^{167}Tm which is illustrated in Fig. 9.3. Significant new data have now been obtained regarding this decay system through use of high resolution, high efficiency Ge(Li) detectors.

The decay of ^{167}Yb is characterized essentially by two distinct groups of γ rays. The first group is composed of a series of low-energy, high-intensity and closely spaced cascade γ rays associated with the well-established low energy rotational states in ^{167}Tm. The second group, on the other hand, is composed of a series of high-energy, low-intensity and closely spaced γ rays originating from high-energy excited states in ^{167}Tm which feed the aforementioned low-energy rotational states. Because of the low intensity characteristics of the high energy γ rays and the relatively short 18-min half-life of ^{167}Yb, the only practical coincidence experiments which could be conducted on this system within a 24-h period would have to involve a high efficiency NaI(Tl) detector coupled with a high resolution Ge(Li) detector, however because of the high density of γ rays characterizing this decay, gated experiments involving a NaI(Tl) detector would be all but impossible to interpret.

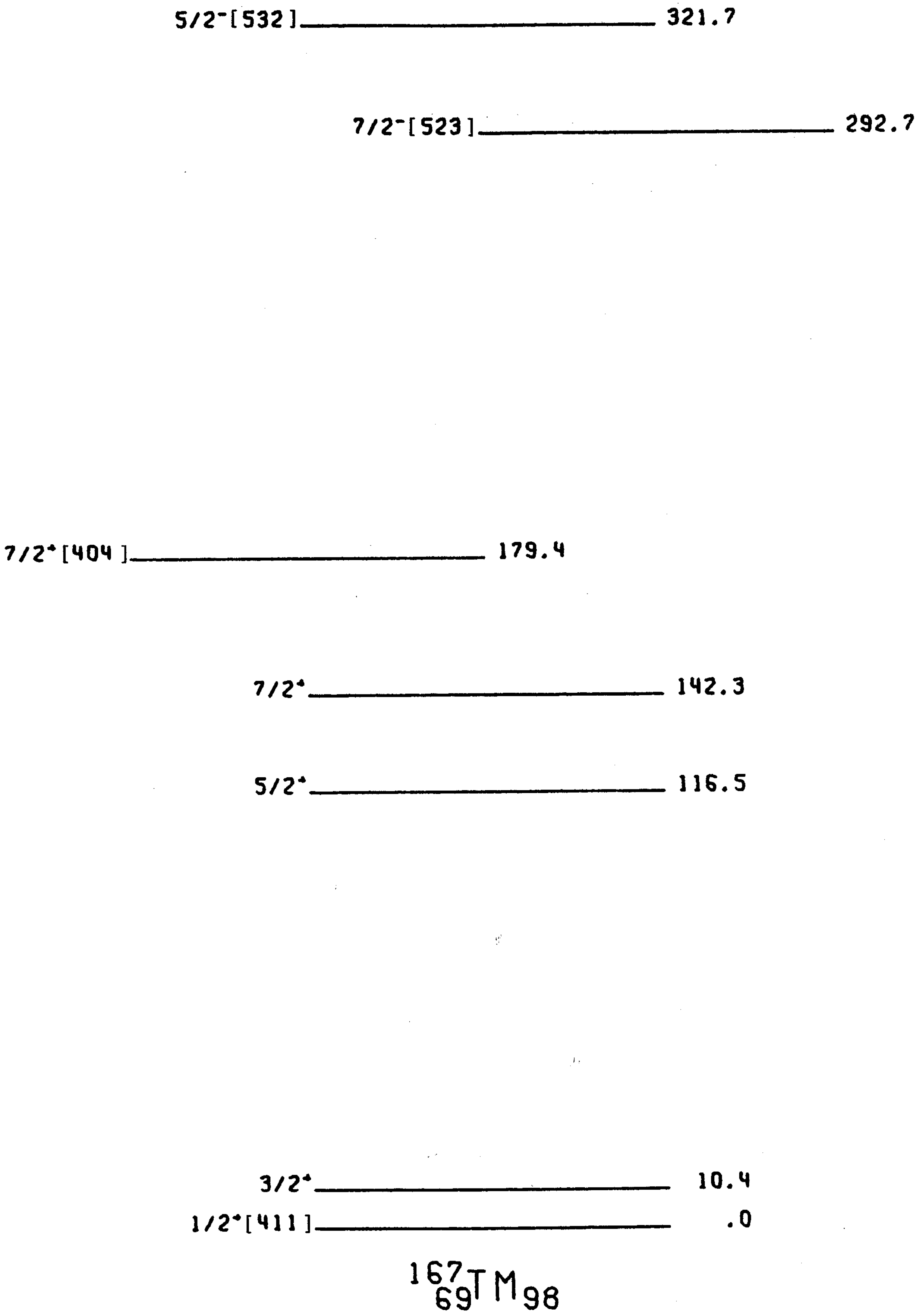

Fig. 9.3. Low energy rotational structure of ^{167}Tm.

On the other hand, the shortcomings of the Ge(Li)-NaI(Tl) coincidence configuration could in theory be eliminated through the use of a Ge(Li)-Ge(Li) two-dimensional megachannel experimental system (Do69). However, on the basis of a Ge(Li)-NaI(Tl) integral coincidence experiment performed on the decay of ^{167}Yb which is discussed later, it was estimated that a minimum of 4-5 days of continual cyclotron use would be required to perform this experiment. Moreover, because of the high dead-time which would be necessary in conducting this experiment, the number of γ rays above the x-ray threshold which could be cleanly gated would be small at best.

On the brighter side of things, the ^{167}Tm ground state rotational band is based on the $1/2^+[411]$ Nilsson single particle state. As a result, one might expect to find very characteristic reduced transition probabilities associated with the γ-ray transitions connecting various excited states to the members of this ground-state rotational band. This feature arises from the fact that the fully anti-symmeterized wave functions of all odd-mass deformed nuclei for which vibrational motion is neglected and a strong coupling model is valid have the following form:

$$\Psi\ (IKM) = \left[\frac{2I+1}{16\pi^2}\right]^{1/2} \{\mathcal{D}^{I}_{MK}\ (\Omega)\ \chi^{\tau}_{\kappa}\ (\times') + (-1)^{I} i^{-J} \mathcal{D}_{M,-K}(\Omega)\ \chi^{\tau}_{\kappa}\ (\times')\}$$

where $\chi(\times')$ describes the intrinsic motion of the odd "optical" nucleon in the deformed field of the core, while $\mathcal{D}(\Omega)$ describes the rotational motion of the deformed core. For a more thorough discussion of the collective model, see Ref. (Pr63).

The energy-independent probability of a γ-ray transition between an initial state i and final state f via a multipolarity λ, (called the reduced transition probability), is obtained from the matrix element of the field operator $M(\lambda,\mu)$ between the wave functions of the initial and final states which has the following form:

$$< \Psi_f(IMK) \; | M(\lambda,\mu) \; | \; \Psi_i(I'K'M') >$$

This matrix element will, in general, be composed of a direct term as well as a cross term contribution. However, only when $(K_i+K_f)\leq\lambda$ will the cross term contribution be non-zero, in which case the expression for the reduced transition probability will take on the following form:

$$B(\lambda:I_i\rightarrow I_f) = A\{C(I_i\lambda K_i(K_f-K_i)|I_fK_f) + b(-1)^{I_f+K_f} C(I_i\lambda K_i-(K_i+K_f)|I_f-K_f)\}^2$$

where A and b are constants characteristic of the initial and final intrinsic states and are determined empirically from observed transition data. It is the coherent sum of Clebsch-Gordon coefficients in the above expression which is responsible for the very characteristic transition probabilities most often associated with K=1/2 rotational bands.

Because of the technical difficulties involved in conducting a prolonged two-dimensional Ge(Li)-Ge(Li) mega-channel coincidence experiment and the doubtful value of such an experiment on the ^{167}Yb system, the approach taken in this study involved carefully measuring energies and intensities of the γ rays associated with the ^{167}Yb decay, conducting all pertinent Ge(Li)-NaI(Tl) coincidence experiments, and using the unique properties of K=1/2 rotational bands as a handle along with log ft values in determining the spins and parities of the states proposed on the basis of the singles and coincidence experiments.

9.2.2. Experimental Results

Samples of the 18.5-min ^{167}Yb were produced by bombarding the oxide of naturally occurring ^{169}Tm with 23.5-MeV protons. Samples were irradiated for approximately 3 min with average beam currents of 2 μA, and the resulting activities were counted for periods not exceeding 3 half-lives.

The γ-ray spectrum of ^{167}Tm above 500 keV taken with a 2.5% efficient Ge(Li) detector with resolution of 2.3 keV FWHM on the 1332-keV γ-ray of ^{60}Co is shown in Fig. 9.4. The low energy spectrum of ^{167}Tm was taken with a newly acquired "super-high" resolution Si(Li) x-ray detector and appears in Fig. 9.5. A total of 110 γ-ray transitions have been observed to follow the decay of ^{167}Yb and are listed in Table 9.2 along with their relative intensities. γ-ray energies appearing in brackets in Table 9.2 correspond to low-intensity γ rays which only appear after long periods of counting and may very well not belong to the ^{167}Yb decay.

The results of an anti-coincidence and integral coincidence experiment using an 8"×8" NaI(Tl) annulus with a 2.5% efficient Ge(Li) detector confirmed the previously described decay characteristics of ^{167}Yb but yielded no important additional information other than placing a lower limit on the amount of time required to perform a two-dimensional Ge(Li)-Ge(Li) mega-channel coincidence experiment.

Since the 179.4-keV $7/2^+$[404] and the 292.4-keV $7/2^+$[523] states have been previously determined (Ta65) to be isomeric, a delayed integral coincidence experiment was conducted utilizing an 8"×8" NaI(Tl) annulus and a 3"×3" NaI(Tl) scintillator together with a newly acquired

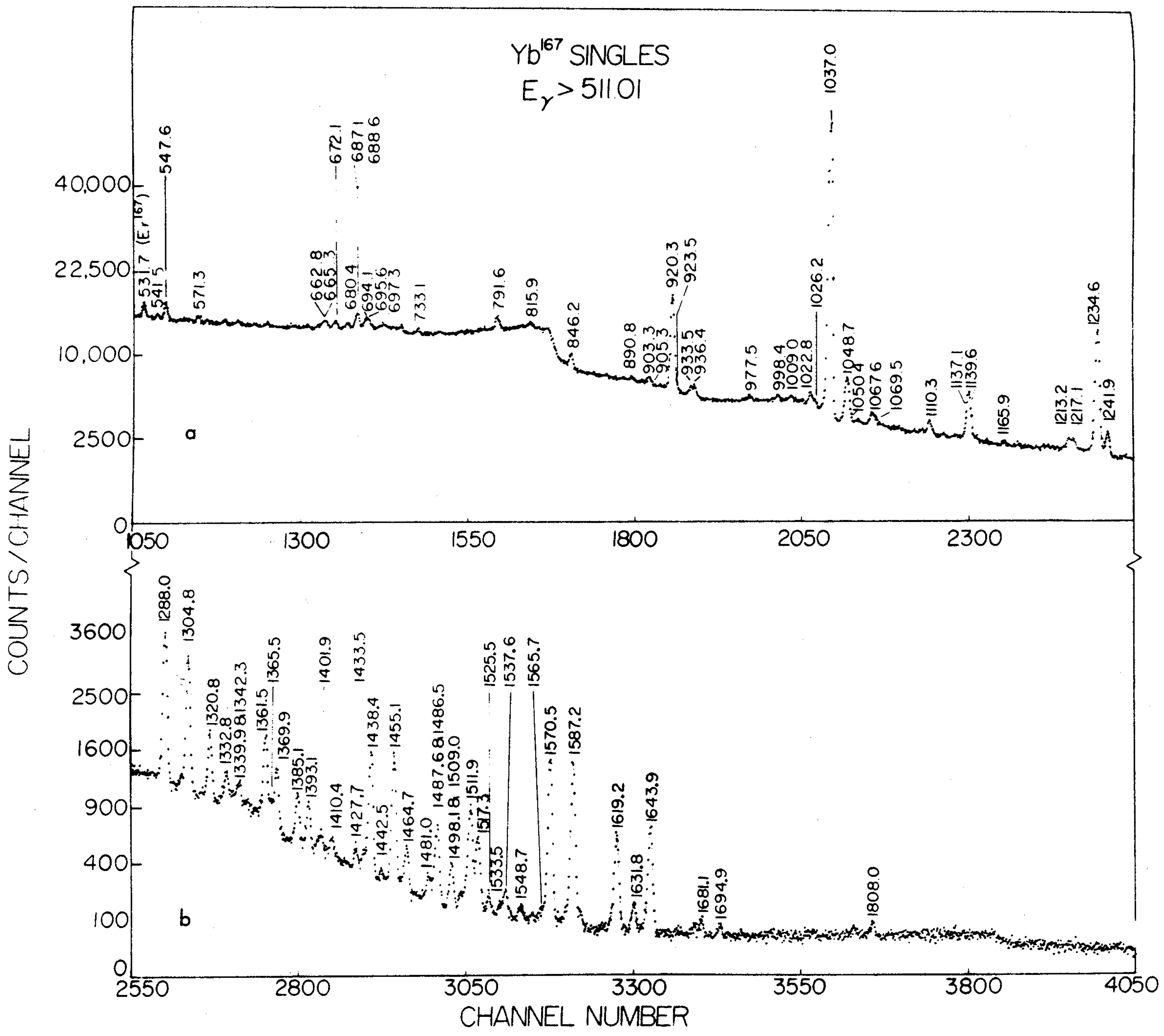

Fig. 9.4. ^{167}Yb singles γ ray spectrum taken with a Ge(Li) detector using a graded lead absorber.

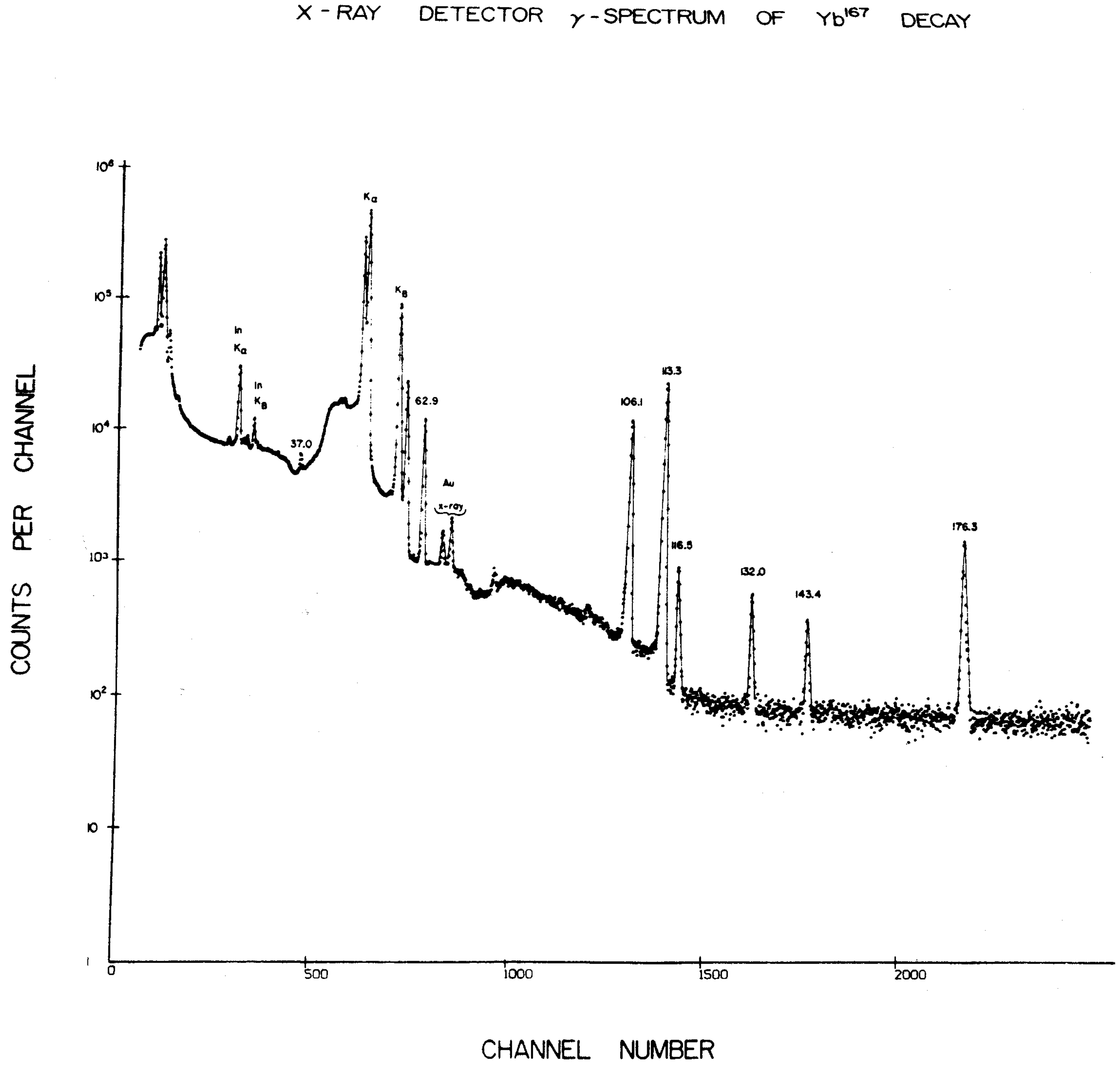

Fig. 9.5. ^{167}Yb low energy γ ray spectrum taken with a high resolution Si(Li) x-ray detector.

Table 9.2.

γ-Ray Transition Data for the ^{167}Yb Decay

Energy (keV)	Photon Intensity	Energy (keV)	Photon Intensity
25.90±0.10	---	794.2±0.5	0.27
37.03±0.05	---	815.9±0.3	0.94
x-rays	27200.	829.3±0.3	1.69
62.88±0.05	524.	832.9±0.3	1.23
106.14±0.05	4770.	846.2±0.2	2.50
113.30±0.05	10900.	903.3±0.3	1.01
116.55±0.05	565.	905.3±0.3	0.49
132.01±0.05	479.	920.3±0.2	18.01
143.41±0.05	337.	923.5±0.3	1.07
(150.5 ±0.3)	4.65	933.5±0.3	1.27
(156.5 ±0.5)	6.01	936.5±0.3	1.40
(162.6 ±0.6)	25.12	970.8±0.4	0.76
(169.7 ±0.5)	25	998.4±0.2	0.85
176.31±0.10	2420.	1009.0±0.2	0.83
(184.0 ±0.5)	1.75	1022.8±0.2	1.50
(198.3 ±0.5)	1.68	1026.2±0.2	0.70
218.6 ±0.3	11.54	1037.0±0.1	≡100.00
225.7 ±0.4	14.48	1048.7±0.2	2.93
282.1 ±0.2	12.88	1050.3±0.2	5.25
290.0 ±0.5	14.43	1067.6±0.3	0.96
343.3 ±0.2	3.11	1069.5±0.3	1.01
(351.8 ±0.2)	2.15	1110.4±0.2	1.76
405.6 ±0.2	2.02	1137.1±0.5	0.59
441.2 ±0.2	1.36	1139.6±0.2	7.47
447.1 ±0.3	0.92	1165.7±0.4	---
457.0 ±0.5	2.05	1213.2±0.2	1.32
460.4 ±0.4	3.66	1217.1±0.2	1.13
470.6 ±0.2	2.29	1234.6±0.1	27.71
511.01 (γ±)	431.05	1241.9±0.1	2.98
541.5 ±0.3	0.81	1288.0±0.3	6.81
547.6 ±0.2	2.48	1304.8±0.2	5.94
(665.1 ±0.5)	0.7	1320.8±0.2	2.34
(672.1 ±0.3)	1.07	1332.8±0.2	0.95
(680.4 ±0.3)	0.6	1336.7±0.5	0.21
687.1 ±0.2	0.6	1339.9±0.4	0.33
(688.6 ±0.4)	1.4	1342.3±0.4	0.78
(694.1 ±0.4)	0.8	1355.3±0.3	0.35
695.6 ±0.4	0.5	1358.3±0.4	0.13
697.3 ±0.4	1.09	1361.6±0.2	2.96
707.7 ±0.4	1.08	1365.5±0.5	0.48
719.7 ±0.4	1.17	1369.9±0.2	1.97
733.1 ±0.3	1.01	1385.1±0.2	1.33
791.6 ±0.2	1.84	1393.1±0.2	1.05

Table 9.2. Continued

Energy (keV)	Photon Intensity	Energy (keV)	Photon Intensity
1401.9±0.3	0.55	1511.9±0.3	2.44
1410.4±0.3	0.57	1517.3±0.3	1.56
1427.7±0.2	0.65	1525.5±0.3	0.28
1433.5±0.4	0.29	1533.6±0.3	0.20
1438.4±0.1	4.00	1537.6±0.3	0.44
1455.1±0.1	4.11	1570.5±0.1	5.38
1460.7±0.4	0.31	1587.2±0.1	4.97
1464.7±0.3	0.91	1619.2±0.2	2.13
1481.0±0.3	0.42	1631.9±0.2	0.36
1486.5±0.3	0.83	1643.9±0.2	2.65
1487.6±0.2	1.26	1681.0±0.5	---
1498.1±0.2	0.79	1694.9±0.5	---
1509.0±0.5	0.32	1808.0±0.5	---

3.6% efficient Ge(Li) detector. The coincidence timing resolution was set at 100 nsec and a delay of ≈200 nsec was added to the Ge(Li) leg of the coincidence circuit. The resulting spectrum is shown in Fig. 9.6. Several peaks were found to be enhanced up to two order of magnitude relative to the 132.0-keV peak, which is not found to be involved in any delayed coincidences. The results of this experiment are summarized in Table 9.3. Based on these results and sum and difference relations, states at 1216.4, 1229.9, 1318.9, 1527.6, 1534.7, 1580.8, 1597.5, and 1654.5 keV have been proposed.

The energy of the $9/2^+$ member of the $7/2^+[404]$ rotational band was established empirically by adjusting its calculated energy determined from the moment of inertia of the same rotational band in neighboring ^{169}Tm. Both the 1216.4-keV and 1318.9-keV states were found to feed the $7/2^+$ band head state strongly, and, in addition, γ rays were found that fit the calculated $9/2^+$ state within 0.6 keV. Moreover, both of these γ rays, when subtracted from the excited states from which they presumably originated, gave results which were consistent within 0.03 keV. This energy consistency, along with the expectation of an observable feeding to the 9/2 member of this $K=7/2$ rotational band if the band head member is strongly fed, led to the establishment of the 296.1-keV state.

A search for the 9/2 members of the $K=1/2^+$ and $K=7/2^-$ bands was made in a similar manner without any apparent success. However, recently (Wi69) these levels were reported to have been populated through the $(\alpha,2n\gamma)$ reaction on ^{165}Ho. The reported energies of these states differed markedly from what one would predict from simple first-order rotational model calculations. Since no really strong evidence exists that these states are populated by the ε/β^+ decay of ^{167}Yb, they have

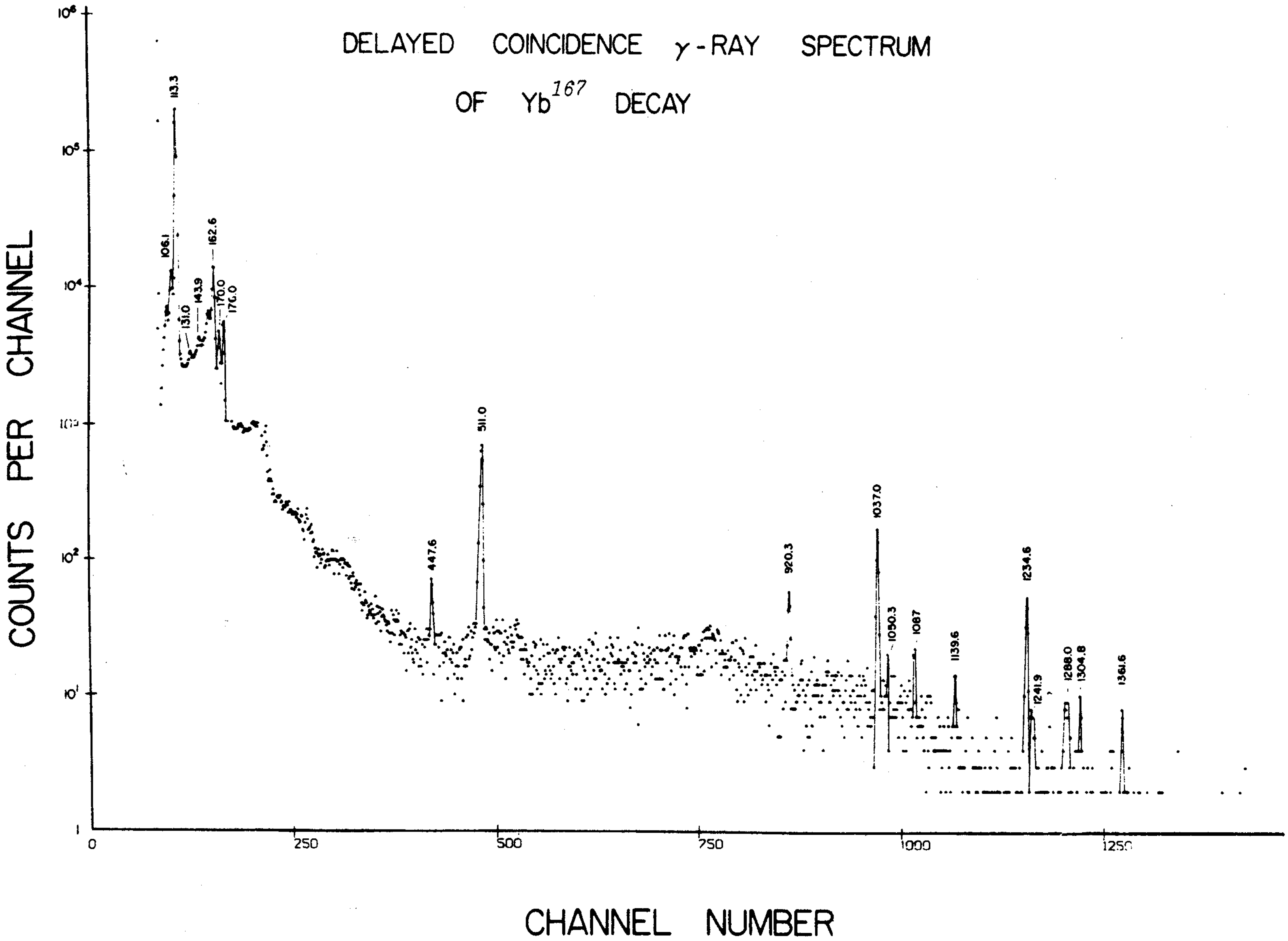

Fig. 9.6. Spectrum of ^{167}Yb γ rays involved in delayed coincidences.

Table 9.3.

Results of Integral Delayed Coincidence Study on ^{167}Yb Decay

γ-ray Energies (keV)	Relative Intensities Singles	Delayed Coin.
106.1	996.11	1607.
113.3	2277.66	28382.
132.0	≡100.00	≡100.00
142.4	70.46	159.
150.5	0.01	113.
162.4	0.05	3102.
169.7	0.05	602.
176.3	505.99	868.
218.6	0.02	275.
225.7	0.03	128.
447.1	0.001	47.
920.3	0.04	117.
923.5	0.002	
1037.0	0.21	423.
1050.0	0.01	18.
1086.2	-----	47.
1139.6	0.02	33.
1234.6	0.06	185.
1241.9	0.01	24.
1288.0	0.01	51.
1304.8	0.01	28.
1346.5	-----	8.
1358.3	0.001	20.
1361.6	0.01	

been put into our decay scheme with dotted lines. This work also served to confirm our placement of $9/2^+$ member of the $7/2^+[404]$ rotational band.

The remaining high energy states were established mainly through restrictive energy sums and feeding consistencies within the various known low-energy rotational bands (Fig. 9.3) of ^{167}Tm.

9.2.3. ^{167}Yb Decay Scheme

The decay scheme developed from our work is illustrated in Fig. 9.7. The resulting level structure forms a consistent framework for accommodating 96% of the observed γ-ray intensity associated with the ^{167}Yb decay. A large portion of the unplaced intensity resides in a single 143.4-keV γ-ray transition. In a recent study of the $(\alpha,2n\gamma)$ reaction on ^{165}Ho (Wi69) an undocumented decay scheme of ^{167}Yb was included for purposes of comparing the results of the two methods of investigation. Besides confirming our placement of several excited states, this decay scheme indicated that the 143.4-keV intensity arose from the feeding of the $9/2^-$ 285.9-keV member of a $1/2^-[541]$ rotational band by the $7/2^-[523]$ Nilsson state via a 6.9-keV transition, which presumably was measured with a β-ray spectrometer. However, the 285.9-keV state plays no other definite role in this decay scheme other than providing a source of the 143.4-keV radiation. One is also struck by the fact that although much effort must have been expended in setting up an experiment for measuring such a low-energy 18-min activity, the very intense 10.4-keV transition conversion line was completely neglected.

If the 285.9-keV state is introduced into our decay scheme, one finds no additional corroborating evidence to support its placement. This fact coupled with the absence of explicit experimental information

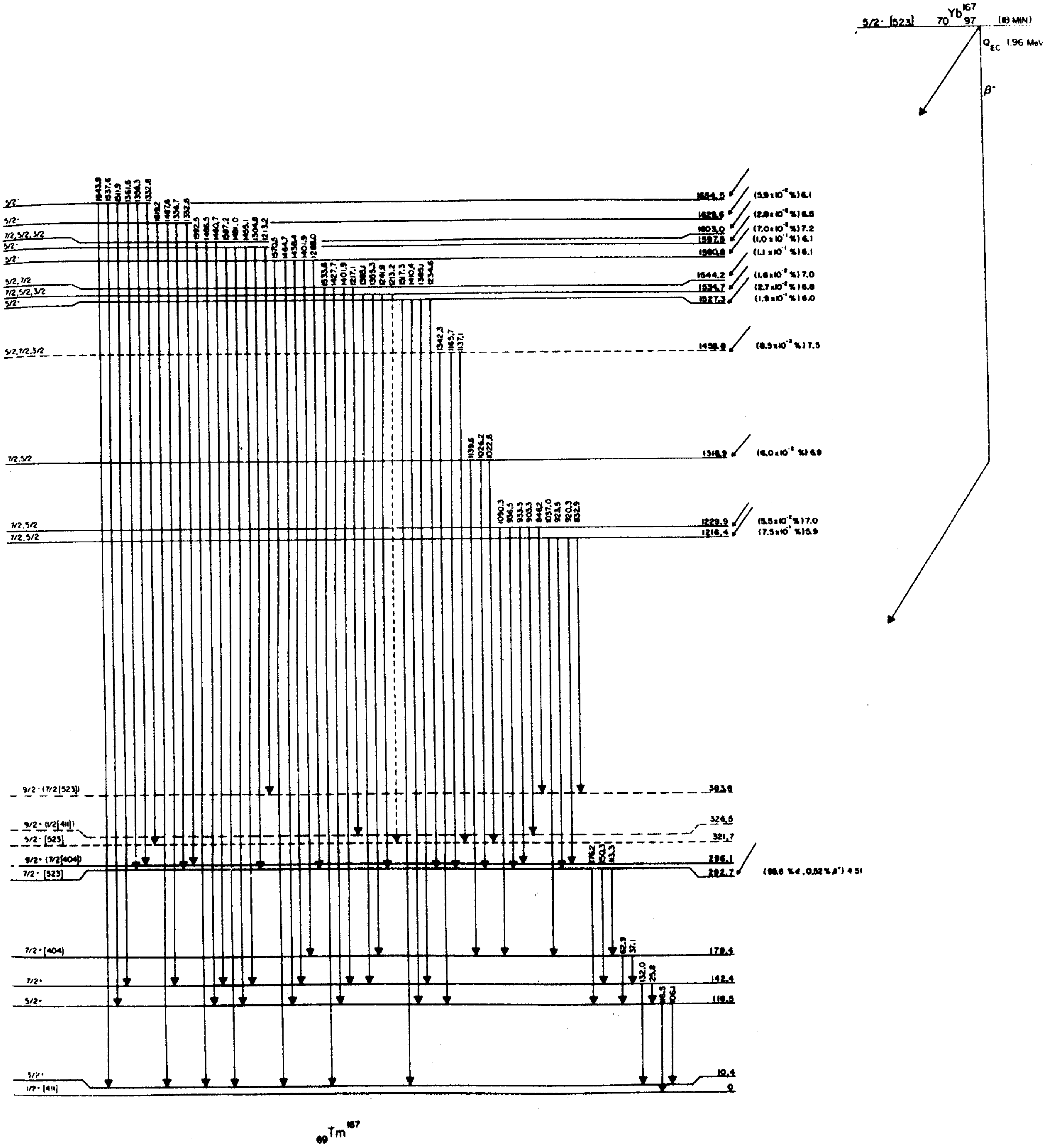

Fig. 9.7. Decay scheme of ^{167}Yb. All energies are given in keV, and (total) transition intensities are given in terms of percent per disintegration of the parent. The β^+/ε ratios are calculated values, and the log *ft* values are calculated on the basis of an 18 min half-life.

concerning the 6.9-keV conversion line led us to exclude the 143.4-keV transition from our decay scheme temporarily.

Although the 25.8-keV and 37.1-keV γ rays have been seen in spectra taken with our Si(Li) x-ray detector, reliable intensities for these transitions are not available, since massless sources of ^{167}Yb were not used in our primary investigation. The intensities of the 25.8-keV and 37.1-keV γ rays used initially in determining the decay scheme of ^{167}Yb were theoretical ones based on the relative electron intensities of Harmatz (Ha59), the multipolarities of Gromov (Gr65), and the theoretical conversion coefficients of Sliv and Band (Sl65). However, the results using these values led to inconsistent β^+/ε feeding to the $5/2^+$ and $7/2^+$ members of the ground-state rotational band. As a result the feedings to these states have been temporarily set equal to zero until accurate intensity measurements of these γ rays are made.

The preliminary assignments of spins and parities have been based primarily on log *ft* values and reduced transition intensities where they apply.

Five newly established excited states of ^{167}Tm were observed to feed the $1/2^+$[411] ground state rotational band with remarkably similar transition intensities. In each case oscillatory transition intensities were observed in the feedings of the 3/2 through 7/2 members of the ground state rotational band. These facts are summarized in Table 9.4. In order to explain this oscillatory feeding behavior exhibited by these five states, calculations of the reduced transition probability ratios corresponding to the feeding of the $K=1/2^+$ rotational band were made on the basis of all reasonable values of the K projection number and spin of the depopulated state and on several assumed multipolarities.

Table 9.4.

Relative Feeding Intensity Data to Members of the Ground State Rotational Band

State (keV)	Spin of State Being Fed		
	3/2	5/2	7/2
1527	1.5	0.6	1.3
1580	5.4	0.9	4.0
1597	4.9	0.4	4.1
1627	2.1	---	1.3
1654	2.6	0.4	2.6

A comparison between experimentally determined reduced transition probability ratios and these calculations for the 1654-keV state appears in Table 9.5. The results of these analyses appear, if one neglects second order effects, to determine uniquely the spin of these five states to be 5/2 and in addition strongly suggest a K=1/2 projection number in each case. All other possibilities lead to absurd contradictions between experimental results and theory. In addition, it is found that the log ft values associated with these excited states of spin 5/2 are all closely clustered about a value of 6.0. Since one would expect much larger log ft values for first forbidden decays with an ℓ- forbiddenness associated with them, the ε decay to these 5/2 states appear to be allowed ℓ-forbidden, which establishes negative parities for these five states. Moreover, these negative parity assignments are consistent with the strong observed feedings to the $7/2^-[523]$ state which is a common feature of each of these states.

The spin assignments of the remaining states are based primarily on log ft values and feeding characteristics of these states.

9.3. Summary

A comparison between the states populated through radioactive decay and (p,t) reaction processes reveals similarities only for lower members of the ground state rotational band and for states occurring above 1300 keV of excitation. Unfortunately, no evidence for direct or indirect feeding of the states based at 600 keV of excitation is found from this decay scheme study leaving unanswered the question of whether a γ-band exists in this region.

The series of three states based at 1380 keV of excitation

Table 9.5.

Theoretical vs Experimental Reduced Transition Probabilities

			Members of the Ground State Rotational Band Being Fed by the 1654 keV State.								
			Experimental			Theoretical					
λ1)	K2)	J3)	3/2	5/2	7/2	1/2	3/2	5/2	7/2	9/2	11/2
2	1/2	3/2	1.00	0.23	1.40	1.94	1.00	1.17	1.40	---	---
1	1/2	5/2	1.00	0.20	1.18	----	1.00	0.11	1.18	----	----
2	1/2	5/2	1.00	0.23	1.40	0.37	1.00	0.06	1.40	2.73	----
2	1/2	7/2	1.00	0.23	1.40	----	1.00	0.02	1.40	0.003	3.77
2	3/2	3/2	1.00	0.23	1.40	17.2	1.00	24.5	1.40	----	----
1	3/2	5/2	1.00	0.20	1.18	----	1.00	1.14	0.36	----	----
2	3/2	5/2	1.00	0.23	1.40	0.58	1.00	0.99	1.40	0.04	----
2	3/2	7/2	1.00	0.23	1.40	----	1.00	1.05	1.40	1.01	1.28
2	5/2	5/2	1.00	0.23	1.40	0.88	1.00	0.56	0.17	0.02	----
2	5/2	7/2	1.00	0.23	1.40	----	1.00	1.78	1.33	0.48	0.07
3	7/2	7/2	1.00	0.27	1.66	0.75	1.00	0.75	0.36	0.11	0.02

---

1) λ=γ-ray multipolarity

2) K=K-projection number of 1654 keV state

3) J=spin of 1654 state

which exhibited some $K=5/2$ band characteristics are also found to be unfed in this decay. This is a little surprising if the spin assignments of these states are correct since the decaying state has spin and parity of $5/2^-$. Again the combined results of these two studies are insufficient to resolve the questions regarding the spins and origins of these three states.

Chapter X

Conclusion

The study of the general systematics of the (*p*,*t*) reaction on spherical and deformed rare earth nuclei has shown that this reaction at the very least is a potent and powerful tool for probing the collective characteristics of nuclei.

The ^{141}Pr(*p*,*t*) experiment illustrated how the (*p*,*t*) reaction on spherical nuclei might be used in selectively identifying states having a vibrational origin. Moreover, (*p*,*t*) differential cross section measurements can in theory be used to determine the spins of these vibrationally excited states.

The (*p*,*t*) reaction on deformed rare earth nuclei clearly established the collective strength associated with this reaction. In each of the deformed nuclei studied, at least six members of the ground state rotational band were found to be strongly excited through this reaction. In two of three deformed nuclei studied, γ vibrational bands were identified, with five members in ^{157}Tb and possibly seven members in ^{163}Ho being populated. In addition, a β vibrational band strongly populated through the ^{159}Tb(*p*,*t*) reaction was also identified. However, only three members of this band could be identified because of high background problems.

The power of using this reaction to identify collective states selectively in deformed nuclei is enourmous. This has clearly been shown in the ^{159}Tb(*p*,*t*) experiment where the disputed origin of the $K=1/2$ band based at 598 keV in the ^{157}Tb nucleus was resolved.

Our data unequivocally indicated that these states had large collective amplitudes in their wave functions and were correspondingly identified as members of a γ-vibrational excitation of the K=3/2 ground state of ^{157}Tb. This assignment has since been corroborated by the recent identification of a rotational band based on the $K^{\pi}=1/2^{+}$[411] single particle proton state located at 923 keV of excitation through ^{156}Gd ($^{3}He,d$) experiments (Bo71). It should be noted that the experimentally determined decoupling parameter associated with this K=1/2 rotational band is consistent with theoretical predictions (Bo71).

In conclusion, I believe that the results of this study have clearly shown the (p,t) reaction to be as powerful a tool for probing the collective characteristics of nuclei two neutrons removed from stability as Coulomb excitation techniques are for stable nuclei.

LIST OF REFERENCES

LIST OF REFERENCES

A

[As71] R. J. Ascuitto, M. K. Glendenning, B. Sørensen, Phys. Lett. 34B, 17(1971).

[Au67] R. L. Auble, D. B. Beery, G. Berzins, L. H. Beyer, R. C. Etherton, W. H. Kelly, and Wm. C. McHarris, Nucl. Inst. and Meth. 51, 61(1967).

[Au68] R. Au, Michigan State University, private communication (1968).

B

[Ba62] R. H. Bassel, R. M. Drisko, and G. R. Satchler, Oak Ridge National Laboratory Report ORNL-3240, 1962 (unpublished).

[Ba64] G. Bassani, Norton M. Hintz, and C. D. Kavalaski, Phys. Rev. 136, B1006(1964).

[Ba67] B. F. Bayman and A. Kallio, Phys. Rev. 156, 1121(1967).

[Ba68] B. F. Bayman and Norton M. Hintz, Phys. Rev. 172, 1113(1968).

[Be69] D. B. Beery, W. H. Helly and Wm. C. McHarris, Phys. Rev. 188, 1851(1969).

[Bj66] J. H. Bjerregaard, Ole Hansen and O. Nathan, Nucl. Phys. 86, 145(1966).

[Bl67] P. H. Blichert-Toft, E. G. Funk and J. W. Mihelich, Nucl. Phys. A100, 369(1967).

[Bo52] A. Bohr, Dan. Mat. Fys. Medd. 26, nr.14(1952).

[Bo53] A. Bohr and B. R. Mottelson, Dan. Mat. Fys. Medd. 27, nr. 16(1953).

[Bo71] J. Boyno, Rodchester University, private communication.

[Br69] S. M. Brahmovar, J. H. Hamilton, A. V. Ramayya, E. F. Zganger, and C. E. Bemis, Nucl. Phys. A125, (1969) C

[Ch70] N. S. Chant and N. F. Mangelson, Nucl. Phys. A140, 81(1970).

D

[Do69] R. Doebler, 1969 Annual Report, Nuclear Chemistry Group, Michigan State University (COO-1773-13).

[Do71] R. Doebler, Ph.D. Thesis, Michigan State University (1971).

F

[Fr67] M. P. Fricke, E. E. Gross, B. J. Morton and A. Zucker, Phys. Rev. 156, 1207(1967).

G

[Go64] M. L. Goldberger and K. M. Watson, Collision Theory, (John Wiley & Sons, 1964).

[Go69] R. Goles, 1969 Annual Report, Nuclear Chemistry Group, Michigan State University (COO-1773-13).

[Gr65] K. Ya Gromov, A. S. Danagulyan, A. T. Strigachev and V. S. Shpenel, U.S.S.R. Yad. Fiz., 1137(1965).

H

[Ha54] T. H. Handley and E. L. Olson, Phys. Rev. 94, 968(1954).

[Ha59] B. Harmatz, T. H. Handley, and J. W. Mihelich, Phys. Rev. 114, 1082(1959).

[Hi70] M. Oothoudt, M. M. Hintz and P. Vedelsly, Phys. Lett. 32B, 270(1970).

I

[Ig69] G. J. Igo, P. D. Barnes, E. R. Flynn and P. D. Armstrong, Phys. Rev. 177, 1831(1969).

K

[Ku65] The DWBA code DWUCK written by P. Kunz of the University of Colorado, 1965 (unpublished).

[Ku71] E. Rost and P. D. Kunz, Nucl. Phys. A162, 376(1971).

L

[Le68] C. M. Lederer, J. M. Hollander, and I. Perlman, Table of Isotopes (John Wiley & Sons, New York 1966).

M

[Ma55] M. G. Mayer and J. H. D. Jensen, Elementary Theory of Nuclear Shell Structure (John Wiley & Sons, Inc., New York, 1955).

[Ma66] J. R. Maxwell, Glenn M. Reynolds, and Norton M. Hintz, Phys. Rev. 151, 1000(1966).

[Mc69] Wm. C. McHarris, D. B. Beery and W. H. Kelly, Phys. Rev. Lett. 22, 1191(1969).

P

[Pa67] P. Paris, J. J. Phys. (Paris) 28, 388(1967).

[Pe62] Lars Persson, Hans Ryde and Karin Oelsner-Ryde, Ark. Fys. 24, nr.34 (1962).

[Pe63] F. Perey. R. J. Silva, and G. R. Satchler, Phys. Lett. 4, 25(1963).

[Pr63] M. A. Preston, Physics of the Nucleus (Addison-Wesley, Inc., Reading, Massachusetts, 1963).

R

[Re67] G. M. Reynolds, J. R. Maxwell and Norton M. Hintz, Phys. Rev. 153, 1283(1967).

[Ri70] J. Rice, Michigan State University, private communication (1971).

[Ro69] J. T. Routti and S. G. Prussin, Nucl. Instr. and Meth. *72*, 125(1969).

S

[Sa64] G. R. Satchler, Nucl. Phys. *55*, 1(1964).

[SaA65] G. R. Satchler in *Lectures in Theoretical Physics*, Vol. VIIC (University of Colorado Press, Boulder, Colorado, 1965).

[Se67] G. G. Seaman, E. M. Bernstein and J. M. Palms, Phys. Rev. *161*, 1223(1967).

[Sl65] L. A. Sliv and I. M. Band, in *Alpha, Beta and Gamma Ray Spectroscopy*, ed. by K. Siegbahn, North Holland Pub. Co., Amsterdam (1965).

T

[Ta65] T. Tamura, Nucl. Phys. *62*, 305 (1965).

[To61] W. Tobocman, *Theory of Direct Nuclear Reactions* (Oxford University Press, 1961).

[Tr70] G. F. Trentelman, Michigan State University, private communication.

W

[Wi60] R. G. Wilson and M. L. Pool, Phys. Rev. *120*, 1296(1960).

[Wi66] C. F. Williamson, J. Boujot, and J. Picard, Centre d' Eludes Nucleaire de Saclay, Report CEA-R3042(1966).

[Wi69] G. Winter, L. Funke, K. Hohmuth, K. H. Kaun, P. Kemnitz and H. Sodan, Nucl. Phys. *A151*, 337(1969).

APPENDICES

APPENDIX A

^{141}Pr(p,t) Spectra

The following pages contain ^{141}Pr(p,t) angular distribution spectra taken with an E-ΔE detector telescope.

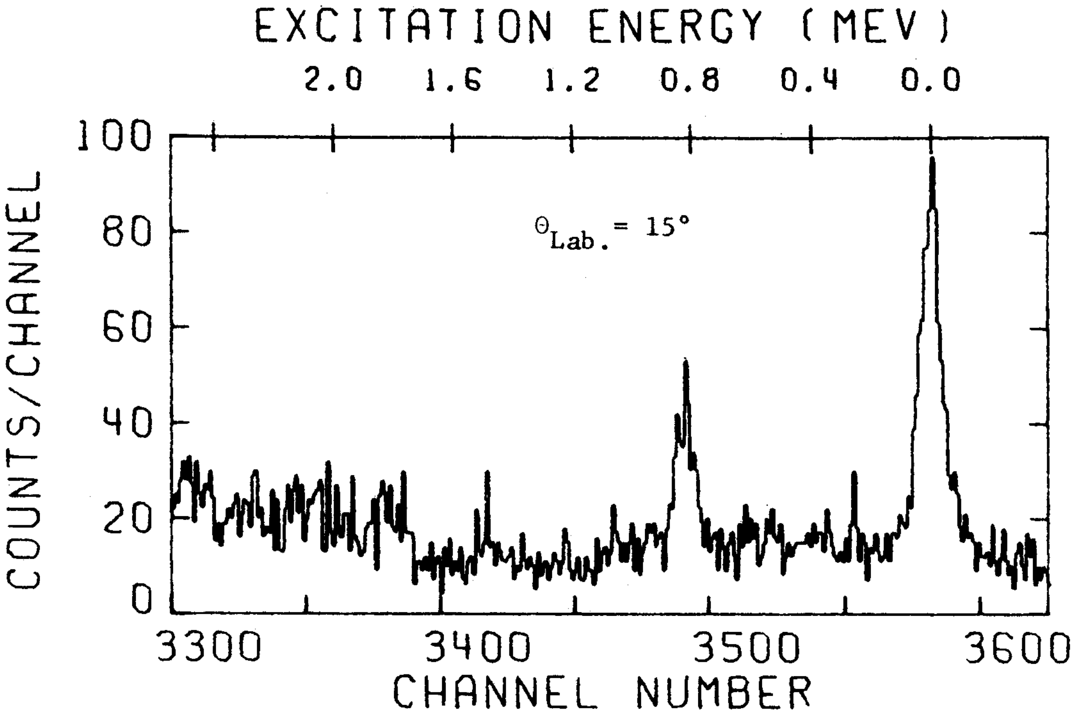
EXCITATION ENERGY (MEV)
2.0
1.6
1.2
0.8
0.4
0.0
COUNTS/CHANNEL
100
80
60
40
20
0
$\Theta_{Lab.}$ = 15°
3300
3400
3500
3600
CHANNEL NUMBER

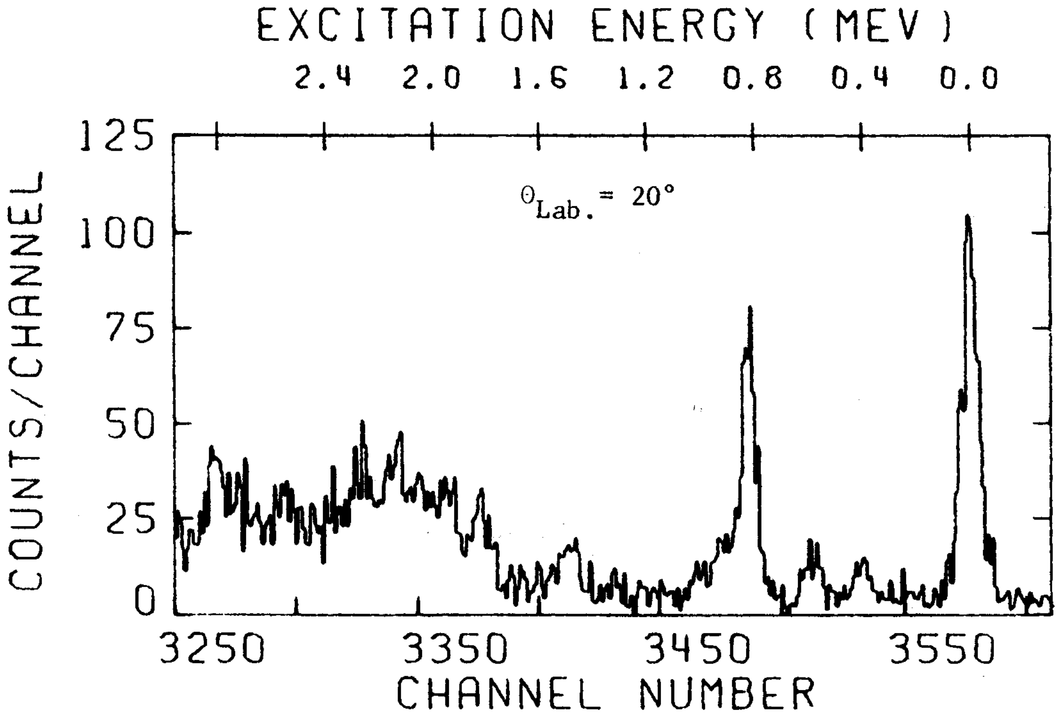
EXCITATION ENERGY (MEV)
2.4
2.0
1.6
1.2
0.8
0.4
0.0
COUNTS/CHANNEL
125
100
75
50
25
0
$\Theta_{Lab.}$ = 20°
3250
3350
3450
3550
CHANNEL NUMBER

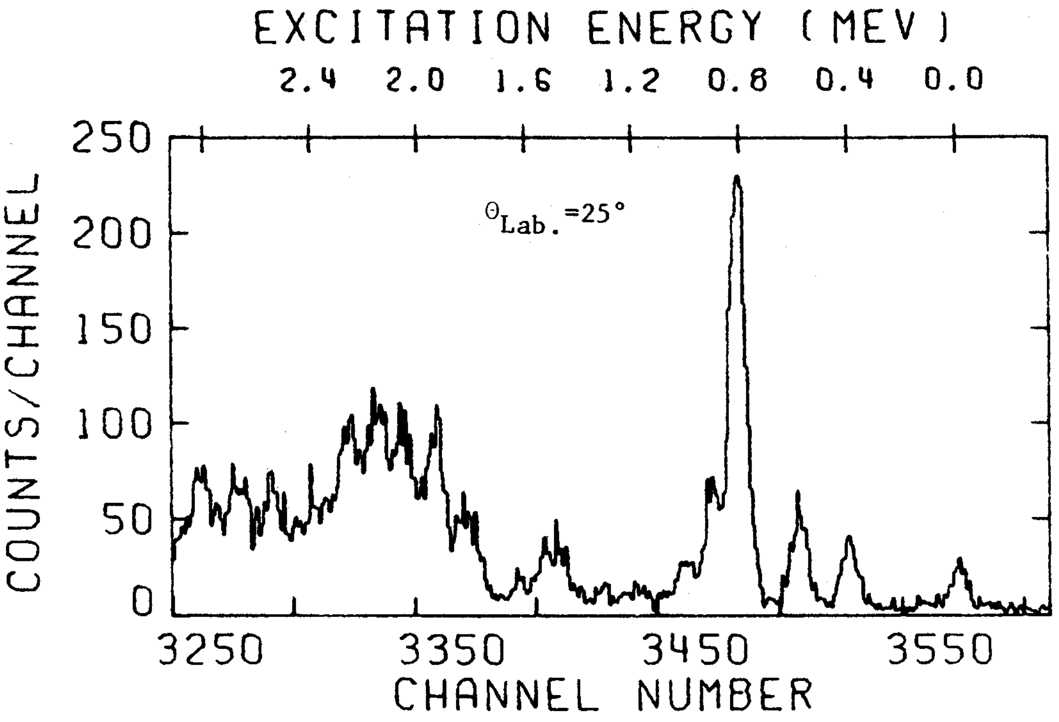
EXCITATION ENERGY (MEV)
2.4
2.0
1.6
1.2
0.8
0.4
0.0
250
200
150
100
50
0
COUNTS/CHANNEL
$\Theta_{Lab.}$=25°
3250
3350
3450
3550
CHANNEL NUMBER

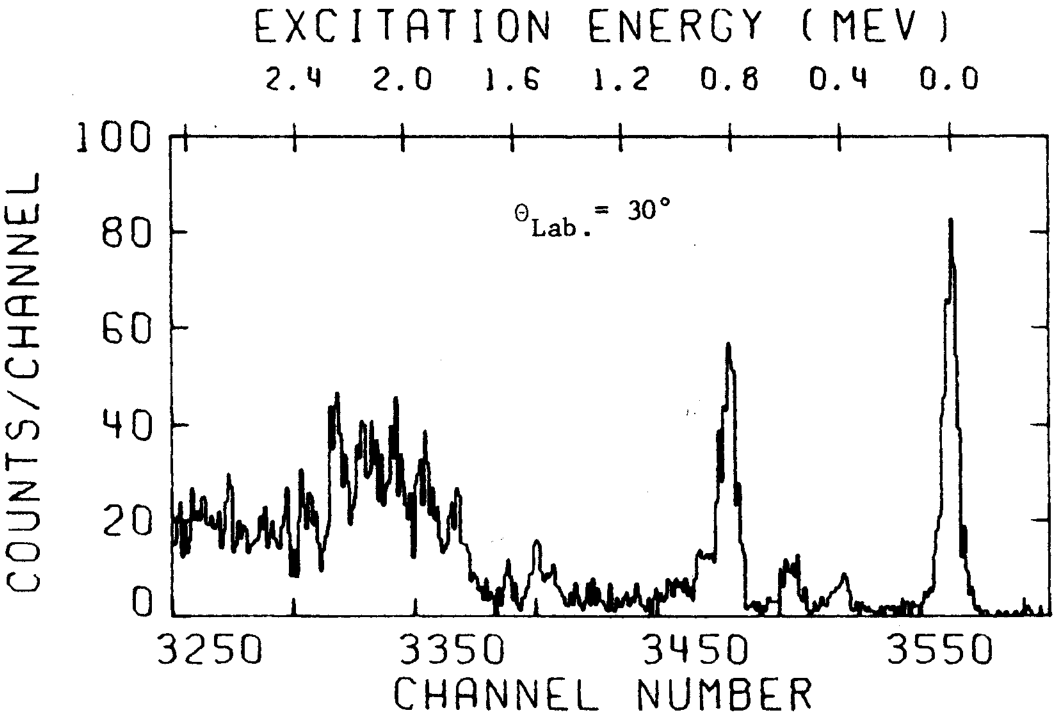
EXCITATION ENERGY (MEV)
2.4
2.0
1.6
1.2
0.8
0.4
0.0
100
80
60
40
20
0
COUNTS/CHANNEL
$\Theta_{Lab.}$= 30°
3250
3350
3450
3550
CHANNEL NUMBER

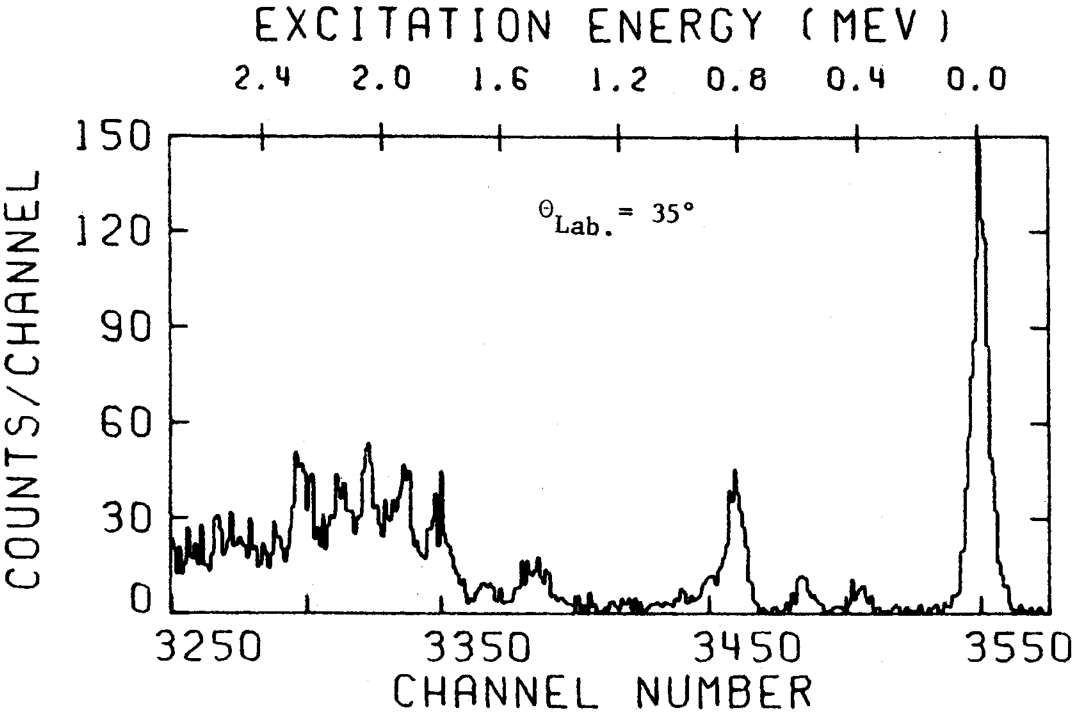
EXCITATION ENERGY (MEV)
2.4
2.0
1.6
1.2
0.8
0.4
0.0
150
120
90
60
30
0
COUNTS/CHANNEL
$\Theta_{Lab.}$ = 35°
3250
3350
3450
3550
CHANNEL NUMBER

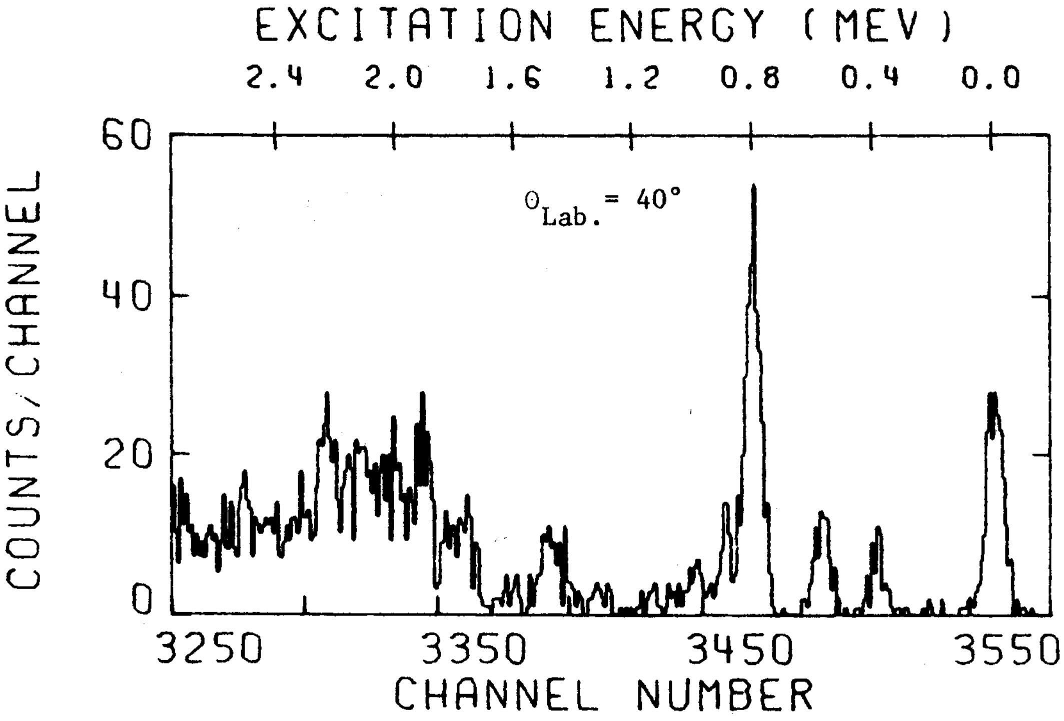
EXCITATION ENERGY (MEV)
2.4
2.0
1.6
1.2
0.8
0.4
0.0
60
40
20
0
COUNTS/CHANNEL
$\Theta_{Lab.}$ = 40°
3250
3350
3450
3550
CHANNEL NUMBER

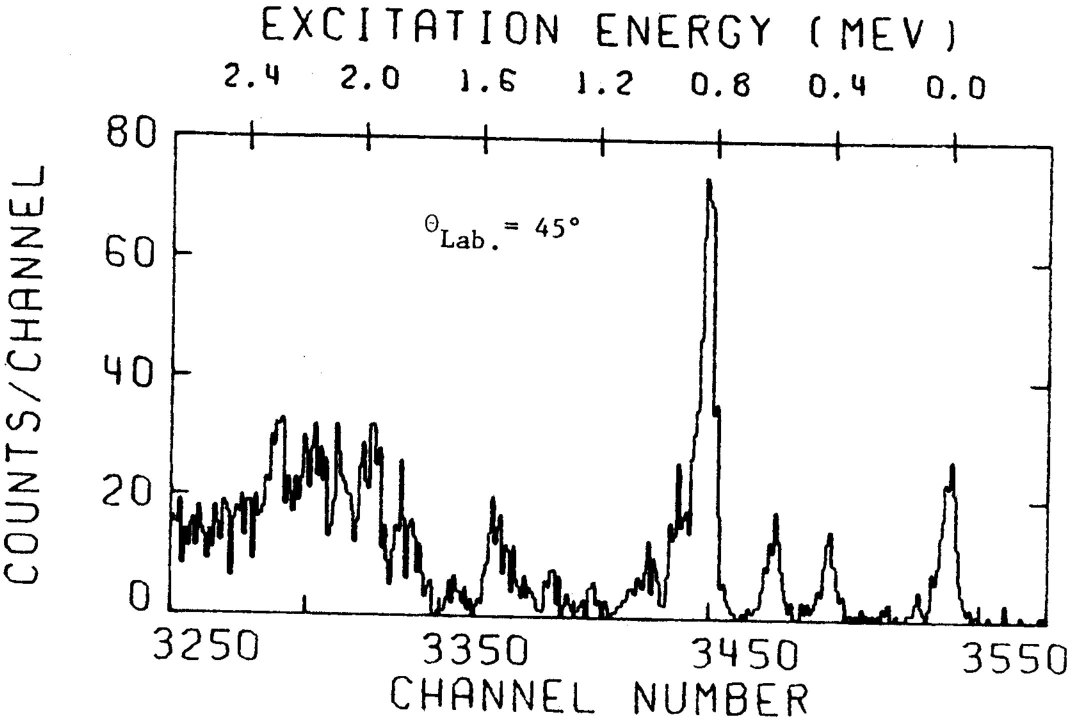
EXCITATION ENERGY (MEV)
2.4
2.0
1.6
1.2
0.8
0.4
0.0
80
60
40
20
0
COUNTS/CHANNEL
$\Theta_{Lab.}$ = 45°
3250
3350
3450
3550
CHANNEL NUMBER

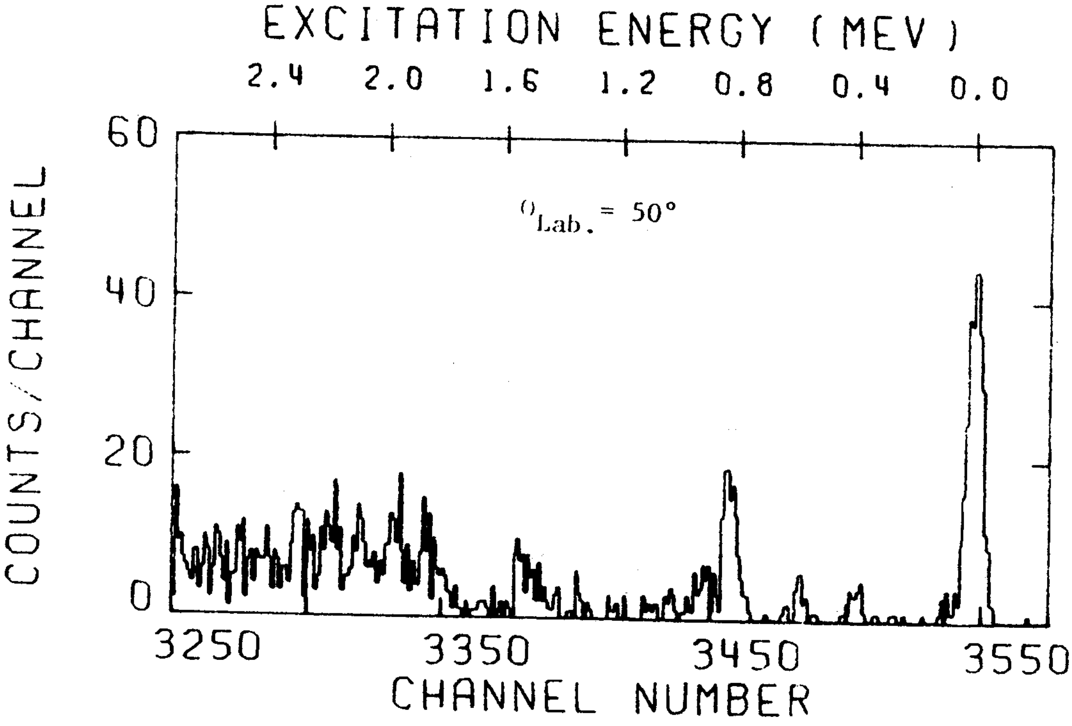
EXCITATION ENERGY (MEV)
2.4
2.0
1.6
1.2
0.8
0.4
0.0
60
40
20
0
COUNTS/CHANNEL
$\Theta_{Lab.}$ = 50°
3250
3350
3450
3550
CHANNEL NUMBER

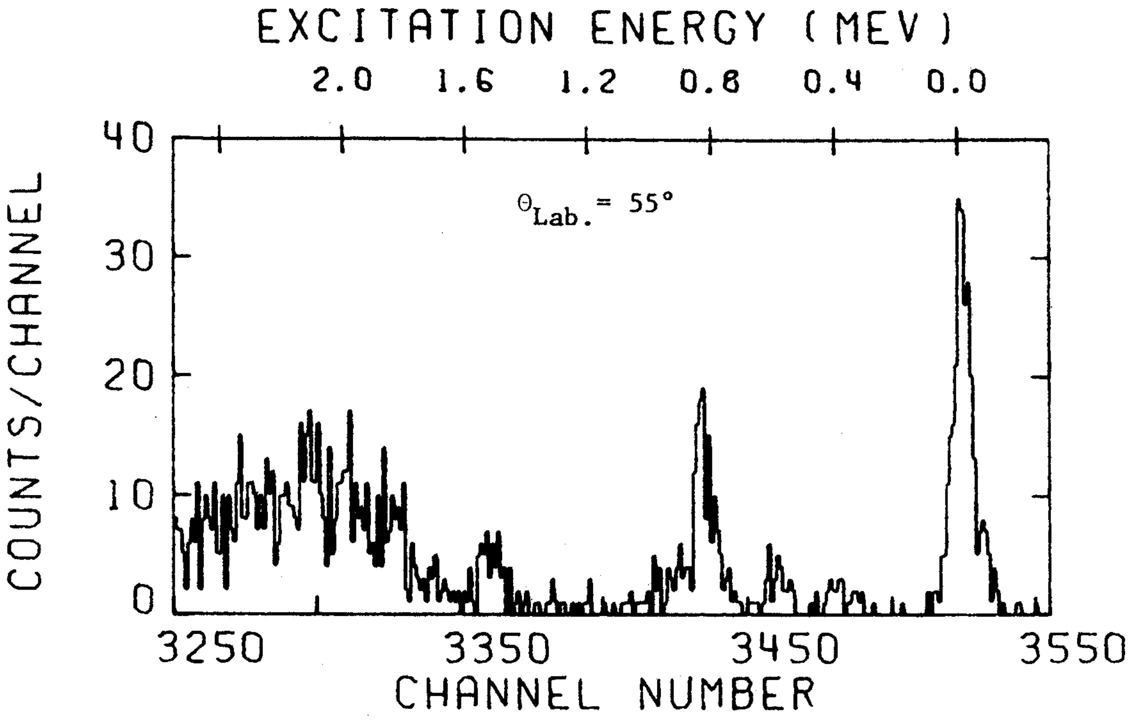
EXCITATION ENERGY (MEV)
2.0
1.6
1.2
0.8
0.4
0.0
COUNTS/CHANNEL
40
30
20
10
0
$\Theta_{Lab.}$ = 55°
3250
3350
3450
3550
CHANNEL NUMBER

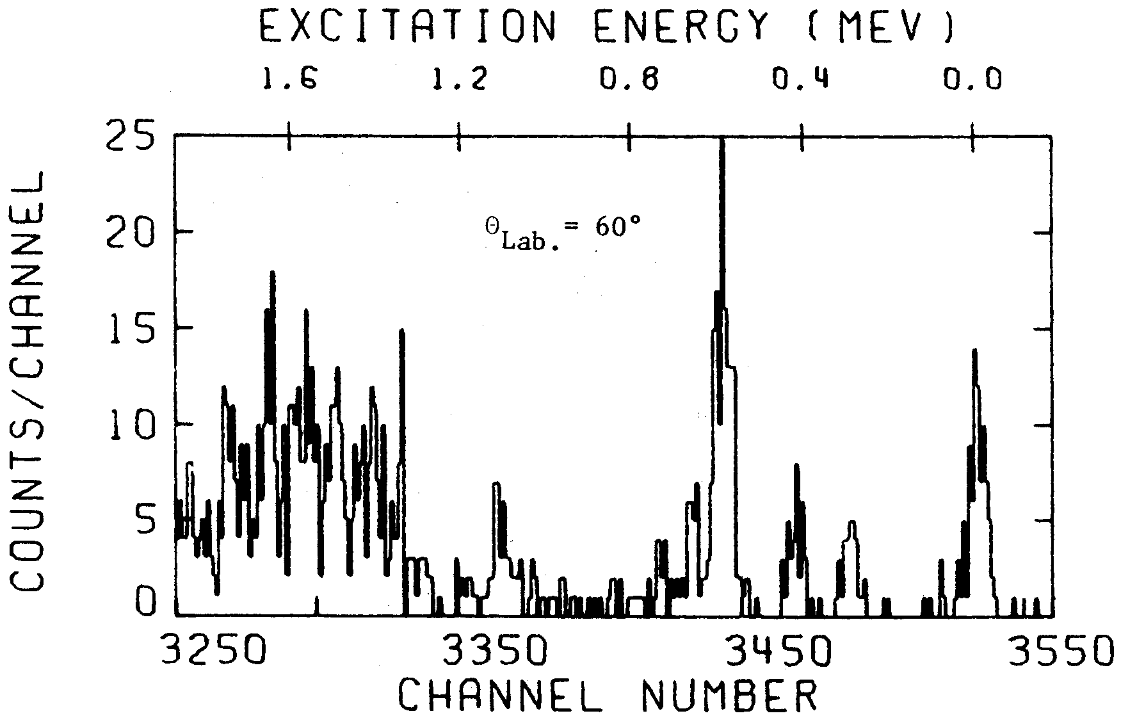
EXCITATION ENERGY (MEV)
1.6
1.2
0.8
0.4
0.0
COUNTS/CHANNEL
25
20
15
10
5
0
$\Theta_{Lab.}$ = 60°
3250
3350
3450
3550
CHANNEL NUMBER

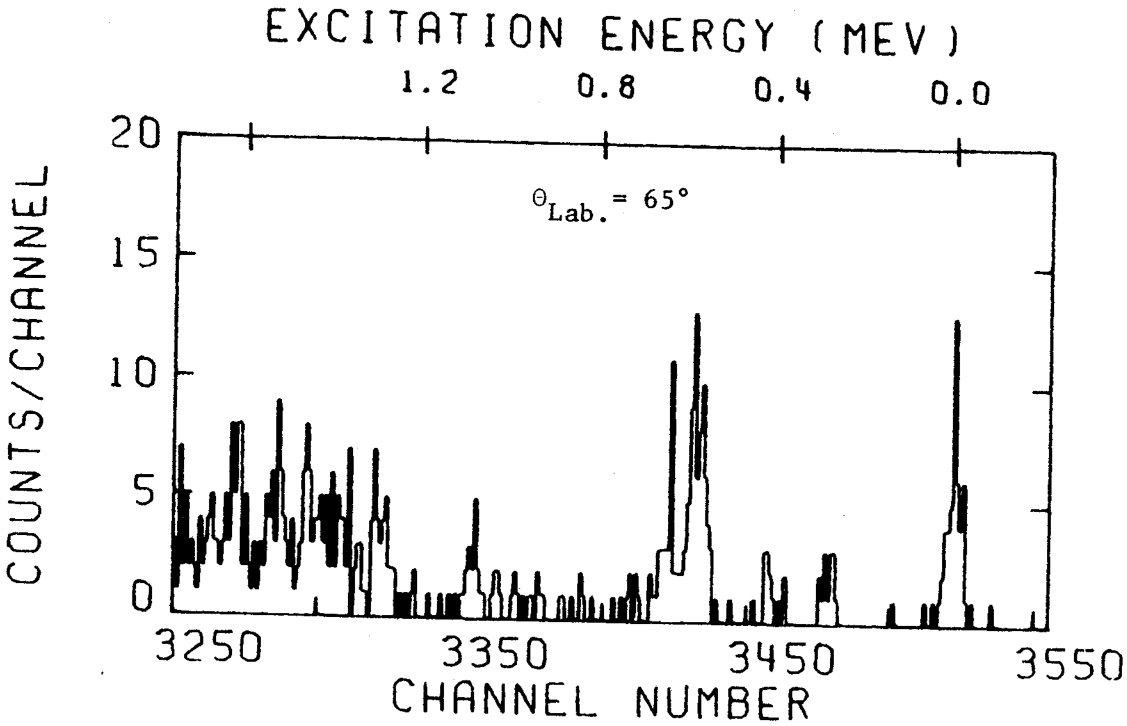
EXCITATION ENERGY (MEV)
1.2
0.8
0.4
0.0
20
15
10
5
0
COUNTS/CHANNEL
$\Theta_{Lab.}$ = 65°
3250
3350
3450
3550
CHANNEL NUMBER

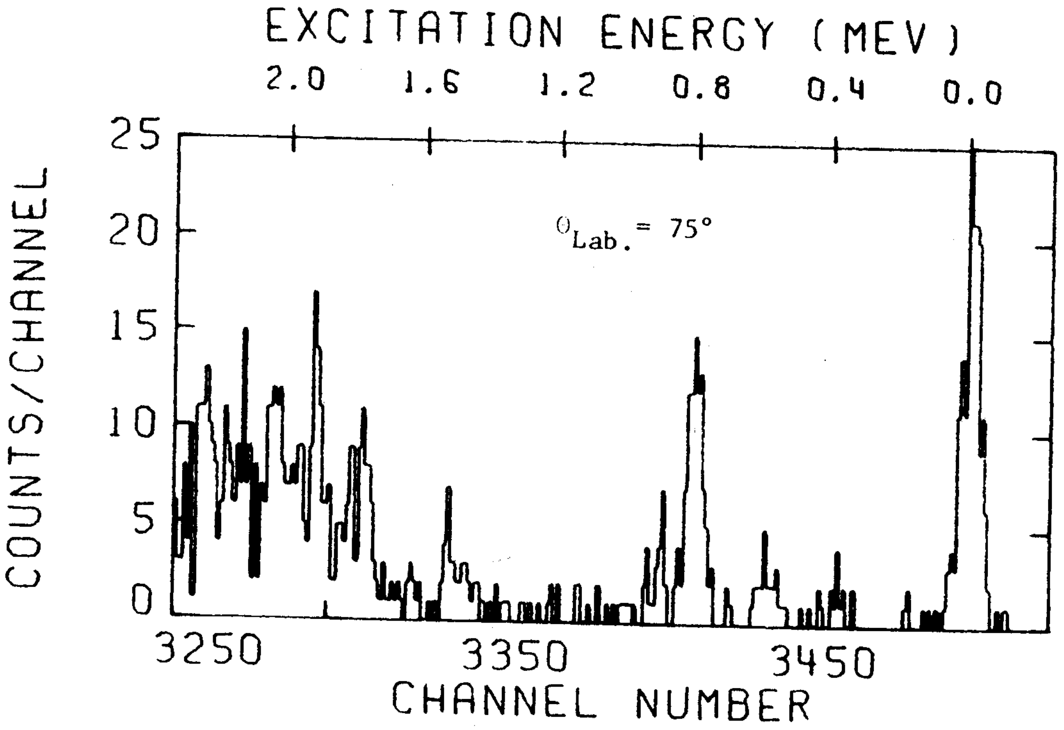
EXCITATION ENERGY (MEV)
2.0
1.6
1.2
0.8
0.4
0.0
25
20
15
10
5
0
COUNTS/CHANNEL
$\Theta_{Lab.}$ = 75°
3250
3350
3450
CHANNEL NUMBER

APPENDIX B

Tabulation of ^{141}Pr(p,t) Differential Cross Sections

The following pages contain listings of the center-of-mass differential cross sections and scattering angles for the various states populated through the ^{141}Pr(p,t) reaction. All cross sections are relative and have been normalized to reflect the magnitudes of measured absolute values. The listed errors are purely statistical.

```
      PR141(P,T)

     EX=  .000 MEV

ANG(CM) SIGMA(CM) ERROR
 (DEG)   (MB/SR)   (%)

 15.21  1.35E-01   4.8
 20.28  6.72E-02   3.9
 25.35  9.47E-03   8.2
 30.41  3.38E-02   4.3
 35.47  4.87E-02   3.1
 40.53  1.44E-02   6.8
 45.58  1.05E-02   8.8
 50.63  1.84E-02   5.7
 55.67  1.43E-02   6.9
 60.71  2.66E-03  10.9
 65.74  3.46E-03  14.7
```

```
      PR141(P,T)

     EX=  .405 MEV

ANG(CM) SIGMA(CM) ERROR
 (DEG)   (MB/SR)   (%)

 15.21  6.04E-03  35.3
 20.28  9.34E-03  12.7
 25.35  1.48E-02   6.3
 30.41  3.07E-03  17.6
 35.47  2.17E-03  17.9
 40.53  3.62E-03  13.6
 45.58  4.51E-03  14.4
 50.63  1.37E-03  20.9
 55.68  5.21E-04  50.9
 60.72  9.81E-04  18.0
 65.75  1.05E-03  26.7
```

```
      PR141(P,T)

     EX=  .590 MEV

ANG(CM) SIGMA(CM) ERROR
 (DEG)   (MB/SR)   (%)

 20.28  1.11E-02  11.2
 25.35  2.16E-02   5.1
 30.41  5.36E-03  12.4
 35.48  3.37E-03  14.3
 40.53  5.96E-03  10.6
 45.59  5.64E-03  12.5
 50.64  1.73E-03  18.6
 55.68  1.21E-03  30.5
 60.72  1.11E-03  16.9
 65.75  9.03E-04  28.8
```

```
      PR141(P,T)

     EX=  .830 MEV

ANG(CM) SIGMA(CM) ERROR
 (DEG)   (MB/SR)   (%)

 15.22  4.36E-02  10.5
 20.28  5.47E-02   4.4
 25.35  9.73E-02   2.3
 30.42  2.45E-02   5.1
 35.48  1.50E-02   5.8
 40.54  2.34E-02   5.4
 45.59  3.38E-02   4.5
 50.64  6.96E-03   9.2
 55.68  6.25E-03  10.6
 60.72  4.49E-03   8.4
 65.75  5.19E-03  12.0
```

PR141(P,T)

EX= .910 MEV

ANG(CM) (DEG)	SIGMA(CM) (MB/SR)	ERROR (%)
20.29	1.24E-02	10.0
25.35	2.72E-02	4.4
30.42	5.95E-03	10.9
35.48	3.18E-03	13.5
40.54	4.08E-03	12.8
45.59	8.76E-03	9.3
50.64	2.62E-03	15.1
55.68	1.50E-03	27.7
60.72	8.22E-04	19.6
65.76	2.41E-03	17.7

PR141(P,T)

EX=1.010 MEV

ANG(CM) (DEG)	SIGMA(CM) (MB/SR)	ERROR (%)
20.29	6.57E-03	14.9
25.35	1.05E-02	7.4
30.42	3.54E-03	15.4
35.48	1.06E-03	25.7
40.54	2.68E-03	15.8
45.59	4.98E-03	13.8
60.72	4.74E-04	25.8

PR141(P,T)

EX=1.330 MEV

ANG(CM) (DEG)	SIGMA(CM) (MB/SR)	ERROR (%)
25.35	2.01E-03	30.2
40.54	1.61E-03	20.4
45.59	1.92E-03	23.1
50.64	9.52E-04	25.0

PR141(P,T)

EX=1.520 MEV

ANG(CM) (DEG)	SIGMA(CM) (MB/SR)	ERROR (%)
15.22	7.46E-03	29.2
20.29	4.19E-03	18.3
25.36	9.91E-03	9.3
30.42	7.95E-03	9.8
35.48	6.23E-03	11.5
40.54	6.76E-03	10.0
45.60	6.24E-03	11.3
50.65	4.40E-03	11.6
55.69	2.54E-03	19.5
60.73	1.42E-03	14.9
65.76	1.35E-03	23.6

```
        PR141(P,T)

      EX=1.620 MEV

ANG(CM)  SIGMA(CM)  ERROR
 (DEG)    (MB/SR)    (%)

 20.29   4.19E-03   19.8
 25.36   3.04E-03   23.1
 30.42   1.94E-03   24.4
 35.48   1.94E-03   23.3
 40.54   6.69E-04   44.7
 45.60   1.39E-03   29.0
 60.73   4.11E-04   27.8
```

```
        PR141(P,T)

      EX=2.050 MEV

ANG(CM)  SIGMA(CM)  ERROR
 (DEG)    (MB/SR)    (%)

 25.36   2.64E-02    7.2
 30.42   9.54E-03   13.7
 35.49   1.15E-02    9.5
 45.60   5.84E-03   21.3
 60.74   1.93E-03   16.8
```

```
        PR141(P,T)

      EX=2.160 MEV

ANG(CM)  SIGMA(CM)  ERROR
 (DEG)    (MB/SR)    (%)

 20.29   2.18E-02   10.7
 25.36   3.23E-02    6.1
 30.43   1.43E-02   10.9
 35.49   1.02E-02   10.6
```

```
        PR141(P,T)

      EX=2.240 MEV

ANG(CM)  SIGMA(CM)  ERROR
 (DEG)    (MB/SR)    (%)

 20.29   1.65E-02   14.8
 25.36   2.84E-02    6.9
 30.43   1.10E-02   12.2
 35.49   1.19E-02    9.4
 40.55   7.29E-03   16.1
 45.60   9.82E-03   13.3
 60.74   2.25E-03   15.1
```

APPENDIX C

^{159}Tb(p,t) Spectra

The following pages contain ^{159}Tb(p,t) angular distribution spectra taken with a broad range magnetic spectrometer.

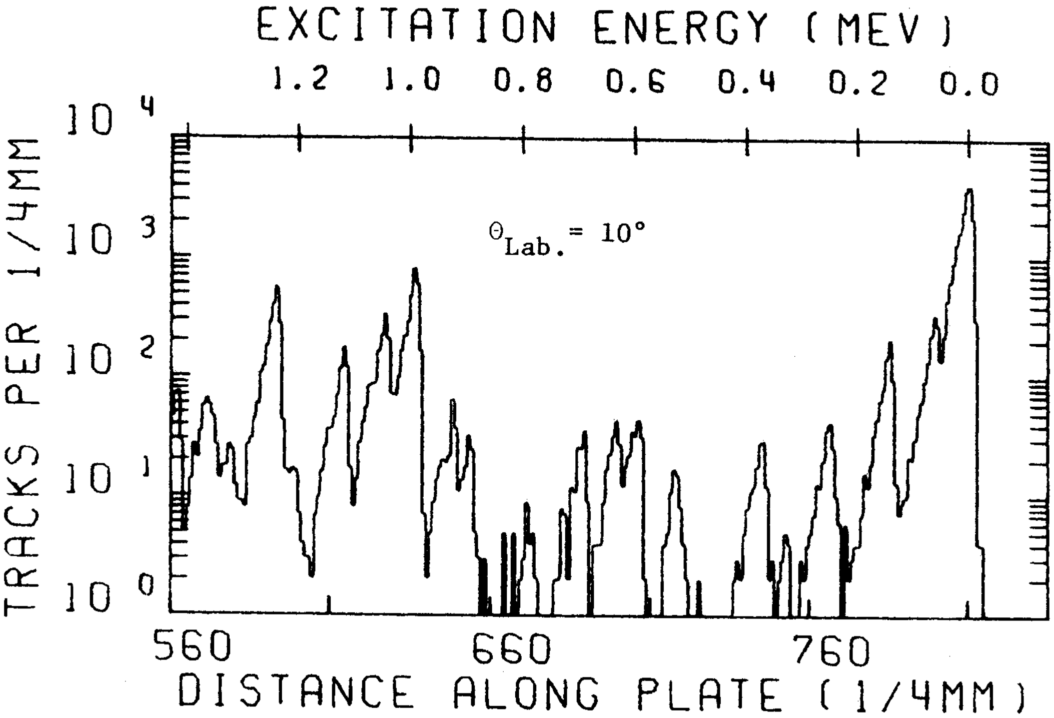
EXCITATION ENERGY (MEV)
1.2
1.0
0.8
0.6
0.4
0.2
0.0
TRACKS PER 1/4MM
10 4
10 3
10 2
10 1
10 0
θLab. = 10°
560
660
760
DISTANCE ALONG PLATE (1/4MM)

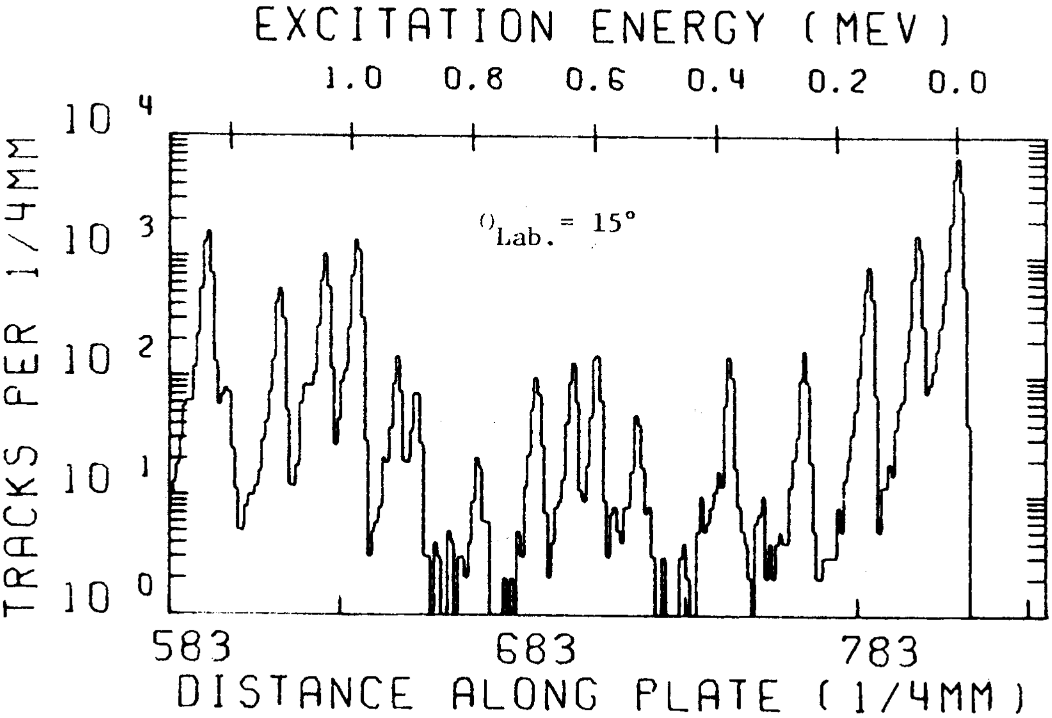
EXCITATION ENERGY (MEV)
1.0
0.8
0.6
0.4
0.2
0.0
TRACKS PER 1/4MM
10 4
10 3
10 2
10 1
10 0
θLab. = 15°
583
683
783
DISTANCE ALONG PLATE (1/4MM)

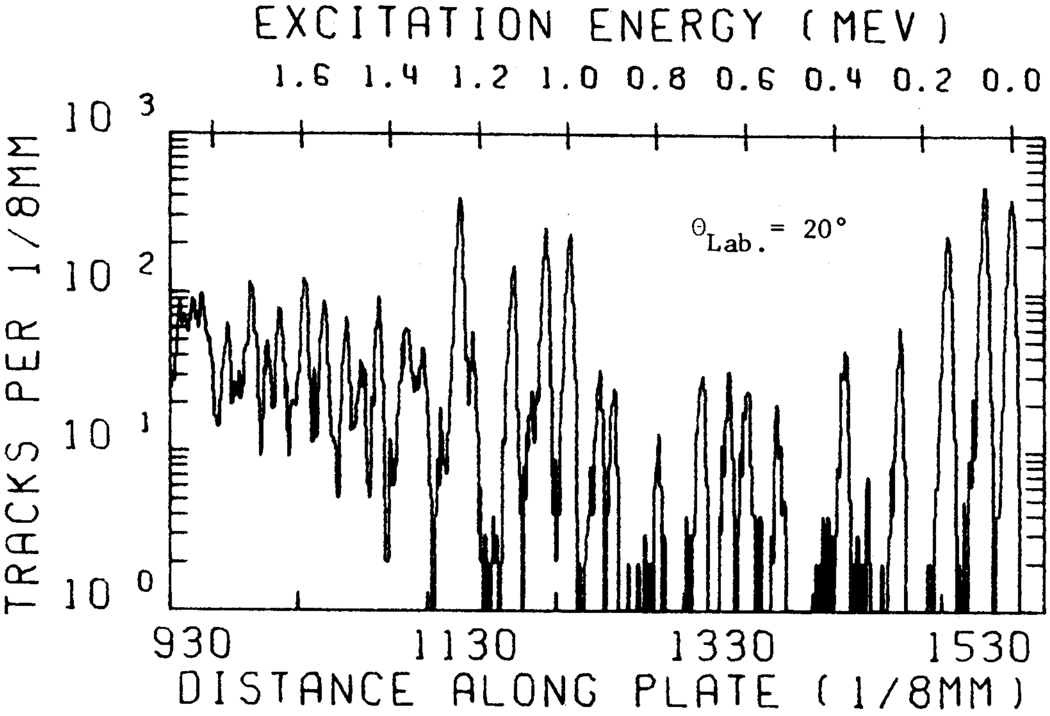
EXCITATION ENERGY (MEV)
1.6 1.4 1.2 1.0 0.8 0.6 0.4 0.2 0.0
$\Theta_{Lab.}$ = 20°
TRACKS PER 1/8MM
10 3
10 2
10 1
10 0
930
1130
1330
1530
DISTANCE ALONG PLATE (1/8MM)

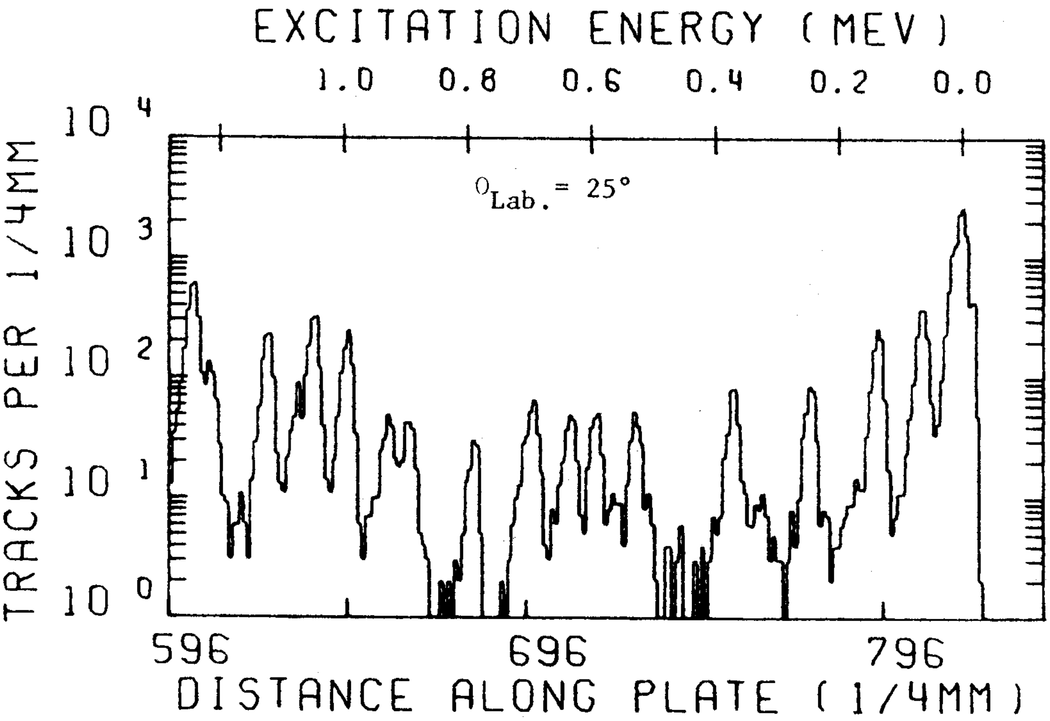
EXCITATION ENERGY (MEV)
1.0 0.8 0.6 0.4 0.2 0.0
$\Theta_{Lab.}$ = 25°
TRACKS PER 1/4MM
10 4
10 3
10 2
10 1
10 0
596
696
796
DISTANCE ALONG PLATE (1/4MM)

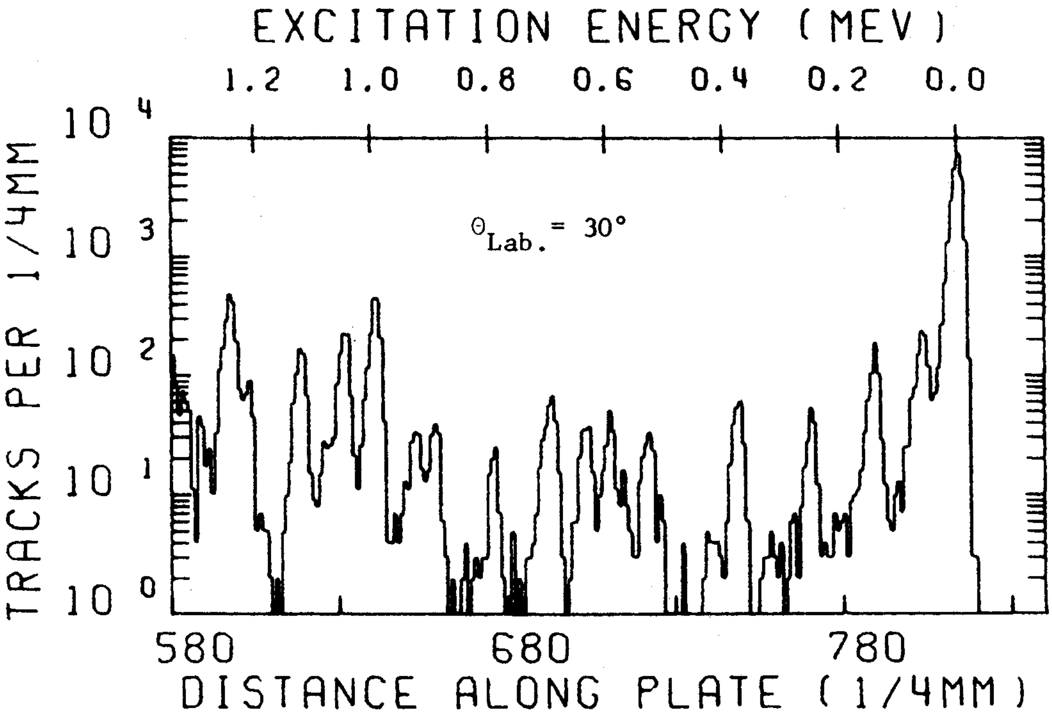
EXCITATION ENERGY (MEV)
1.2
1.0
0.8
0.6
0.4
0.2
0.0
10^4
10^3
10^2
10^1
10^0
TRACKS PER 1/4MM
$\Theta_{Lab.} = 30°$
580
680
780
DISTANCE ALONG PLATE (1/4MM)

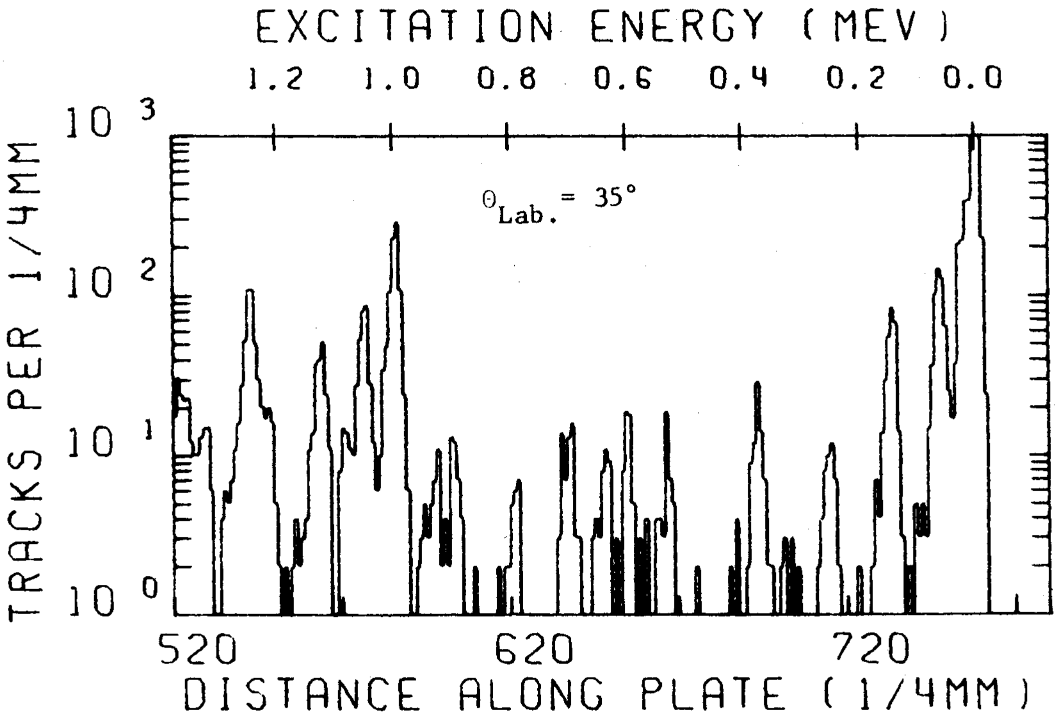
EXCITATION ENERGY (MEV)
1.2
1.0
0.8
0.6
0.4
0.2
0.0
10^3
10^2
10^1
10^0
TRACKS PER 1/4MM
$\Theta_{Lab.} = 35°$
520
620
720
DISTANCE ALONG PLATE (1/4MM)

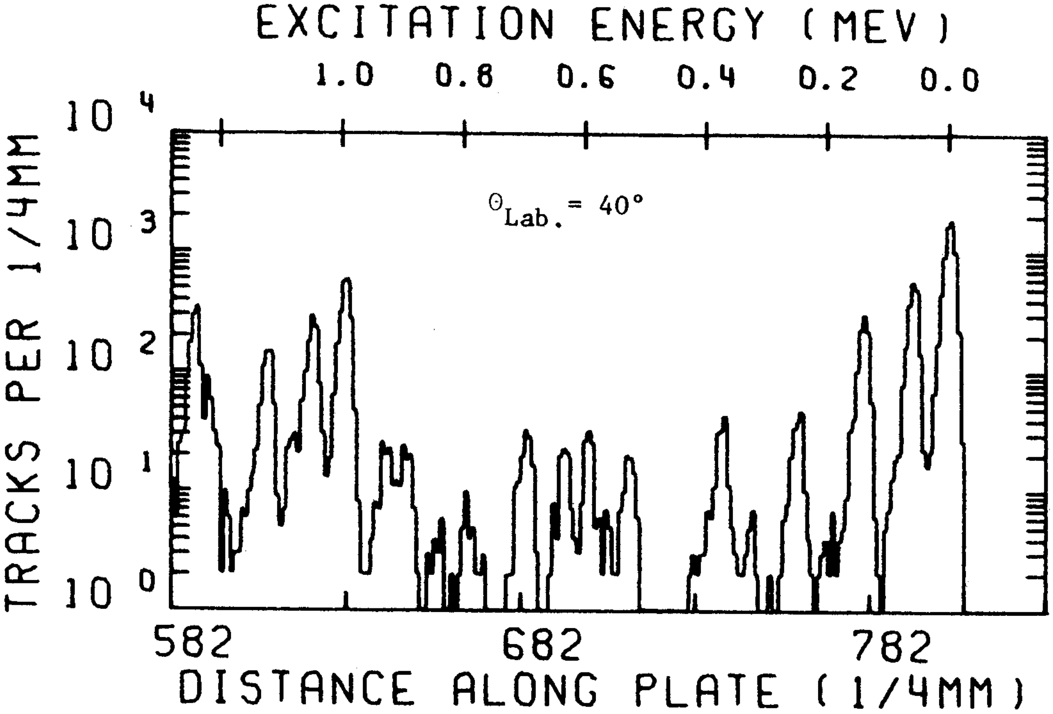
EXCITATION ENERGY (MEV)
1.0
0.8
0.6
0.4
0.2
0.0
$\Theta_{Lab.}$ = 40°
TRACKS PER 1/4MM
10 4
10 3
10 2
10 1
10 0
582
682
782
DISTANCE ALONG PLATE (1/4MM)

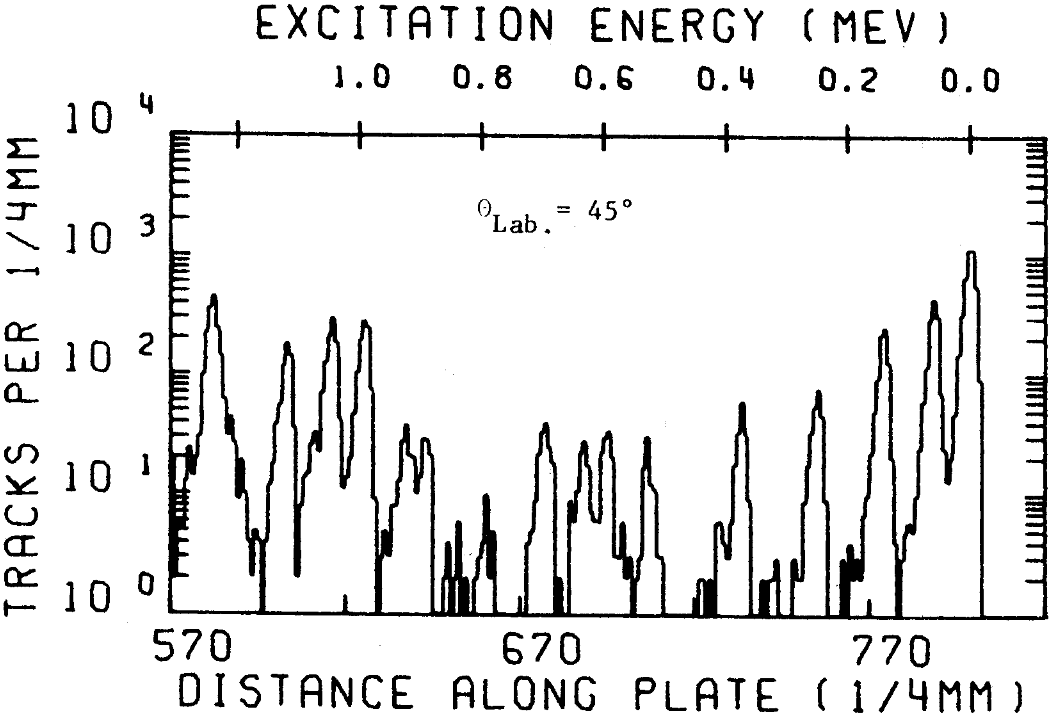
EXCITATION ENERGY (MEV)
1.0
0.8
0.6
0.4
0.2
0.0
$\Theta_{Lab.}$ = 45°
TRACKS PER 1/4MM
10 4
10 3
10 2
10 1
10 0
570
670
770
DISTANCE ALONG PLATE (1/4MM)

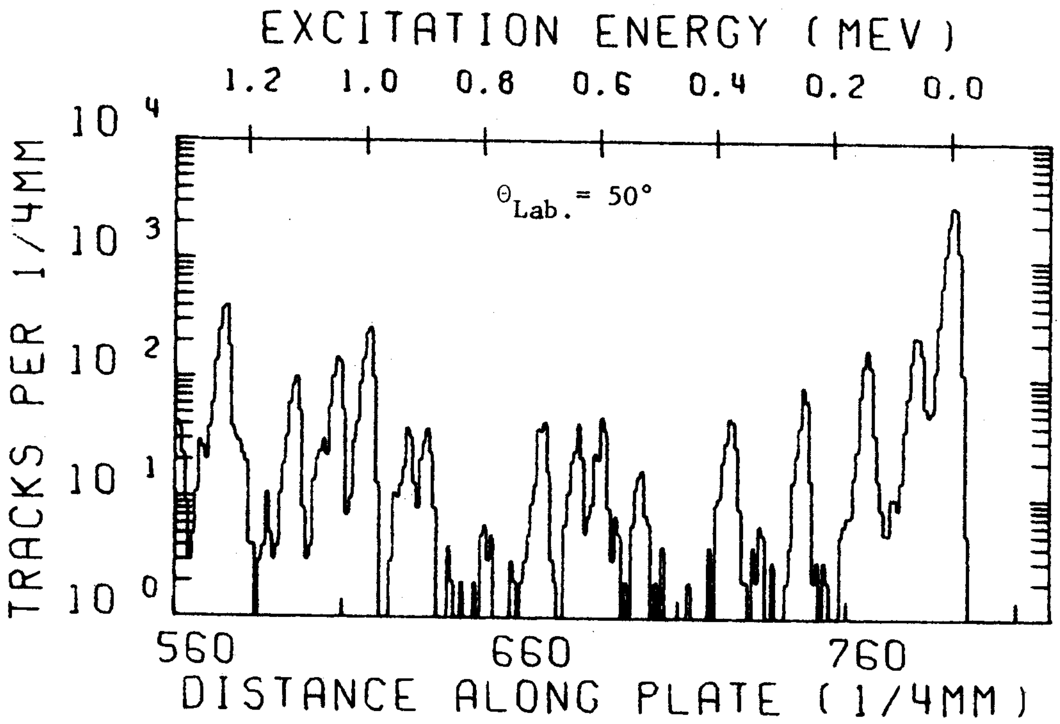
EXCITATION ENERGY (MEV)
1.2
1.0
0.8
0.6
0.4
0.2
0.0
$\Theta_{Lab.} = 50°$
TRACKS PER 1/4MM
10^4
10^3
10^2
10^1
10^0
560
660
760
DISTANCE ALONG PLATE (1/4MM)

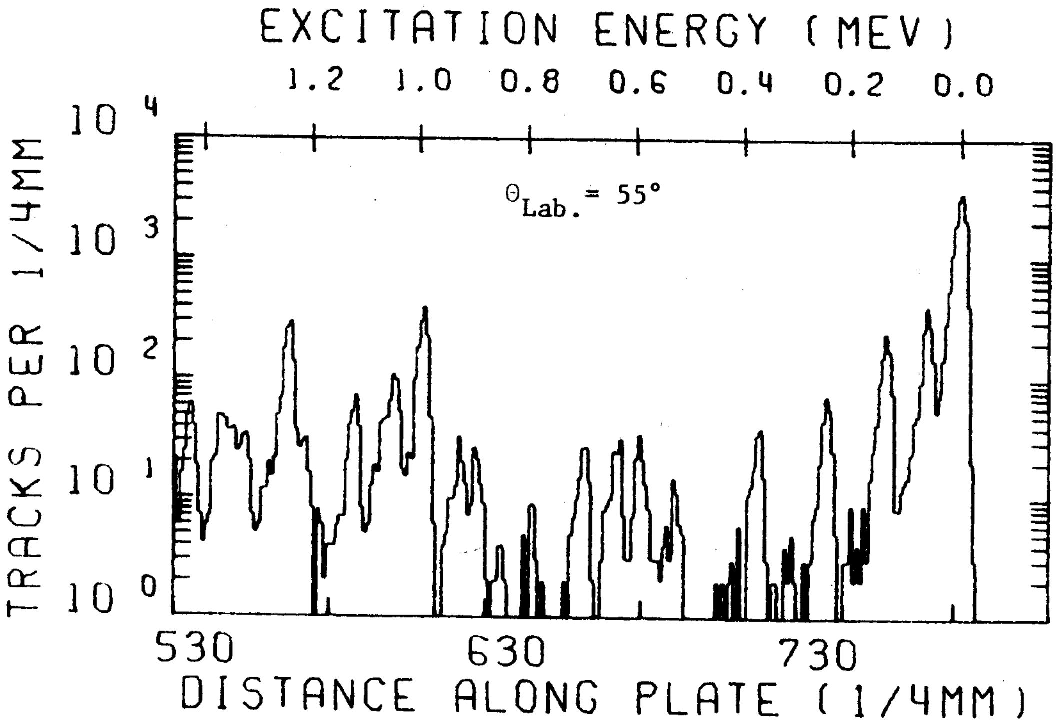
EXCITATION ENERGY (MEV)
1.2
1.0
0.8
0.6
0.4
0.2
0.0
$\Theta_{Lab.} = 55°$
TRACKS PER 1/4MM
10^4
10^3
10^2
10^1
10^0
530
630
730
DISTANCE ALONG PLATE (1/4MM)

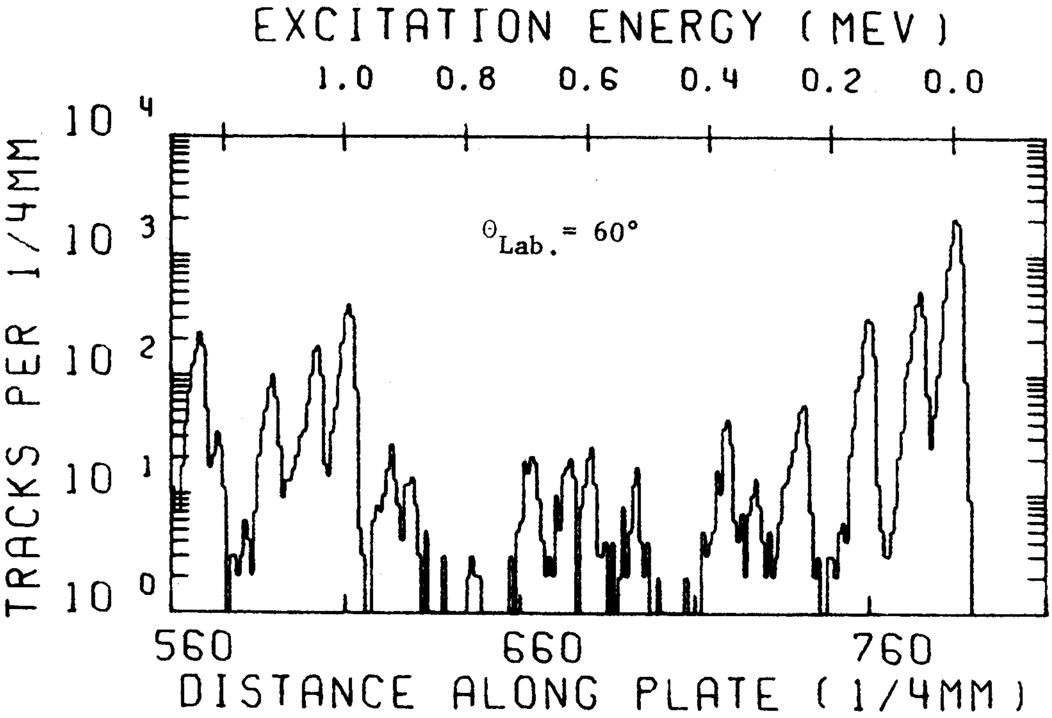
EXCITATION ENERGY (MEV)
1.0
0.8
0.6
0.4
0.2
0.0
$\theta_{Lab.}$ = 60°
TRACKS PER 1/4MM
10^4
10^3
10^2
10^1
10^0
560
660
760
DISTANCE ALONG PLATE (1/4MM)

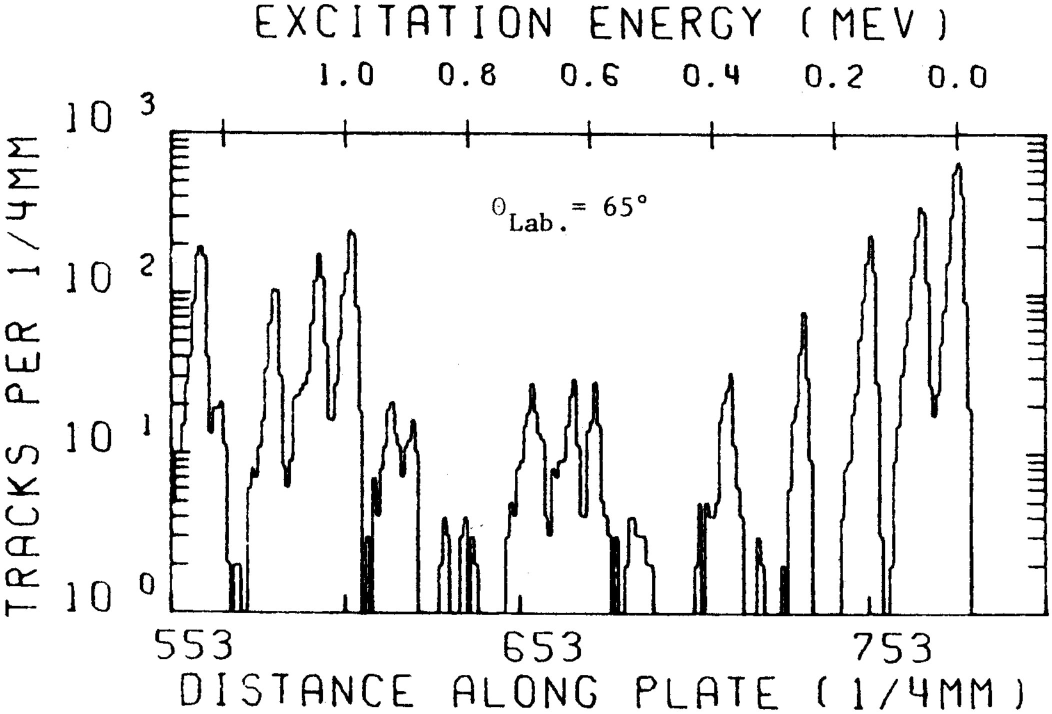
EXCITATION ENERGY (MEV)
1.0
0.8
0.6
0.4
0.2
0.0
$\theta_{Lab.}$ = 65°
TRACKS PER 1/4MM
10^3
10^2
10^1
10^0
553
653
753
DISTANCE ALONG PLATE (1/4MM)

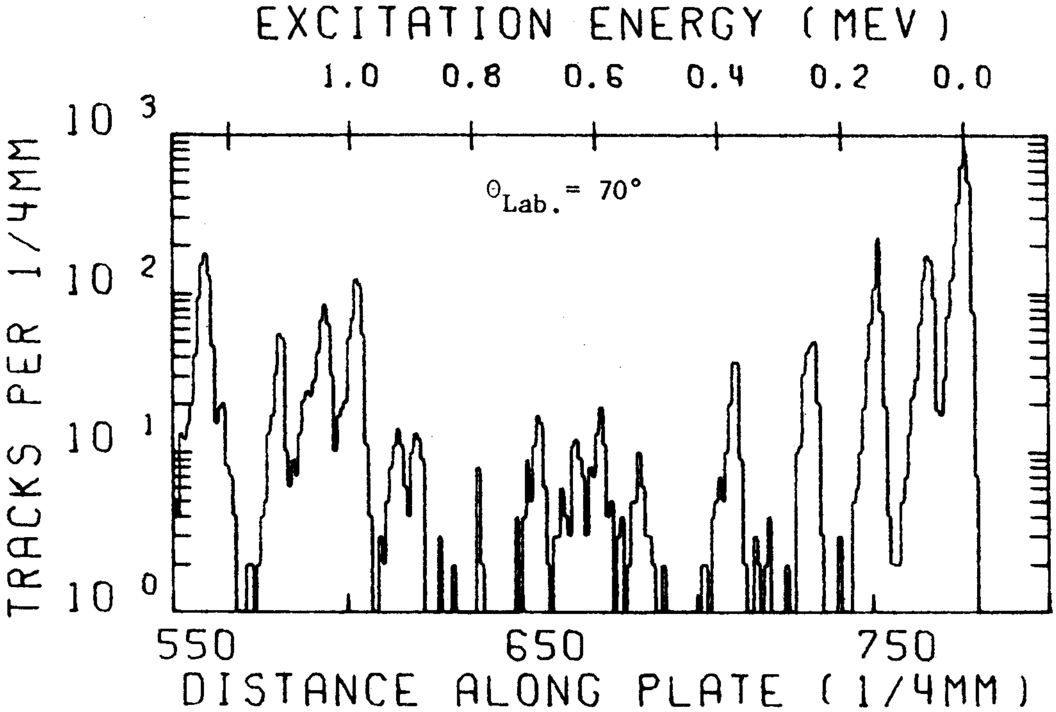
EXCITATION ENERGY (MEV)
1.0
0.8
0.6
0.4
0.2
0.0
$\Theta_{Lab.}$ = 70°
TRACKS PER 1/4MM
10^3
10^2
10^1
10^0
550
650
750
DISTANCE ALONG PLATE (1/4MM)

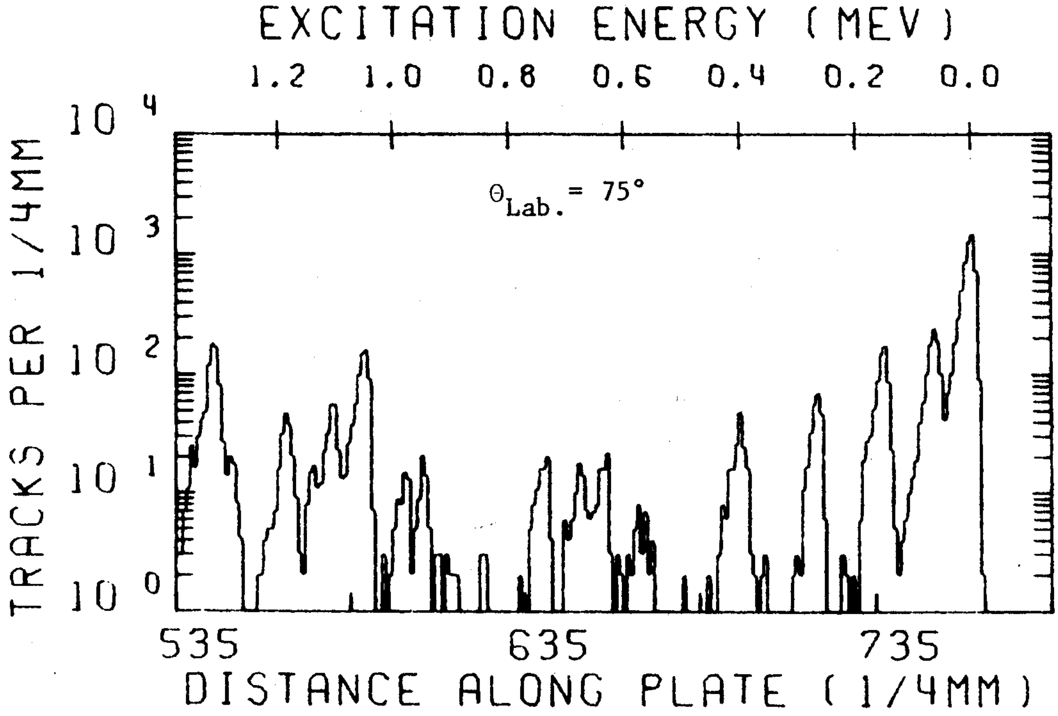
EXCITATION ENERGY (MEV)
1.2
1.0
0.8
0.6
0.4
0.2
0.0
$\Theta_{Lab.}$ = 75°
TRACKS PER 1/4MM
10^4
10^3
10^2
10^1
10^0
535
635
735
DISTANCE ALONG PLATE (1/4MM)

APPENDIX D

Tabulation of ^{159}Tb(p,t) Differential Cross Sections

The following pages contain listings of the center-of-mass differential cross sections and scattering angles for the various states populated through the ^{159}Tb(p,t) reaction. All cross sections are relative and have been normalized to reflect the magnitude of measured absolute values. The listed errors are purely statistical.

```
        TB159(P,T)

      EX= .000 MEV

ANG(CM) SIGMA(CM) ERRØR
 (DEG)   (MB/SR)   (%)

 10.13  1.66E-01    .7
 15.19  2.34E-02    .7
 20.25  8.44E-03   2.1
 25.31  1.75E-02   1.0
 30.36  4.61E-02    .6
 35.42  4.65E-02   1.3
 40.47  1.68E-02   1.2
 45.51  9.78E-03   1.5
 50.56  2.62E-02    .9
 55.59  3.39E-02    .9
 60.63  1.97E-02   1.1
 65.66  6.38E-03   2.0
 70.68  1.08E-02   1.9
 75.70  1.66E-02   1.3
```

```
        TB159(P,T)

      EX= .061 MEV

ANG(CM) SIGMA(CM) ERRØR
 (DEG)   (MB/SR)   (%)

 10.13  1.30E-02   2.8
 15.19  5.32E-03   1.5
 20.25  9.36E-03   2.0
 25.31  2.40E-03   2.6
 30.36  1.76E-03   3.3
 35.42  4.24E-03   4.3
 40.47  4.95E-03   2.3
 45.51  3.22E-03   2.7
 50.56  2.17E-03   3.3
 55.59  3.48E-03   2.7
 60.63  4.78E-03   2.3
 65.66  3.63E-03   2.7
 70.68  2.77E-03   3.7
 75.70  3.01E-03   3.1
```

```
        TB159(P,T)

      EX= .144 MEV

ANG(CM) SIGMA(CM) ERRØR
 (DEG)   (MB/SR)   (%)

 10.13  6.95E-03   3.6
 15.19  2.90E-03   2.0
 20.25  5.00E-03   2.7
 25.31  1.50E-03   3.2
 30.36  1.11E-03   4.0
 35.42  2.20E-03   5.9
 40.47  2.63E-03   3.1
 45.51  1.89E-03   3.5
 50.56  1.50E-03   4.0
 55.60  2.10E-03   3.4
 60.63  3.08E-03   2.9
 65.66  2.03E-03   3.6
 70.68  2.20E-03   4.2
 75.70  1.99E-03   3.9
```

```
        TB159(P,T)

      EX= .254 MEV

ANG(CM) SIGMA(CM) ERRØR
 (DEG)   (MB/SR)   (%)

 10.13  1.69E-03   7.3
 15.19  5.60E-04   4.6
 20.25  1.05E-03   6.0
 25.31  5.33E-04   5.5
 30.36  3.03E-04   7.9
 35.42  3.49E-04  14.9
 40.47  4.49E-04   7.5
 45.52  5.86E-04   6.3
 50.56  5.98E-04   6.3
 55.60  6.11E-04   6.4
 60.63  6.58E-04   6.2
 65.66  5.41E-04   7.0
 70.69  8.28E-04   6.8
 75.70  7.45E-04   6.3
```

```
       TB159(P,T)

      EX= .325 MEV

ANG(CM) SIGMA(CM) ERROR
 (DEG)   (MB/SR)   (%)

 10.13  1.55E-04  24.2
 15.19  3.16E-05  19.6
 20.25  8.95E-05  20.4
 25.31  9.84E-05  11.6
 30.37  4.30E-05  20.9
 40.47  5.61E-05  21.3
 45.52  2.77E-05  28.8
 50.56  4.01E-05  24.2
 60.63  1.18E-04  14.6
 65.66  1.58E-05  40.8
```

```
       TB159(P,T)

      EX= .379 MEV

ANG(CM) SIGMA(CM) ERROR
 (DEG)   (MB/SR)   (%)

 10.13  1.24E-03   8.6
 15.19  5.02E-04   4.9
 20.25  9.51E-04   6.3
 25.31  5.07E-04   5.6
 30.37  3.96E-04   6.9
 35.42  6.13E-04  11.3
 40.47  4.26E-04   7.7
 45.52  3.78E-04   7.8
 50.56  4.71E-04   7.1
 55.60  3.36E-04   8.6
 60.63  3.93E-04   8.0
 65.66  3.76E-04   8.4
 70.69  5.21E-04   8.5
 75.71  5.11E-04   7.6
```

```
       TB159(P,T)

      EX= .527 MEV

ANG(CM) SIGMA(CM) ERROR
 (DEG)   (MB/SR)   (%)

 10.13  6.09E-04  12.2
 15.19  1.93E-04   7.9
 20.25  3.69E-04  10.1
 25.31  3.11E-04   7.2
 30.37  2.62E-04   8.4
 35.42  3.41E-04  15.1
 40.47  2.04E-04  11.2
 45.52  1.91E-04  11.0
 50.56  1.53E-04  12.4
 55.60  1.29E-04  13.9
 60.64  1.44E-04  13.2
 65.66  6.30E-05  20.4
 70.69  1.44E-04  16.2
 75.71  1.07E-04  16.7
```

```
       TB159(P,T)

      EX= .598 MEV

ANG(CM) SIGMA(CM) ERROR
 (DEG)   (MB/SR)   (%)

 10.13  1.78E-03   7.1
 15.19  5.35E-04   4.8
 20.25  6.42E-04   7.6
 25.31  3.05E-04   7.3
 30.37  2.99E-04   7.9
 35.42  4.03E-04  13.3
 40.47  2.76E-04   9.6
 45.52  2.67E-04   9.3
 50.56  3.68E-04   8.0
 55.60  2.84E-04   9.3
 60.64  2.04E-04  11.1
 65.67  2.36E-04  10.5
 70.69  2.70E-04  11.9
 75.71  2.34E-04  11.3
```

```
       TB159(P,T)

     EX= .640 MEV

ANG(CM) SIGMA(CM) ERROR
 (DEG)   (MB/SR)   (%)

 10.13  1.60E-03   7.5
 15.19  4.61E-04   5.1
 20.25  6.30E-04   7.7
 25.31  3.47E-04   6.8
 30.37  3.05E-04   7.8
 35.42  3.10E-04  15.8
 40.47  2.37E-04  10.4
 45.52  2.49E-04   9.6
 50.56  3.04E-04   8.8
 55.60  3.02E-04   8.2
 60.64  2.12E-04  10.9
 65.67  3.10E-04   9.2
 70.69  2.32E-04  12.8
 75.71  2.14E-04  11.8
```

```
       TB159(P,T)

     EX= .699 MEV

ANG(CM) SIGMA(CM) ERROR
 (DEG)   (MB/SR)   (%)

 10.13  1.10E-03   9.1
 15.19  3.65E-04   5.8
 20.25  6.94E-04   7.3
 25.31  4.37E-04   6.1
 30.37  5.29E-04   5.9
 35.42  4.73E-04  12.5
 40.47  3.27E-04   8.8
 45.52  3.64E-04   8.0
 50.56  3.98E-04   7.7
 55.60  2.67E-04   9.6
 60.64  2.52E-04  10.0
 65.67  3.68E-04   8.4
 70.69  2.81E-04  11.6
 75.71  2.40E-04  11.1
```

```
       TB159(P,T)

     EX= .795 MEV

ANG(CM) SIGMA(CM) ERROR
 (DEG)   (MB/SR)   (%)

 10.13  2.46E-04  19.3
 15.19  8.02E-05  12.3
 20.25  2.20E-04  13.0
 25.31  1.66E-04   9.7
 30.37  1.46E-04  11.3
 35.42  2.09E-04  19.3
 40.47  9.19E-05  16.7
 45.52  6.23E-05  19.3
 50.57  5.42E-05  20.9
 55.60  7.41E-05  18.3
 60.64  3.53E-05  26.7
 65.67  3.68E-05  26.7
 70.69  4.18E-05  30.2
 75.71  2.37E-05  35.4
```

```
       TB159(P,T)

     EX= .896 MEV

ANG(CM) SIGMA(CM) ERROR
 (DEG)   (MB/SR)   (%)

 10.13  9.73E-04   9.7
 15.19  2.77E-04   6.6
 20.25  5.13E-04   8.5
 25.31  3.05E-04   7.3
 30.37  2.65E-04   8.4
 35.42  2.95E-04  16.2
 40.48  2.09E-04  11.0
 45.52  2.37E-04   9.9
 50.57  2.97E-04   8.9
 55.61  2.17E-04  10.7
 60.64  1.34E-04  13.7
 65.67  1.47E-04  13.4
 70.69  1.82E-04  14.4
 75.71  1.69E-04  13.2
```

TB159(P,T)

EX= .927 MEV

ANG(CM) (DEG)	SIGMA(CM) (MB/SR)	ERROR (%)
10.13	1.38E-03	8.1
15.19	4.65E-04	5.1
20.25	5.97E-04	7.9
25.31	3.13E-04	7.2
30.37	2.50E-04	8.6
35.42	2.17E-04	18.9
40.48	2.22E-04	10.7
45.52	3.18E-04	8.5
50.57	3.09E-04	8.7
55.61	2.64E-04	9.7
60.64	2.12E-04	10.9
65.67	2.47E-04	10.3
70.70	2.47E-04	12.4
75.71	1.63E-04	13.5

TB159(P,T)

EX= .994 MEV

ANG(CM) (DEG)	SIGMA(CM) (MB/SR)	ERROR (%)
10.13	2.63E-02	1.9
15.19	4.95E-03	1.6
20.25	4.91E-03	2.8
25.31	1.26E-03	3.6
30.37	2.97E-03	2.5
35.42	6.70E-03	3.4
40.48	5.26E-03	2.2
45.52	2.31E-03	3.2
50.57	2.20E-03	3.3
55.61	3.27E-03	2.7
60.64	3.78E-03	2.6
65.67	2.39E-03	3.3
70.70	1.88E-03	4.5
75.72	1.96E-03	3.9

TB159(P,T)

EX=1.048 MEV

ANG(CM) (DEG)	SIGMA(CM) (MB/SR)	ERROR (%)
10.13	9.99E-03	3.0
15.19	3.40E-03	1.9
20.25	5.10E-03	2.7
25.31	1.85E-03	3.0
30.37	1.58E-03	3.4
35.43	2.37E-03	5.7
40.48	2.58E-03	3.1
45.52	2.21E-03	3.2
50.57	1.23E-03	4.4
55.61	1.00E-03	5.0
60.64	1.92E-03	3.6
65.67	1.60E-03	4.1
70.70	1.33E-03	5.3
75.72	6.68E-04	6.7

TB159(P,T)

EX=1.120 MEV

ANG(CM) (DEG)	SIGMA(CM) (MB/SR)	ERROR (%)
10.13	6.25E-03	3.8
15.19	2.01E-03	2.5
20.25	3.07E-03	3.5
25.31	1.36E-03	3.4
30.37	1.16E-03	4.0
35.43	1.60E-03	7.0
40.48	1.52E-03	4.1
45.53	1.40E-03	4.1
50.57	8.93E-04	5.1
55.61	6.57E-04	6.1
60.64	9.85E-04	5.1
65.67	1.05E-03	5.0
70.70	7.49E-04	7.1
75.72	5.70E-04	7.2

```
              TB159(P,T)

             EX=1.238 MEV

   ANG(CM)  SIGMA(CM)  ERROR
    (DEG)    (MB/SR)    (%)

    10.13   1.98E-02    2.1
    15.19   5.77E-03    1.5
    20.25   8.93E-03    2.0
    25.31   3.90E-03    2.0
    30.37   3.44E-03    2.3
    35.43   3.53E-03    4.7
    40.48   2.87E-03    3.0
    45.53   3.84E-03    2.4
    50.57   3.61E-03    2.6
    55.61   2.71E-03    3.0
    60.65   2.23E-03    3.4
    65.68   2.04E-03    3.6
    70.70   2.63E-03    3.8
    75.72   2.02E-03    3.3
```